AD_____

Award Number: W81XWH-10-1-0026

TITLE: P53 Suppression of Homologous Recombination and Tumorigenesis

PRINCIPAL INVESTIGATOR: Bijal Karia, B.S.

CONTRACTING ORGANIZATION: University of Texas Health Science Center at San Antonio
San Antonio, TX 78229

REPORT DATE: January 2011

TYPE OF REPORT: Annual Summary

PREPARED FOR: U.S. Army Medical Research and Materiel Command
Fort Detrick, Maryland 21702-5012

REPORT DOCUMENTATION PAGE

Form Approved
OMB No. 0704-0188

1. REPORT DATE	2. REPORT TYPE	3. DATES COVERED
January 2011	Annual Summary	1 January 2010 – 31 December 2010

4. TITLE AND SUBTITLE

P53 Suppression of Homologous Recombination and Tumorigenesis

5a. CONTRACT NUMBER

5b. GRANT NUMBER
W81XWH-10-1-0026

5c. PROGRAM ELEMENT NUMBER

6. AUTHOR(S)

Bijal Karia

E-Mail: BIJALKARIA79@GMAIL.COM

5d. PROJECT NUMBER

5e. TASK NUMBER

5f. WORK UNIT NUMBER

7. PERFORMING ORGANIZATION NAME(S) AND ADDRESS(ES)

University of Texas Health Science Center at San Antonio
San Antonio, TX 78229

8. PERFORMING ORGANIZATION REPORT NUMBER

9. SPONSORING / MONITORING AGENCY NAME(S) AND ADDRESS(ES)
U.S. Army Medical Research and Materiel Command
Fort Detrick, Maryland 21702-5012

10. SPONSOR/MONITOR'S ACRONYM(S)

11. SPONSOR/MONITOR'S REPORT NUMBER(S)

12. DISTRIBUTION / AVAILABILITY STATEMENT
Approved for Public Release; Distribution Unlimited

13. SUPPLEMENTARY NOTES

14. ABSTRACT

Maintaining genomic stability is critical for organismal fitness. Consequently, the absence of tumor suppressor gene activity, such as p53, results in increased genomic instability and increased cancer predisposition. Homologous recombination (HR), as measured by the in vivo pun assay, is a DNA repair mechanism that our laboratory uses to measure genomic instability. We compared eyespot frequency in normal wild type mice, mice that are absent in p53 protein (null) and those that have the hotspot mutations R172H and R172P (equivalent to R175 in human breast cancer). Previously, we have shown that in the absence of p53 the normal frequency of spontaneous HR is significantly elevated. However, the mechanism by which p53 suppresses HR is unclear. The p53 R172P mutant mice retains limited transcriptional functionality (regulating cell cycle genes but not apoptotic genes) while the p53 R172H mutant mice lack any transcriptional activity but retain some protein: protein interaction capability. We observed significantly increased HR frequency in the p53 R172H mutant versus the p53 R172P mutant mice. This suggests that p53 regulation of cell cycle genes but not apoptotic genes may be responsible for its ability to suppress HR frequency. Also, the loss of key protein: protein interactions may have contributed to this suppression. It has been previously reported that p53 R172H mutant mice come down with early aggressive tumors compared to the p53 R172P mutant mice. This correlates with the increased HR frequency we observed in the R172H mutant mice implicating p53 suppression of genomic instability as a major mechanism for p53 tumor suppression. This work provides novel insight into the mechanism of cancer development in the absence or mutation of p53 and the mechanism of p53 control of HR in an in vivo system. p53 is often a targeted therapy and further insight into the function of p53 in DNA repair pathways can be vital to finding novel points of targeted therapy. Our data will add insight to the important paradigm of genomic instability and its relation to breast cancer etiology.

15. SUBJECT TERMS
HOMOLOGOUS RECOMBINATION, P53 HOTSPOT MUTATIONS, BREAST CANCER, GENOMIC INSTABILITY, TUMORIGENESIS

16. SECURITY CLASSIFICATION OF:			17. LIMITATION OF ABSTRACT	18. NUMBER OF PAGES	19a. NAME OF RESPONSIBLE PERSON
a. REPORT	b. ABSTRACT	c. THIS PAGE			USAMRMC
U	U	U	UU	48	19b. TELEPHONE NUMBER *(include area code)*

Table of Contents

Introduction

The purpose of this project is to determine the mechanism for how the tumor suppressor, p53, suppresses homologous recombination. P53 is implicated in 50% of all human cancers and inactivated in some form in 100% of human cancers. Homologous recombination (HR) is an error proof repair mechanism that is able to repair any type of DNA lesion with high fidelity. However, when the HR machinery uses an incorrect template for repair large deletions in the genome can occur leading to a predisposition for cancer. P53 has been implicated in suppressing homologous recombination in order to maintain genomic stability, however the mechanism is still unknown. In the first year of this grant huge strides have been made in the numbers of mice breed and relevant cells collected for the purposes of experiments outlined in the aims below. The PI has optimized the pun assay and RAD51 foci experiments in order to start collecting data during the second year of the grant period. The first year accomplishments include a second author publication regarding the PI's work in mastering the pun assay and RAD51 foci experiments using a different mouse in the lab. This expertise will help the PI publish work for the aims outlined below. The PI has also attended several conferences, presented posters, and has had several committee meetings to evaluate the work progress.

P53 is a potent tumor suppressor that shields the genome from daily interrogations of endogenous and exogenous damage, most importantly through its ability to arrest the cell cycle. In response to damage, p53 up regulates transcription of p21 leading to G1 arrest, which allows adequate time for repair of lesions before entering S phase (1, 2). Furthermore, p53 has been linked to G2/M arrest through multiple overlapping p53-dependent and p53-independent pathways that inhibit cdc2 (3). As a final resort if the damage is severe enough p53 has been shown to induce apoptosis in certain situations (2, 4).

P53 has also been linked to various DNA repair pathways such as non-homologous end joining (NHEJ) and homologous recombination (HR). Homologous recombination is a high fidelity DNA repair mechanism that can repair almost any type of DNA lesion when in correct equilibrium. When this delicate balance is disrupted as seen in *Blm* null cells resulting in hyperrecombination or hyporecombination in *Brca1* null cells the ensuing result is genomic instability (5).

It has been reported previously that p53 down regulates spontaneous homologous recombination in chromosomally integrating plasmid substrate models. Bertrand *et al*. using a plasmid-based system with PJS3-10 (mouse L cell lines) overexpressed the mutant $p53^{175\ (Arg>His)}$, which showed a 5-20 fold increase in spontaneous recombination compared to wild type control cells. Further analysis showed that the effect of the p53 mutation acted on both rad51 dependent gene conversion events and deletion events (6).

Willers *et al*. also showed an increase in recombination frequency in a temperature sensitive p53 mutant (Ala135 to Val) using a plasmid substrate that stably integrated into p53 null mouse embryonic fibroblasts (MEFs). This study further established the uncoupling of p53's function in suppressing HR and its role as a cell cycle checkpoint protein (7).

The Wiesmuller lab has explored the role of p53 in HR using a rare cutting endonuclease ISCE-1 in breast cancer cells with varying p53 mutations. This study used a DSB repair assay to show that some p53 mutants retain partial ability to repair double strand breaks by repressing aberrant HR and less infrequently through NHEJ and SSA(8).

P53 is mutated in 50% of all human cancers and most likely inactivated by some other mechanism in the other 50%. Patients with Li Fraumeni syndrome suffer from a germ line mutation in p53 and subsequently endure an early onset of cancer. Mouse models have been created to recapitulate this phenomenon and are surprisingly viable. 80% of P53 null mice come down with lymphomas within 6 months and the rest suffer from sarcomas. MEFs from these mice show aneuploidy, allelic loss and gene amplification. Most of these germline mutations are missense mutations occurring in the DNA binding domain of p53. One such mutant is the p53-R172P and p53-R172H mouse model (9). The p53-R172P mouse is able to induce partial cell cycle arrest in response to DNA damage but is defective in promoting apoptosis. Mice homozygous for this mutation escape the early onset of lymphomas that is typical for p53 null mice, however these mice eventually do succumb to tumors that have a normal diploid number of chromosomes in contrast to p53 null tumors. The p53-R172H mouse shows an inability to transactivate p53 target genes as well as a defect in apoptosis induction (10). A majority of mice homozygous for p53-R172H developed lymphomas similar to p53 null mice with a smaller percent developing sarcomas. P53-R172H heterozygous mice developed sarcomas and a surprising number of osteosarcomas and carcinomas that metastasized, which was not seen in p53 heterozygous mice (9). Interestingly, the p53-R172H tumors showed a high level of aneuploidy similar to p53 null mice but unlike p53-R172P mice. Given this we sought to look at the HR frequency of these two mutants to determine if there is a difference in in the ability to suppress HR similar to WT given the different functionalities of these to mutants. HR is measure of genomic instability, even though it can fix any type of genotoxic lesion, when used incorrectly it can cause large deletions and lesions in the genome. Using the in vivo pun assay we have seen an increase in HR frequency in many mouse models of the DNA damage repair pathway. HR frequency

is increased in BLM null, p53 null and parp null mice and decreased in Brca1 and Brca2 null animals (5, and unpublished work).

Given the power of this assay here we used the *in vivo* p^{un} assay to determine the consequence of HR suppression in two breast cancer hotspot p53 mutant mouse models with differing loss of function. The p53-R172P mice, which are defective in their ability to induce apoptosis but are able to induce cell cycle genes, retained the ability to suppress HR similar to wild type p53 animals. The more aggressive p53-R172H mouse showed increase HR similar to p53 null mice, which do not produce any p53 protein at all.

Specific Aim 1: Determine whether p53 mutants R172P and R172H suppress spontaneous levels of homologous recombination the same as wild-type p53.

In the first year of the training grant great effort was put forth to establish a robust breeding colony of R172P, R172H, Wild type and p53 null mice in order to have sufficient numbers of animals to perform the in vivo pun assay.

Mouse Strains and Breeding Cohorts

Mice heterozygous for the point mutations $p53^{R172P}$ and $p53^{R172H}$ both on a C57BL/6 genetic background were kindly provided by Dr. G. Lozano (M.D. Anderson). In addition, two crosses were made to C57BL/6 $p^{un/un}$ mice obtained from the Jackson Laboratory (Bar Harbor, ME) to establish the homozygous $p^{un/un}$ genotype. Mice heterozygous for a targeted null allele of *p53* were previously crossed into a C57BL/6J $p^{un}/^{un}$ genetic background as described in Aubrecht *et al*. (11). Breeding cohorts of $p53^{R172P/+}$ $p^{un/un}$, $p53^{R172H/+}$ $p^{un/un}$ and $p53^{neo/+}$ $p^{un/un}$ mice were established and maintained by intercrossing heterozygous mice in each respective cohort to produce the desired experimental mice ($p53^{R172P/R172P}$, $p53^{R172H/R172H}$, $p53^{neo/neo}$) along with littermate controls ($p53^{R172P/+}$, $p53^{R172H/+}$, $p53^{neo/+}$, $p53^{+/+}$).

Genotyping

The $p53^{R172P}$, $p53^{R172H}$ and $p53^{neo}$ genotypes were determined as previously described (11). The $p^{un/un}$ genotype was identified by the phenotypic dilute (grey) coat color.

p^{un} Eyespot HR Assay

Mice were sacrificed at weaning age and their eyes harvested and dissected to expose the retinal pigment epithelium (RPE) as previously described (12). Briefly, each RPE whole mount was digitally photographed and analyzed for eyespots using a Zeiss Lumar version 12 stereomicroscope, Zeiss AxioVision MRm camera, and Zeiss AxioVision 4.6 software (Thornwood, NY) as described previously (13, appendix). The criteria for what constitutes an eyespot was previously defined in bishop *et al*. as being a pigmented cell that is separated by 2 other pigmented cells (12). Next, the RPE images were uploaded into Adobe Photoshop and the edge of the RPE was delineated using the ellipse tool and free transform path function. Two measurements were made (i) a frequency of eyespots (HR events) per RPE, and (ii) distribution of the eyespots within the RPE (their position) reflecting the developmental time at which the eyespots were produced.

Statistics

The Kruskal-Wallis test (non-parametric, one-way analysis of variance for multiple group comparison) followed by the Dunn's Multiple Comparison test was performed using GraphPad Prism (La Jolla, CA).

The recessive R172P mutation retains the ability to suppress HR in vivo

P53 is a potent tumor suppressor and plays an important role in protecting the genome from endogenous and exogenous damage. HR is the only DNA repair mechanism that is able to mend any

lesion with high fidelity when it is working correctly. P53, although not a direct player in HR, helps the cell decide whether HR will be the best route to take. The R172P point mutation in p53 results in a mouse that is unable to transcribe apoptotic genes but is still able to arrest the cell cycle and retains most of its protein: protein interactions.
The frequency of p^{un} reversion was determined in $p53^{R172P/R172P}$ $p^{un/un}$ mice using the *in vivo* p^{un} assay (Table 1 and Figure 1). There was no significant increase in the number of eyespots compared to wild type. Suggesting that p53-R172P mutant mice retain the ability to suppress homologous recombination similar to wild type mice. The inability to transcribe apoptotic genes in this particular mutant had no impact on its ability to suppress HR, suggesting that the mechanism for p53 involvement in HR may be cell cycle mediated or through protein: protein interactions.

The aggressive R172H mutant mice show increased HR frequency similar to p53 null mice in vivo

The R172H point mutation results in a protein being formed but it is unable to bind and transcribe any of the p53 target genes. Also many of the normal protein: protein interactions have also been disrupted. The p53- R172H mutation is more detrimental than the R172P mutation in that the former mice have an earlier onset of tumors and a higher incidence of metastatic tumors in the heterozygous genotype.
The frequency of p^{un} reversion events in the p53-R172H mouse was significantly higher than the wild type controls and p53-R172P mutant mice ($p < .001$) (Table 1 and figure 1). Interestingly, the p^{un} reversion frequency was similar to that of a p53 null animal that produces no p53 protein at all (~ 10 eyespots).

Table 1. Summary of RPE analyzed and p^{un} reversion frequency by *p53* genotype

	TOTAL			AVERAGE					
Genotype	RPE	Eyespots	Cells	Eyespots per RPE	SD	Cells per RPE	SD	Spot Size	SD
$p53^{+/+}$ $p^{un/un}$	41	153	441	3.7	2.3	10.7	11	2.8	3.5
$p53^{neo/neo}$ $p^{un/un}$	22	258	680	11.7	6.6	31	26.6	2.6	3.4
$p53^{R172P/R172P}$ $p^{un/un}$	29	118	323	4.1	2.6	11.5	15.4	2.7	5.2
$p53^{R172H/R172H}$ $p^{un/un}$	35	340	742	9.7	4.6	21.2	13.9	2.2	2.5

Because these mouse models are not a true separation of function (none exist in mouse models) we will need to do further explore the relationship between p53's transcription factor capability and protein: protein interaction capability and its disruption in mutant mice.

Given these results we will need to delineate the 2 mechanisms of p53 to determine which have been disrupted between the R172P and R172H mutant to cause the change in HR suppression. Further experiments including microarray analysis to determine transactivation differences as well as Co-IP experiments to determine broken protein: protein interactions will need to be performed. The genes to look at in the microarray in order to focus the experiment and not fish will be to look at HR genes, cell

cycle, apoptotic genes that may be dysregulated. Same is true for protein: protein interaction experiments- look at HR proteins such as BRCA/2, Rad51, RPA, 53bp1, bcl2 to determine if there are broken interactions in the R172H mutation and not in the R172P mutant.

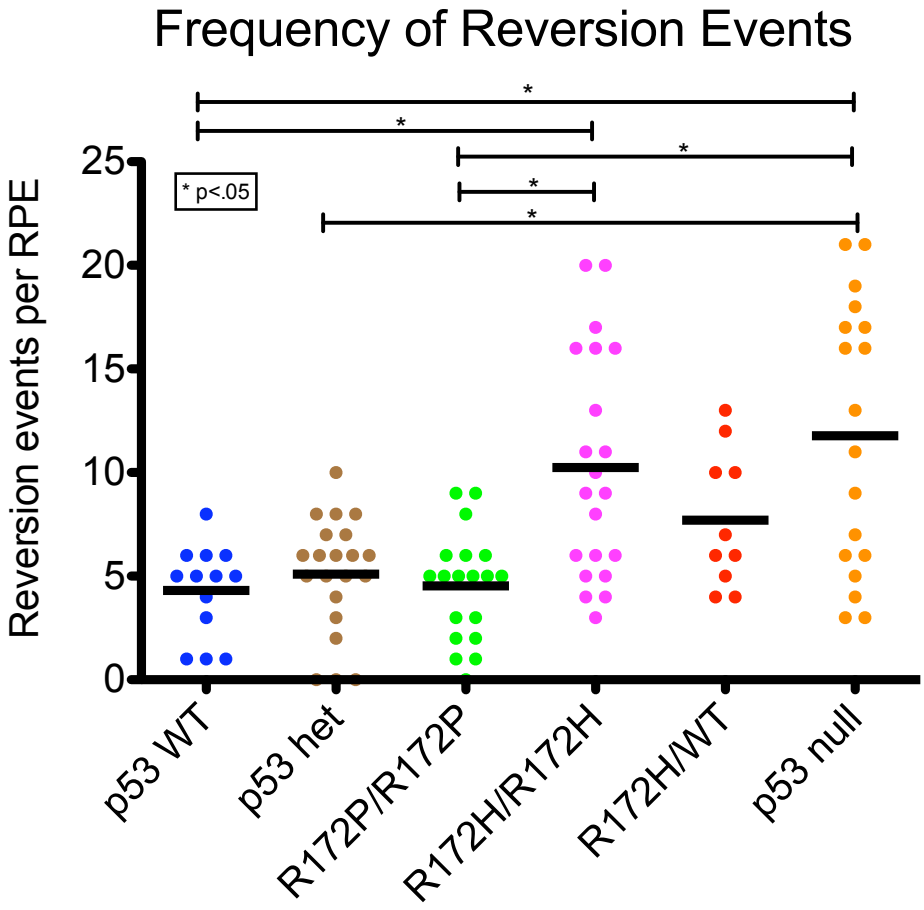

Figure 1. The frequency of eyespots was determined using the pun assay. The data indicates that p53 R172P mutant mice retained the ability to suppress HR similar to WT p53 mice. However, p53 R172H mutant mice showed increased HR frequency similar to p53 null mice. $p<0.001$.

A more sophisticated measurement that can be made using the pun eye assay is the relative position of the eyespot on the RPE. We performed this analysis (Figure 2.) and were surprised to see that there was a difference in these results in comparison to previous findings by the PI's mentor. Previous work showed that p53 null animals showed an increased number of eyespots closer to the optic nerve (towards the center) indicating a time in early development ~E8. This was not seen in the current work and can be explained by the difference in where the cutoff is made in the edge of the RPE. The current work shows a larger portion of the RPE whereas the previous work was a tighter

circle around the RPE. This would lead to more spots being counted on the edge of the RPE that what was previously reported (14). There is no significant difference between the p53 mutants and WT in terms of their positional distribution on the RPE. Thus these events are not time in development as was previously reported for p53 null mice (14).

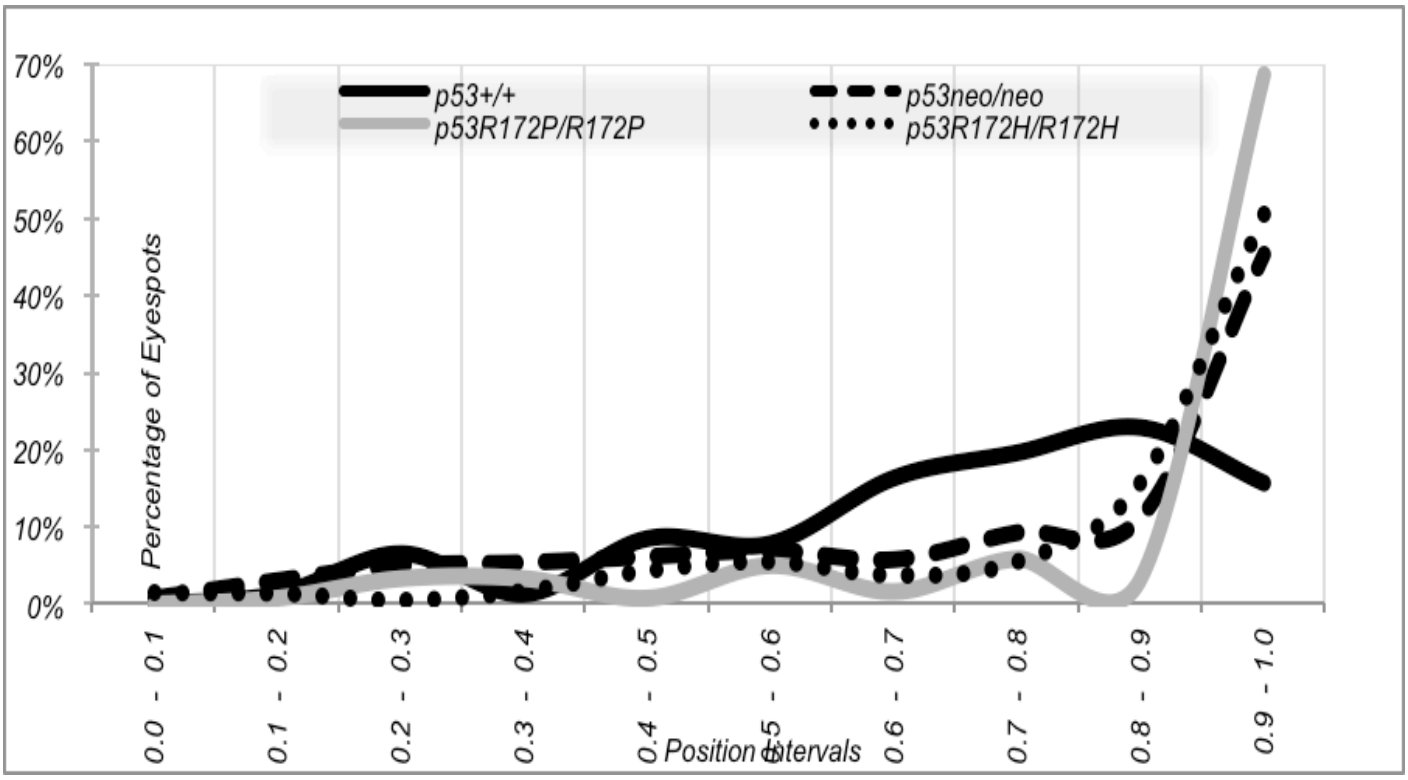

Figure 2. The Relative Position distribution of eyespots was determined using the pun assay. P<0.05

- Rad51 Foci using primary MEFs (months 5-12)
  - An initial experiment has been performed but is in the process of being replicated with additional biological replicates and the use of more sophisticated confocal microscopy versus epifluorescence.

Specific Aim 2: Determine the influence of the two p53 mutant mice on BER and NER activity as a mechanism by which p53 suppresses homologous recombination..

- Time frame: 1 year
  - The NER and BER assays are currently being optimized in the lab. All resources and relevant p53 mutant cells have been collected. This aim will be the focus in the second year.

Specific Aim 3. Determine whether either of the p53 mutants can alter the damage induced HRR response and if their reduced functionality impacts damage induced BER and NER activity.

- Time frame: 1 year
  - Continue to expand R172P, R172H and neo cohorts (months 1-12)
    - Currently I have a robust breeding colony for all three genotypes. Heterozygous mice from each colony are kept and mated for MEF production, spontaneous and exposure pun assay.
  - Perform timed matings to intercross heterozygous mice in each cohort (months 1-12)
    - $p53^{R172P/+}$ $p^{un/un}$, $p53^{R172H/+}$ $p^{un/un}$ and $p53^{neo/+}$ $p^{un/un}$
    - Additional cross between $p53^{R172H/+}$ $p^{un/un}$ and $p53^{neo/+}$ $p^{un/un}$ mice to obtain $p53^{R172H/neo}$
  - Expose pregnant dams to 1Gy of X-ray at E12.5 (months 1-12)
    - 7 pregnant dams have been exposed and the analysis is currently being done.
  - Assess the frequency of damage induced p^{un} HRR deletion for each *p53* genotype by performing the p^{un} eyespot assay (months 5-12)
    - Data from 7 exposed dams has been collected and currently being processed.
  - Set up timed matings for primary MEFs of each *p53* genotype (months 1-12)
    - Intercross heterozygous mice: $p53^{R172P/+}$ $p^{un/un}$, $p53^{R172H/+}$ $p^{un/un}$ and $p53^{neo/+}$ $p^{un/un}$
    - Additional cross between $p53^{R172H/+}$ $p^{un/un}$ and $p53^{neo/+}$ $p^{un/un}$ mice to obtain $p53^{R172H/neo}$
  - Expose pregnant dams to 1Gy of X-ray at E12.5 for MEFs (months 1-12)
    - Mice have been setup for exposures and MEF harvest
  - Perform BER and NER assays on damage induced primary MEFs of each p53 genotype (months 5-12)
  - Perform RAD51 foci kinetics on damage induced primary MEFs of each p53 genotype (months 5-12)

- An initial experiment has been performed but is in the process of being replicated with additional biological replicates and the use of more sophisticated confocal microscopy versus epifluorescence.

- Set up timed matings for nuclear extracts of each *p53* genotype (months 1-12)
  - Intercross heterozygous mice: $p53^{R172P/+}$ $p^{un/un}$, $p53^{R172H/+}$ $p^{un/un}$ and $p53^{neo/+}$ $p^{un/un}$
  - Additional cross between $p53^{R172H/+}$ $p^{un/un}$ and $p53^{neo/+}$ $p^{un/un}$ mice to obtain $p53^{R172H/neo}$
- Expose pregnant dams to 1Gy of X-ray at E12.5 for MEFs (months 1-12)
- Perform BER and NER assays on damage induced nuclear extracts of each p53 genotype to determine If NER/BER activity is recapitulated *in vivo* (months 5-12)

Key Research Accomplishments

- R172P mutant mice are able to suppress HR similar to wild type suggesting the mechanism is not due to the transactivation of apoptotic genes but through cell cycle or protein: protein interactions.
- R172H mutant mice have a decrease in HR similar to p53 null mice, which do not produce p53 protein. This suggests a protein: protein interaction defect and a possible indirect regulatory role for p53 in the regulation of HR.

Reportable outcomes:

Peer-Reviewed Publications:

- Claybon A, Karia B, Bruce C, Bishop AJ (2010) PARP1 suppresses homologous recombination events in mice in vivo. Nucleic Acids Res 38:7538–7545

- Ravi D, Chen Y, Karia B, Brown A, Gu TT, Li J, Carey MS, Hennessy BT, Bishop AJ: 14-3-3 sigma expression effects G2/M response to oxygen and correlates with ovarian cancer metastasis. *PloS one* 2011, 6(1):e15864.

Conference/Poster Presentations:

- **Bijal Karia**, Alexander J.R. Bishop. P53 Suppression of Homologous Recombination and Tumorigenesis. Keystone Symposia: Genomic Instability and DNA Repair. Keystone, Colorado. January 30 - February 4, 2011

- **Bijal Karia**, Alexander J.R. Bishop. P53 Suppression of Homologous Recombination and Tumorigenesis. 15th International P53 Workshop. Philadelphia, Pennsylvania October 8-12, 2010

- **Bijal Karia**, Alexander J.R. Bishop. P53 Suppression of Homologous Recombination and Tumorigenesis. Greehey Children's Cancer Research Institute Symposium. San Antonio, Texas February 25-26 2010

Conclusions

The main focus of this grant was to train me for future as an independent breast cancer investigator. Using the funds from this grant I have attended 3 meetings related to genomic instability (Keystone Symposia), p53 (p53 international workshop) and breast cancer (San Antonio breast cancer symposium). My attendance at these meetings allowed me to make contacts with breast cancer investigators all over the world. I was exposed to cutting-edge research that was being done in the field of breast cancer research. My poster presentation allowed for good discussion and feedback from other investigators that will help shape future experiments and thinking about breast cancer.

I have had 2 dissertation committee meetings (5-10-2010, 2-21-2011) in which the discussion of my progress was key. My committee gave me invaluable advice on analysis of experiments, interpretations, statistical help and time management for progression of my PHD. I have also presented my work to the department of cellular and structural biology two times since this grant was awarded (5-18-2010, 12-23-2010). This has been a great experience for honing my speaking and presentation skills. I have learned how to better answer difficult questions regarding my work and to think critically about my project.

I have also attended seminars twice a week to better keep up with ongoing research in many fields. This has been a great lesson in critically thinking about the work of others and how they answered questions and solved problems.

I have completed the cancer core course given through the cellular and structural biology department with a grade of “A.” This completes all classes necessary for my PHD requirements.

I continually meet with my mentors on a weekly basis to discuss experiment results, future experiment planning and troubleshooting strategies.

In this first year I have made significant progress. Animal models are very difficult but I have managed to learn and master mouse husbandry and now have a thriving healthy breeding colony. The cohorts mentioned in the statement of work have all been established and experiments are underway. Assays for measuring RAD51 foci, NER, BER have been learned by the PI and are currently being used in the lab. The most significant finding that has come from the first year experiments is that there is a difference between the 2 p53 mutants in terms of homologous recombination frequency. Given the separation of function of these 2 mutants we can now tease out the mechanism for how p53 suppresses homologous recombination both in a spontaneous situation and following damage. Future experiments will include microarray analysis to determine differential expression of target genes between the mutants as well as CO-IP experiments to determine if broken interactions exist between the mutants that might explain the difference in HR frequency.

“So what”

the significance of these initial findings is that we are closer to determining what p53 mutations are exactly doing and not doing in cells. If we can determine what main “normal” functions of p53 are altered or lost or broken in cancer cells we can develop better targets and therapies that address these issue particularly. For example if it is determined that the more aggressive R172H mutation has a broken protein: protein interaction that causes it to have hyper recombination leading to genomic instability leading to cancer than there is a chance for targeted therapy to repair this interaction in order to restore normal DNA repair function. The research that has been done in this field by previous investigators has been on in vitro plasmid based models with questionable results. Here we use an in vivo assay in a clean genetic system that provides an excellent model for determining genomic instability by way of measuring HR.

References

1. Lane DP. Cancer. p53, guardian of the genome. Nature. 1992 Jul 2;358(6381):15-6.
2. Sherr CJ. Cancer Cell Cycles. Science. 1996 Dec 6;274(5293):1672-7.
3. Taylor WR, Stark GR. Regulation of the G2/M transition by p53. Oncogene. 2001 Apr 5;20(15):1803-15.
4. Ko LJ, Prives C. p53: Puzzle and Paradigm. Genes Dev. 1996 May 1;10(9):1054-72.
5. Brown AD, Claybon AB, Bishop AJ. A conditional mouse model for measuring the frequency of homologous recombination events in vivo in the absence of essential genes. Mol Cell Biol. 2011 Sep;31(17):3593-602. Epub 2011 Jun 27.
6. Bertrand P, Rouillard D, Boulet A, Levalois C, Soussi T, Lopez BS. Increase of spontaneous intrachromosomal homologous recombination in mammalian cells expressing a mutant p53 protein. Oncogene. 1997 Mar 6;14(9):1117-22.
7. Willers H, McCarthy EE, Wu B, Wunsch H, Tang W, Taghian DG, Xia F, Powell SN. Dissociation of p53-mediated suppression of homologous recombination from G1/S cell cycle checkpoint control. Oncogene. 2000 Feb 3;19(5):632-9.
8. Akyüz N, Boehden GS, Süsse S, Rimek A, Preuss U, Scheidtmann KH, Wiesmüller L. DNA substrate dependence of p53-mediated regulation of double-strand break repair. Mol Cell Biol. 2002 Sep;22(17):6306-17.
9. Lang GA, Iwakuma T, Suh YA, Liu G, Rao VA, Parant JM, Valentin-Vega YA, Terzian T, Caldwell LC, Strong LC, El-Naggar AK, Lozano G. Gain of function of a p53 hot spot mutation in a mouse model of Li-Fraumeni syndrome. Cell. 2004 Dec 17;119(6):861-72.
10. Olive KP, Tuveson DA, Ruhe ZC, Yin B, Willis NA, Bronson RT, Crowley D, Jacks T. Mutant p53 gain of function in two mouse models of Li-Fraumeni syndrome. Cell. 2004 Dec 17;119(6):847-60.
11. Aubrecht J, Secretan MB, Bishop AJ, Schiestl RH. Involvement of p53 in X-ray induced intrachromosomal recombination in mice. Carcinogenesis. 1999 Dec;20(12):2229-36.
12. Bishop AJ, Kosaras B, Carls N, Sidman RL, Schiestl RH. Susceptibility of proliferating cells to benzo[a]pyrene-induced homologous recombination in mice. Carcinogenesis. 2001 Apr;22(4):641-9.
13. Claybon A, Karia B, Bruce C, Bishop AJ. PARP1 suppresses homologous recombination events in mice in vivo. Nucleic Acids Res. 2010 Nov;38(21):7538-45. Epub 2010 Jul 21.

14. Bishop AJ, Hollander MC, Kosaras B, Sidman RL, Fornace AJ Jr, Schiestl RH. Atm-, p53-, and Gadd45a-deficient mice show an increased frequency of homologous recombination at different stages during development. Cancer Res. 2003 Sep 1;63(17):5335-43.

OPEN ACCESS Freely available online

PLoS one

14-3-3 σ Expression Effects G2/M Response to Oxygen and Correlates with Ovarian Cancer Metastasis

Dashnamoorthy Ravi[1,2], Yidong Chen[1,3], Bijal Karia[1,2], Adam Brown[1,2], Ting Ting Gu[1], Jie Li[4], Mark S. Carey[4,5], Bryan T. Hennessy[4,6], Alexander J. R. Bishop[1,2]*

1 Greehey Children's Cancer Research Institute, University of Texas Health Science Center, San Antonio, Texas, United States of America, **2** Department of Cellular and Structural Biology, University of Texas Health Science Center, San Antonio, Texas, United States of America, **3** Department of Epidemiology and Biostatistics, University of Texas Health Science Center, San Antonio, Texas, United States of America, **4** Department of Gynecologic Medical Oncology, University of Texas MD Anderson Cancer Center, Houston, Texas, United States of America, **5** Division of Gynecologic Oncology, Department of Obstetrics and Gynecology, University of British Columbia, Vancouver, Canada, **6** Department of Medical Oncology, Beaumont Hospital, Dublin, Ireland

Abstract

Background: *In vitro* cell culture experiments with primary cells have reported that cell proliferation is retarded in the presence of ambient compared to physiological O_2 levels. Cancer is primarily a disease of aberrant cell proliferation, therefore, studying cancer cells grown under ambient O_2 may be undesirable. To understand better the impact of O_2 on the propagation of cancer cells *in vitro*, we compared the growth potential of a panel of ovarian cancer cell lines under ambient (21%) or physiological (3%) O_2.

Principal Findings: Our observations demonstrate that similar to primary cells, many cancer cells maintain an inherent sensitivity to O_2, but some display insensitivity to changes in O_2 concentration. Further analysis revealed an association between defective G2/M cell cycle transition regulation and O_2 insensitivity resultant from overexpression of 14-3-3 σ. Targeting 14-3-3 σ overexpression with RNAi restored O_2 sensitivity in these cell lines. Additionally, we found that metastatic ovarian tumors frequently overexpress 14-3-3 σ, which in conjunction with phosphorylated RB, results in poor prognosis.

Conclusions: Cancer cells show differential proliferative sensitivity to changes in O_2 concentration. Although a direct link between O_2 insensitivity and metastasis was not determined, this investigation showed that an O_2 insensitive phenotype in cancer cells to correlate with metastatic tumor progression.

Citation: Ravi D, Chen Y, Karia B, Brown A, Gu TT, et al. (2011) 14-3-3 σ Expression Effects G2/M Response to Oxygen and Correlates with Ovarian Cancer Metastasis. PLoS ONE 6(1): e15864. doi:10.1371/journal.pone.0015864

Editor: Janine Santos, University of Medicine and Dentistry of New Jersey, United States of America

Received August 26, 2010; **Accepted** November 25, 2010; **Published** January 10, 2011

Funding: This work was supported by the NIEHS (K22-ES12264) and a Voelcker Fund Young Investigator Award from the Max and Minnie Tomerlin Voelcker Fund to A.J.R. Bishop. Kleberg Center for Molecular Markers at the M. D. Anderson Cancer Center, The M.D. Anderson Cancer Center Physician Scientist Program, the McNair Scholars Program supported by the Robert and Janice McNair Foundation and an American Society of Clinical Oncology (ASCO) cancer foundation Career Development Award (CDA), Cancer Foundation and by a Science Foundation Ireland (SFI)/Health Research Board (HRB (Ireland)) Translational Research Award (TRA), all to B.T. Hennessy. B. Karia is supported by DOD CDRMP Breast Cancer Research Program Predoctoral Traineeship Award (BC093931). A. Brown is supported by NIA T32 training grant (T32AG021890). Y. Chen is supported by NIH/NCI cancer center grant (P30 CA054174-17) and NIH/NCRR CTSA grant (1UL1RR025767). The funders had no role in study design, data collection and analysis, decision to publish, or preparation of the manuscript.

Competing Interests: The authors have declared that no competing interests exist.

* E-mail: bishopa@uthscsa.edu

Introduction

Cell lines derived from cancer patients provide an experimentally manipulable model system that facilitates investigations into cancer biology and its therapy. The unlimited proliferation potential of cancer cells is a major hallmark of malignancy, however the use of standard tissue culture protocols often restricts cell proliferation, as observed with primary cell lines [1,2,3,4]. Although the use of physiological conditions is known to impact *in vitro* proliferation of cancer cells [5,6,7] and primary cells are known to propagate better at physiological O_2, the impact of physiological O_2 on *in vitro* cancer cell proliferation is relatively unexplored. However, it has been reported that altered concentrations of O_2 results in clear differences in cell proliferation and response to drug treatment in the cancer cells [8,9,10].

Oxygen, in addition to nutrients and growth factors, is vital for proper cell growth and its availability has a direct impact on cellular metabolism, signaling pathways, proliferation, differentiation and survival [3,11,12,13]. Many *in vitro* investigations have demonstrated the advantages of physiological O_2 for tissue culture. For example, the biological behavior of primary cell cultures with a physiological concentration of O_2 (2.7–5.3%) is far superior compared to the standard practice of growing cells under atmospheric or "ambient" O_2 concentration (21% O_2) [4]. In fact, these two growth conditions are known to result in distinct metabolic and molecular characteristics [13].

The importance of considering O_2 tension in cancer biology is well established. For example, the fact that many cancers exist in a 'hypoxic' state has led to the development of hypoxia-targeted therapy [14,15]. In general the hypoxic concentration of O_2 is

<1% for most solid tumors, however the hypoxic concentration could vary based on the cell types and the normal perfusion status [16] and additionally, hypoxia tends to inhibit cell proliferation [17]. Physiological O_2 tension varies from 2.7–5.3% in the interstitial space [18], where many primary tumors reside, to 14.7% in the arterial circulation and lungs, where migrating and potentially metastatic cancer cells are often found. Therefore, cancer studies that are only conducted in ambient (21%) O_2 may miss pertinent biological observations. This may be particularly important when attempting to study the progression of cancer to metastatic disease, which is a significant event in cancer etiology and is associated with poor prognosis [19]. Considering the differences in O_2 tension in different compartments of the body, an understanding of the effect of O_2 concentration on cancer cell proliferation could provide useful insights into the mechanisms involved in the pathological progression of cancer.

Cancer cells that have acquired mutations in either oncogenes or tumor suppressor genes display a characteristic uncontrolled proliferation phenotype [20]. For example, tumor suppressors such as p53 or RB act as "molecular gatekeepers" known to affect cell cycle progression. Mutation of such factors facilitates unlimited proliferation in cancer cells [20]. Cell cycle progression involves a sequential series of events catalyzed by cyclins and cyclin-dependent kinases (CDKs) [21], and in normal cells is a tightly regulated process. The tumor suppressor p53 is a master regulator of G1/S and G2/M phase transition in the cell cycle [22] and is known to have an important role in responding to oxygen concentration, particularly hypoxia (<1% O_2) [23] or hyperoxia (95% O_2) [24]. Although examining the effect of extreme O_2 conditions is both important and revealing, it must be noted that these previous studies did not investigate the response of p53 at physiological (3%) O_2 and ambient (21%) O_2. p21 and 14-3-3 σ are transcriptional targets of p53 that are involved in regulating G1/S and G2/M transitions of the cell cycle by targeting CDK2 and CDC2 (also known as CDK1), respectively [22,25]. The CDKs, in turn, regulate RB protein function, to mediate cell cycle progression through G1/S and G2/M [26]. Therefore, disruption of RB function could also impact the control of cell cycle progression [26]. Considering that differences in O_2 concentration result in altered cell cycle progression in primary cells but cancer cells frequently display cell cycle control defects, there is clearly the potential that these defects may impact how cancer cells respond to altered O_2 levels in a manner that could have a profound influence on cancer progression.

Here we examined the biological behavior of ovarian cancer cells under physiological and ambient O_2. Interestingly, some of the ovarian cancer cell lines had a normal response to O_2 concentration, (*i.e.* reduced cell proliferation with increased O_2 concentration) while the proliferation of other ovarian cancer cell lines was unaffected by this O_2 increase. Further, our investigations revealed that 14-3-3 σ and its role in the cell cycle influence the proliferative response to altered O_2 levels. Considering the variation in partial pressure of oxygen throughout the body and the potential importance that this context may have on cancer progression, it is crucial to understand the affect of O_2 concentration on cancer cell proliferation and cancer progression. We provide evidence that acquisition of O_2 insensitivity may be a component in cancer progression and a hallmark of successful metastatic disease.

Results

Physiological oxygen results in increased cell proliferation in ovarian cancer cells

In our initial studies we compared the effect of physiological (3% O_2) and ambient (21% O_2) oxygen concentration using A2780 ovarian cancer cells and observed that 12 days of cell culture under these conditions resulted in a 2.6 fold growth suppression under 21% O_2 (Figure 1). Therefore, we examined the affect of O_2 concentration on the growth potential of six ovarian cancer cell lines using physiological (3% O_2) and ambient (21% O_2) oxygen concentrations. Since the serum present in cell culture medium can also have a dominant influence on growth, we also tested the affect of various concentrations of serum. Regardless of the amount of serum present in the growth medium, culturing in 21% O_2 generally resulted in a significant decrease in cell proliferation for four of the ovarian cancer cell lines (A2780, OVCAR5, OVCAR8 and HOC8) compared to 3% O_2 (Figure 2). The only exception observed was with HOC8 cells in the presence of the highest concentration of serum (10% v/v), where an insignificant O_2-dependent growth effect was observed (Figure 2). Presumably the lack of response in Hoc8 results from a dominant influence of serum, which was not observed with A2780, OVCAR5 and OVCAR8. In contrast, there was no significant effect on the growth of SKOV3 and HeyA8 cell lines by increasing the O_2 concentration to 21%, irrespective of serum concentrations (Figure 2). The observed exception was HeyA8 cultured under 2% serum, which showed decreased cell proliferation at 21% O_2 compared to 3% O_2 ($p<0.001$). In contrast to the effect of O_2 levels, increasing the concentration of serum resulted in a proportional growth increase in the ovarian cancer cell lines A2780, OVCAR5 and OVCAR8 ($p<10^{-5}$, Figure 2). The concentration of serum had a moderate influence on growth in SKOV3 and HeyA8 (Figure 2); a serum concentration between 2 and 6% had a significant effect ($p<10^{-5}$) in SKOV3, while HeyA8 serum concentration between 2 and 10% serum had the greatest effect at 3% O_2 ($p<10^{-5}$) (Figure 2). Increasing serum concentration from 6% to 10% had little effect on growth of HeyA8, SKOV3 and HOC8 (Figure 2). Together, it appears that both oxygen levels and serum concentration affect the growth of these ovarian cancer cell lines, but in an independent fashion. As expected from work by others with primary cells [4], we observed that the majority of the ovarian cancer cells displayed decreased cell proliferation at ambient O_2 concentration compared to physiological O_2 concentration. However, two cell lines did not appear to have inhibited cell proliferation at the higher (ambient) O_2 levels. We therefore categorized the ovarian cancer cell lines based on these differences, being either O_2 sensitive (A2780, OVCAR5, OVCAR8 and HOC8) or insensitive (SKOV3 and HeyA8) (Figure 2). Overall, these differences suggest heterogeneity in growth regulation responses to physiological cues of O_2 levels in these cultured cell lines.

It is possible that the apparent O_2 insensitivity and differences in proliferation resulted from differences in the doubling time of each cell line. For example, if SKOV3 and HeyA8 (the O_2 insensitive cell lines) proliferate more slowly, O_2 dependent proliferation changes may be too trivial to measure. Therefore, we measured the cell doubling time for all ovarian cancer cell lines. Our results showed that under standard tissue culture conditions (10% serum and 21% O_2) the doubling time for all ovarian cancer cell lines were somewhat similar (<24 hours) except for HOC8, which had an extended doubling time of about 45.5 ± 4.9 hours (Table S1, and see Methods S1). Therefore, most of the ovarian cancer cell lines were dividing at an approximately equal rate, and gross difference in doubling time is unlikely to be a factor in the observed proliferation differences between cell lines under different conditions.

Oxygen sensitivity correlates with dynamic changes in the S and G2 phases of the cell cycle

Considering the differences in proliferation observed for ovarian cancer cell lines grown under either 3% or 21% O_2, we examined

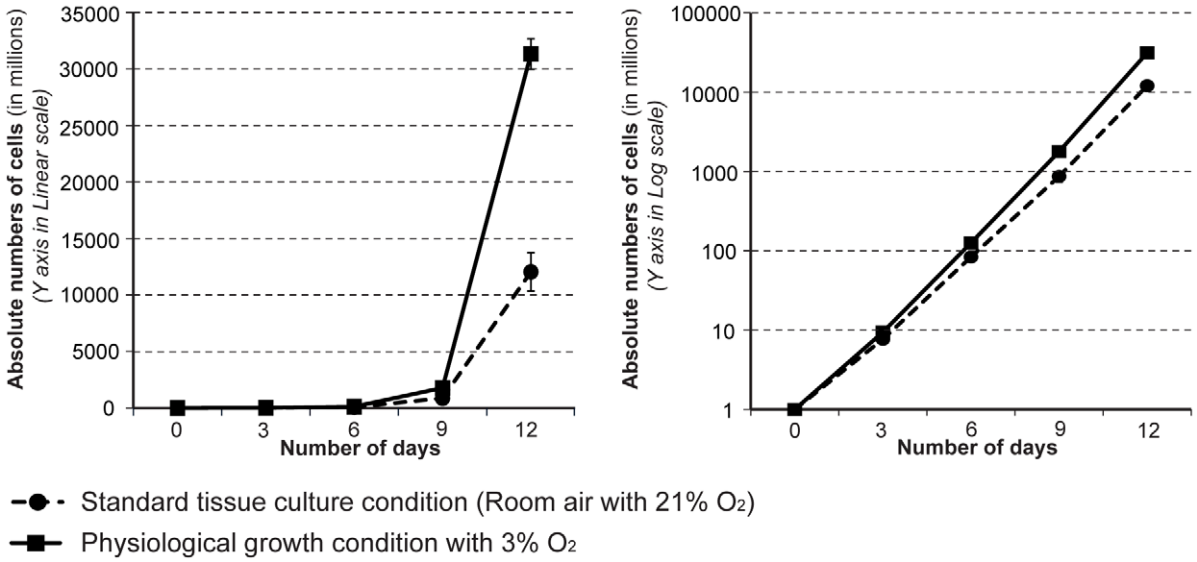

Figure 1. Cancer cell proliferation is markedly suppressed by the standard cell culture conditions used for *in vitro* experiments. Equal numbers of A2780 ovarian cancer cells were seeded in a 10 cm petri dish and were routinely maintained under 3% O_2 (physiological) or 21% O_2 (ambient). The increase in cell numbers was determined by counting manually once in three days, and the total cell numbers were estimated and plotted using linear scale (in Graph A) and log scale (in Graph B).
doi:10.1371/journal.pone.0015864.g001

whether O_2 concentration alters the cell cycle profile of each cell line. Irrespective of serum concentration, comparing 3% O_2 to 21% O_2 resulted in a significant decrease in the percentage of cells that were in the G1 phase of the cell cycle and a significant increase in the percentage of cells in S phase (Table 1), which was expected based on previous observations made with primary cells [27]. Furthermore, in three of the O_2 sensitive cell lines (A2780, OVCAR5 and OVCAR8) the percentage of the cell population in the G2 phase was increased significantly in 21% O_2. However a significant increase in G2 was not observed in the fourth O_2

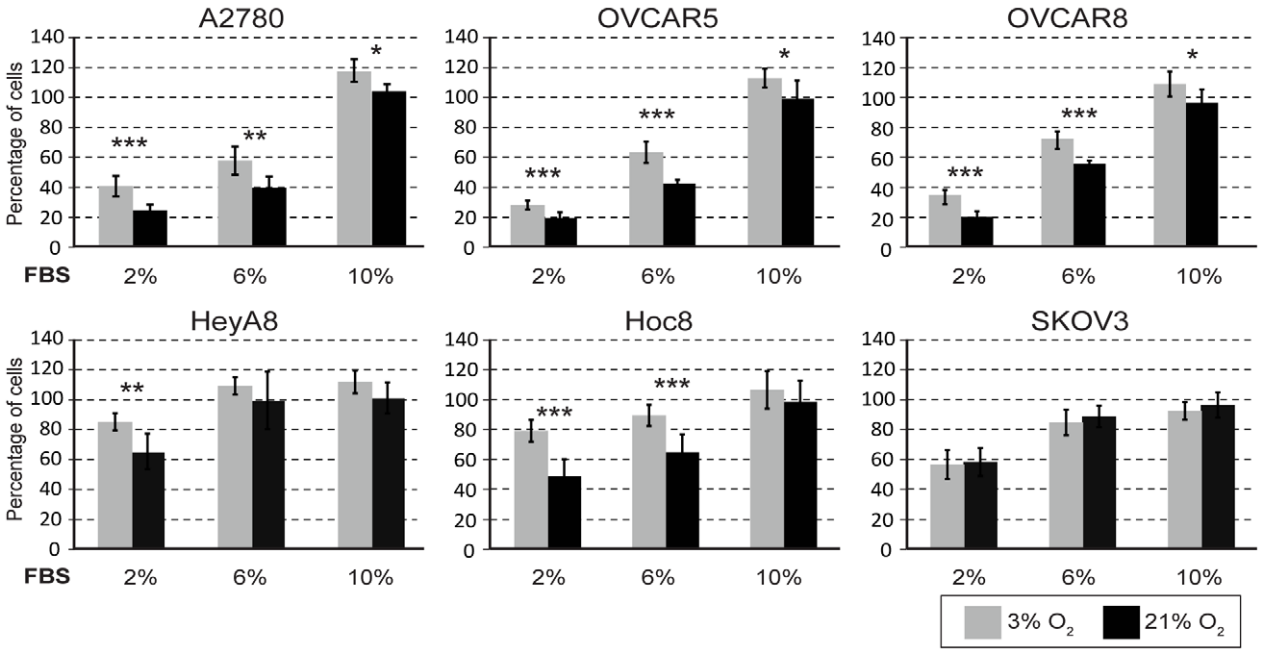

Figure 2. Ovarian cancer cells grown under physiological and ambient O_2 show differential proliferation response. Ovarian cancer cell lines were cultured under 3% or 21% O_2 and the extent of proliferation was determined following 3 days of growth (see Materials and Methods section). For each cell line, the percent of cell proliferation at 3% O_2 (light shaded bars) and at different concentrations of serum was compared with proliferation under standard tissue culture conditions consisting of 21% (ambient) O_2 (dark shaded bars) and 10% FBS. The error bars represent the standard deviations of mean and statistical significant (by student T Test) differences in proliferation between 3% and 21% O_2 for each concentration of serum is indicated by an asterisk [(*) $p<0.05$, (**) $p<0.001$ and (***) $p<0.0001$].
doi:10.1371/journal.pone.0015864.g002

sensitive cell line, HOC8 (Table 1). Similar to HOC8, the O_2 insensitive cell lines, SKOV3 and HeyA8, did not display a significant alteration in the proportion of cells in the G2 phase of the cell cycle when grown under 3% O_2 or 21% O_2 (Table 1). Considering that the O_2 sensitive cell lines proliferated more slowly at 21% O_2 compared to 3% O_2 despite having smaller proportions of their cell population in G1 and a increased proportions in S and G2, we conclude that these cells must be progressing more slowly through the cell cycle. However, for the O_2 insensitive cell lines and HOC8 (with the significantly extended doubling time), we did not observe a significant increase in the percentage of cells in G2 when the O_2 levels were increased. These results suggest that although the G1 and S phases of the cell cycle are responding similarly to changes in O_2 concentration in both O_2 sensitive and insensitive cell lines, it is the G2 phase of the cell cycle that is not responsive to O_2 concentration in the O_2 insensitive cell lines. Therefore, the difference in cell cycle response observed with these ovarian cancer cell lines might be at the level of regulation during the cell cycle progression from G2 to M phase. It is also possible that the changes observed with G2 and O_2 sensitivity in these cancer cell lines is reflected in the mitotic component of the cell cycle. Our observation of the mitotic cells present in the O_2 sensitive and insensitive cell lines grown under 3% and 21% O_2 supports this conclusion; the O_2 sensitive cell lines show a proportionate decrease in the mitotic cell population observed at 21% O_2 compared to 3% O_2, (Figure 3), corresponding to an accumulation of cells at G2 at 21% O_2 (Table 1). Similarly, in the O_2 insensitive cell lines (HeyA8 and SKOV3) the proportion of mitotic cells remained unaltered regardless of O_2 concentrations (Figure 3). This is expected because, as noted previously (Table 1), the proportion of cells at G2 in the O_2 insensitive cell lines were also unaffected by O_2 concentration. We conclude that most cancer cells retain an ability to regulate cell cycle in response to changes in O_2 concentration comparable to wild type cells [27]. However, some cancer cells may lose O_2 concentration dependent control of cell cycle (as in the O_2 insensitive cancer cell lines), resulting in a distinct phenotype.

Oxygen insensitivity correlates with altered G2/M components

Thus far we have demonstrated that O_2 sensitive cell cycle response at the G2/M transition is lacking in the O_2 insensitive cell lines. We therefore went on to characterize this observation further by determining what component of G2/M regulation is deficient in the O_2-insensitive cancer cells. The major effector of G2/M transition is CDC2 [22,28]. CDC2 forms a complex with cyclin B [29,30], which phosphorylates various structural proteins resulting in the collapse of the nuclear envelope, condensation and segregation of chromosomes [30,31] and inactivation of other cell cycle regulatory proteins such as WEE1, RB and CDC25C [30,32]. In normal cells, the overall levels of CDC2 protein are kept constant throughout the cell cycle [33] and are regulated by post-translational modification [33] and cellular localization [30,31]. Once the Tyr15 residue on CDC2 is dephosphorylated by CDC25C, activated CDC2 forms a complex with cyclin B, accumulates in the nucleus, and promotes the G2/M transition[30,33,34]. This occurs in a stepwise fashion through increasing amounts of nuclear CDC2 protein [30]. Our examination of total CDC2 protein and phosphorylated CDC2 protein revealed that both are considerably lower in the O_2-insensitive cell lines (HeyA8 and SKOV3) compared to the O_2-sensitive cell lines (Figure 4A). Although the levels of CDC2 were relatively high in the O_2-sensitive cell lines (A2780, OVCAR5 and OVCAR8) (Figure 2), we observed a decrease in Tyr15 phosphorylation status regardless of O_2

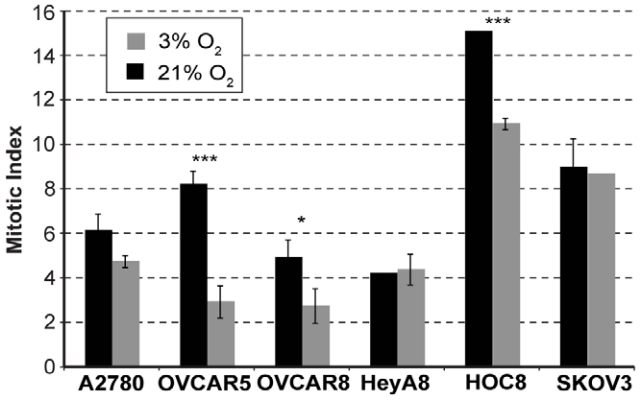

Figure 3. Mitotic index in the ovarian cancer cell lines grown under 3% or 21% O_2. Mitotic index in the ovarian cancer cell lines that were cultured under 3% or 21% O_2 for 3 days were determined by counting nuclei with condensed chromosomes, among the minimum of 1000 cells present in each experiment. Statistical significance was determined by ANOVA and the significant difference in the mitotic index between 3% and 21% O_2 is denoted by an asterisk [(*) $p<0.05$, (***) $p<0.0001$].
doi:10.1371/journal.pone.0015864.g003

concentration for A2780, OVCAR5 and OVCAR8 with increasing serum levels (Figure 4A). This correlates with the observation that increasing serum concentration causes increased cellular proliferation and results in a concomitant reduction in the proportion of cells in G2/M (compare with Table 1). However, no overt O_2-dependent alteration in either total or phosphorylated cyclin B or CDC25C was observed in the O_2 sensitive cell lines (A2780, OVCAR5, OVCAR8 and HOC8) compared to O_2 insensitive cell lines (HeyA8 and SKOV3) (Figure 4A). Therefore, it appears that the observed decrease in the cell population in G2 in 21% O_2 might not be dependent on phosphorylation-mediated inactivation of CDC2. It should be noted that these experiments were performed in asynchronously growing cells, and therefore it is possible that transient differences in CDC2 status were missed. Interestingly, the levels of CDC2, Cyclin B and CDC25c (the negative regulator of CDC2) were considerably lower in O_2 insensitive cell lines (HeyA8 and SKOV3) compared to O_2 sensitive cell lines (A2780, OVCAR5, OVCAR8 and HOC8) (Figure 4A). These observations suggest an inherent deficiency in the core components involved in the G2/M progression in the O_2 insensitive cell lines.

p53, p21 and 14-3-3 σ are factors which have the ability negatively to influence CDC2 activity and G2/M transition [22]. Current understanding is that p53 and p21 influence cell cycle in hypoxic and hyperoxic conditions [23,24,35,36]. Considering the reduced levels of CDC2 and the apparently defective G2/M checkpoint in the O_2 insensitive cell lines (HeyA8 and SKOV3), we explored the possibility that impairment was due to a defect in any of these molecular regulators. Western blot analysis found p53 and p21 to be overexpressed in one O_2-insensitive cell line (HeyA8). However, both were absent in the other O_2-insensitive cell line (SKOV3), and the expression pattern for these proteins remained unaltered regardless of changes in O_2 or serum concentration (Figure S1), suggesting that neither p53 nor p21 is relevant to CDC2's function in O_2 sensitivity. Interestingly, we observed a considerable elevation in the expression of 14-3-3 σ (Figure 4A) in the O_2 insensitive cell lines (HeyA8 and SKOV3) compared to the O_2-sensitive cell lines. Although, the level of 14-3-3 σ expression was considerably lower in all O_2-sensitive cell lines compared to HeyA8 and SKOV3, we did observe an increase in the expression of 14-3-3 σ at 21% O_2 with A2780 (Figure 4A). Although

Table 1. FACS profile for cell cycle analysis with ovarian cancer cells that were grown under cell culture conditions consisting of increasing serum and O_2 concentration.

Cells	Serum	G1			S			G2		
		3% O_2	21% O_2	*p*-value	3% O_2	21% O_2	*p*-value	3% O_2	21% O_2	*p*-value
	2%	66.8±0.9	62.5±0.2	0.0011	25.6±1	27.5±0.1	0.02800	7.6±0.4	9.96±0.1	0.0007
A2780	6%	76.9±2.1	64.3±0.7	0.0006	17.5±0.9	29±0.1	<0.0001	5.6±1.4	6.7±0.6	**NS**
	10%	84.1±3.2	69.5±1.4	0.0028	14.3±1.9	26.5±1.3	0.0080	1.5±1.3	4±0.7	0.0411
	2%	66.4±0.7	60.2±0.4	0.0001	25.8±0.2	29.3±0.6	0.0006	7.7±0.5	10.4±0.3	0.0017
OVCAR5	6%	79±1.5	70.2±0.5	0.0014	17.4±1.5	25.1±0.9	0.0015	3.4±0.4	4.7±0.6	**NS**
	10%	90.6±1.2	84±1.6	0.0077	8.2±1.4	14.6±1.5	0.0052	1.1±0.1	1.2±2.1	**NS**
	2%	74.7±10.7	69±1	**NS**	15.5±2.5	23.7±0.6	0.0052	13.7±2.3	6±0	0.0043
OVCAR8	6%	66±1	59±1	0.0010	25.7±1.5	30±0	0.0079	7±0	9.7±0.6	0.0013
	10%	69±4.6	61.7±1.5	0.0582	24.3±1.5	30.7±1.2	0.0045	5.3±3.8	6.3±0.6	**NS**
	2%	69.3±1.5	58.7±2.1	0.0020	25±1	34±1	0.0003	4.3±1.5	5.7±1.5	**NS**
HeyA8	6%	62.7±0.6	53.7±1.5	0.0006	30.3±1.2	37.3±2.5	0.0118	5.3±0.6	8±3.5	**NS**
	10%	61.7±1.2	50.3±2.3	0.0016	30.7±1.2	37.3±1.2	0.0021	6.7±2.3	11±1.6	**NS**
	2%	80±1.7	72.3±1.5	0.0045	15±0	18.7±1.5	0.0141	5±1.7	8±1	**NS**
HOC8	6%	80.3±1.2	72.7±1.2	0.0012	15.3±1.5	22.7±1.5	0.0041	3.3±1.5	3.7±1.5	**NS**
	10%	78.7±2.5	73.3±0.6	0.0232	16.3±0.6	23.7±0.6	<0.0001	4.3±2.5	3±1	**NS**
	2%	74±2	62.1±1.7	0.0014	13.5±3.5	27.7±1.2	0.0026	12±2	10.3±2.5	**NS**
SKOV3	6%	76.7±1.5	65.3±3.2	0.0052	14±1	25.7±1.5	0.0003	9.3±1.5	9±2	**NS**
	10%	80.3±1.2	68±1.7	0.0005	12.7±1.5	26±1	0.0002	7±1	6.3±0.6	**NS**

NS "Not Significant"

doi:10.1371/journal.pone.0015864.t001

contradictory to the known inhibitory role of 14-3-3 σ on CDC2 activity, we concluded that high levels of 14-3-3 σ combined with reduced levels of CDC2 in a proliferating cancer cell may indicate a lack of control of G2/M progression in response to O_2 levels.

To clarify the consequence of the low levels of CDC2 protein observed in the O_2-insensitive cell lines, we determined the functional activity of the remaining CDC2 by examining the phosphorylation of two of its substrates, RB and WEE1. Phosphorylation of RB at the Ser 807 residue is mediated by CDC2 [32], and we observed this phosphorylation regardless of CDC2 levels or O_2 levels with 10% serum for all cell lines except HOC8 (Figure 4B), indicating unimpaired CDC2 activity in these cell lines. A reduction in phosphorylated RB correlated with reduction of serum concentration (Figure 4B) and correlated with increased accumulation of total RB in the O_2-sensitive cell lines (A2780, OVCAR5 and OVCAR8), but not in HOC8 (Figure 4B). Total RB was barely detectable in the O_2-insensitive cell lines (HeyA8 and SKOV3) (Figure 4B), with the exception of 2% serum at 3% O_2 condition in the HeyA8 cell line. Interestingly, a comparison between the RB expression pattern (Figure 4B) and cell proliferation (Figure 2) revealed that HOC8, HeyA8 and SKOV3 cells grow better in cell culture medium with a low concentration of serum (2%) compared to A2780, OVCAR5 and OVCAR8. It therefore appears that the total RB protein level response remains intact in O_2-sensitive cell lines and that this response is probably more relevant to serum concentrations than O_2 levels. The other target for CDC2-mediated inactivation by phosphorylation is WEE1, which can also reciprocally inhibit CDC2 function by phosphorylation [37]. We observed increased phosphorylation of WEE1 in the O_2 sensitive cell lines (A2780, OVCAR5 and OVCAR8), barely detectable levels in HOC8, (Figure 4B) and a complete absence in the O_2-insensitive cell lines (HeyA8 and SKOV3, Figure 4B). This pattern was largely recapitulated for total WEE1 protein levels (Figure 4B). Therefore, the absence of phospho-WEE1 in the O_2-insensitive cell lines does not indicate an absence of CDC2 activity, but rather an absence of the WEE1 substrate. From these results we concluded that despite the reduced amounts of CDC2 in the O_2-insensitive cell lines, CDC2 is functionally active and uninhibited by the increased levels of 14-3-3 σ. It should be noted that RB and CDC2 act upon each other to regulate each others function [38], and phosphorylation status of RB [26] or CDC2 [39] could influence E2F mediated expression of cyclins that are essential for cell cycle progression. Therefore, considering this complex relationship between RB and CDC2, the phosphorylation pattern of RB is insufficient to predict G2/M progression.

In summary, the O_2-sensitive cell lines (A2780, OVCAR5 and HOC8) showed increased expression of CDC2 and cyclin B combined with low level of 14-3-3 σ expression. This suggests that the cell cycle components required for a dynamic proliferative response to differences in the O_2 concentration is present in these cell lines. However in the O_2-insensitive cell lines that express high levels of 14-3-3 σ and low levels of CDC2 and CDC25C such a dynamic cell cycle response to changes in O_2 concentration could be impaired. We therefore pursued the possibility that this inverse correlation between 14-3-3 σ and CDC2 might be important for the O_2-sensitive regulation of G2/M transition.

14-3-3 σ and mitotic progression in oxygen sensitivity

Our previous observations suggest an association between elevated level of 14-3-3 σ and O_2-insensitivity that needs to be confirmed. Therefore, we wanted to confirm that 14-3-3 σ does indeed affect O_2-dependent proliferation. For this part of the study, we restricted our analysis to two cell lines with wild type p53: the O_2-sensitive A2780 [40], and O_2-insensitive HeyA8 cell lines [41].

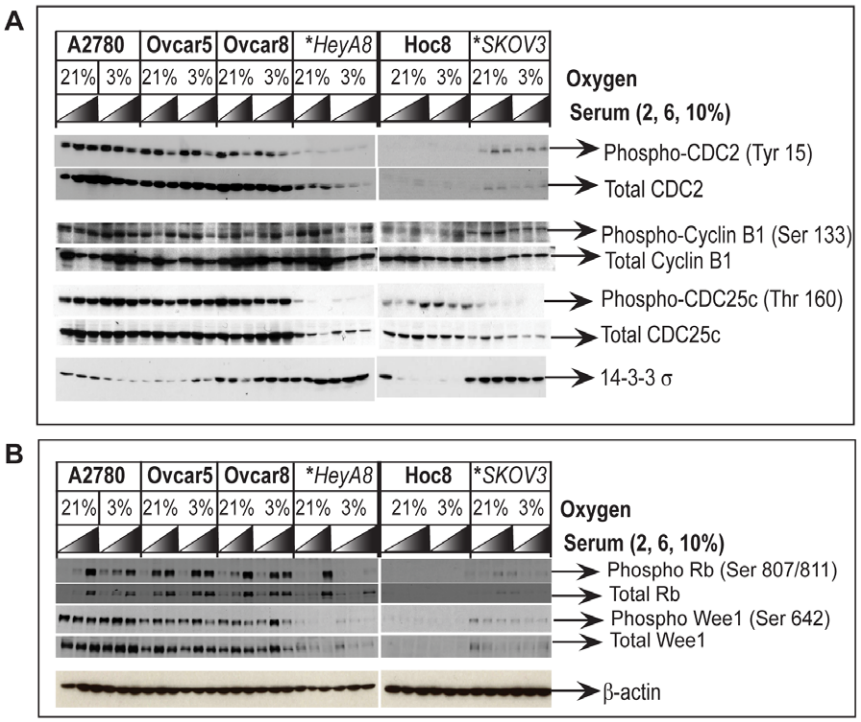

Figure 4. Western blot analysis of G2 cell cycle regulatory proteins and the relevance to O_2 sensitivity in the ovarian cancer cell lines. Protein lysates prepared from the ovarian cancer cell lines maintained in growth medium consisting of increasing concentrations of serum and 21% or 3% O_2 were analyzed by Western blot. (A) Compared to O_2 sensitive cell lines, decreased expression of the core components involved in G2/M cell cycle progression CDC2/cyclin B1 complex and its activator CDC25c is observed in the O_2 insensitive cell lines (indicated by asterisk and italics), while the expression of 14-3-3 σ, a protein that inhibits CDC2 is elevated in the O_2 insensitive cell lines. (B) Phosphorylation of RB and Wee1 were monitored as an indicator for CDC2 function because both RB and Wee1 are known targets for phosphorylation by CDC2. Equal loading of protein extracts were monitored by probing the stripped Western blots with the primary antibody for β-actin.
doi:10.1371/journal.pone.0015864.g004

So far we have used Western blot analysis to monitor the overall expression levels of 14-3-3 σ and CDC2 (Figure 4A). However, since the functional responses of these proteins are dependent on their cellular localization, we used immunofluorescence to determine their cellular location under 3% O_2 and 21% O_2. In the O_2-sensitive A2780 cell line, the localization of 14-3-3 σ was restricted to the cytoplasm under 3% O_2 (Figure 5A), but was found in both the nucleus and cytoplasm at 21% O_2 (Figure 5A). CDC2 was distributed throughout the cell and its localization was unaffected by O_2 concentration. It therefore appears that nuclear exclusion of 14-3-3 σ correlates with a decreased fraction of cells in the G2/M phase and an uninhibited cell cycle progression when A2780 is grown at 3% O_2, as noted before (Table 1). In contrast, the O_2-insensitive HeyA8 cell line showed high levels of 14-3-3 σ and low levels of CDC2 (Figure 4A), with a considerable amount of 14-3-3 σ in the cytoplasm (Figure 5A). Further, 14-3-3 σ remained excluded from the nucleus even at 21% O_2 in the HeyA8 cells (Figure 5A). These observations were further verified by Western blot analysis of nuclear and cytosolic cell fractions obtained from these cells (Figure 5B). Finally, to confirm the effect on G2/M transition, we determined the proportion of those cells in M phase for different O_2 concentrations using the mitosis specific marker phospho-histone H3. In the O_2-sensitive A2780 cells, under 21% O_2, we observed a decrease in the mitotic index ($P<0.001$), compared to 3% O_2 (Figure 5C). No such O_2-dependent change in mitotic index was observed for the O_2-insensitive HeyA8 cells (Figure 5C). These results support our initial conclusion, that the O_2-insensitive cells lines have a deficiency in regulating cell cycle progression at G2/M in response to increased O_2 levels (Figure 2).

The levels and cellular localization of 14-3-3 σ correlate with O_2-sensitive proliferation. To demonstrate a direct relationship, we examined whether over-expression of 14-3-3 σ could render O_2-sensitive A2780 cells insensitive to O_2 and conversely whether reducing the levels of 14-3-3 σ in O_2-insensitive HeyA8 cells could restore O_2-sensitivity. Transient over-expression of 14-3-3 σ in A2780 cells reduced cell proliferation (Figure 5D) and resulted in loss of O_2-sensitivity. Therefore, merely increasing 14-3-3 σ expression results in its inability to regulate G2/M in the absence of any further genetic alterations. Conversely, RNAi-mediated silencing of 14-3-3 σ expression in HeyA8 cells (Figure 5E - Western blot) resulted in a substantial increase in proliferation under 3% O_2 (Figure 5E - Bar graph). Interestingly, when the cells from the same siRNA transfection were placed at 21% oxygen, 14-3-3 σ protein expression was induced, reducing the knockdown effect of the siRNA. This observation also suggests an O_2-dependent transcriptional response by 14-3-3 σ. Despite this transcriptional response, we still observed a muted growth phenotype at 21% O_2 under these conditions. Together these experiments demonstrate that 14-3-3 σ is a critical factor for controlling ovarian cancer cell proliferation in response to O_2 concentration.

14-3-3 σ is frequently highly expressed in ovarian cancer and its ineffectiveness in controlling CDC2 is relevant to ovarian tumor pathology

Considering that increased expression of 14-3-3 σ provides some indication of impaired G2/M control, it is possible that cancer cell lines that express high levels of 14-3-3 σ are O_2-insensitive. The O_2-insensitive ovarian cancer cell lines we have

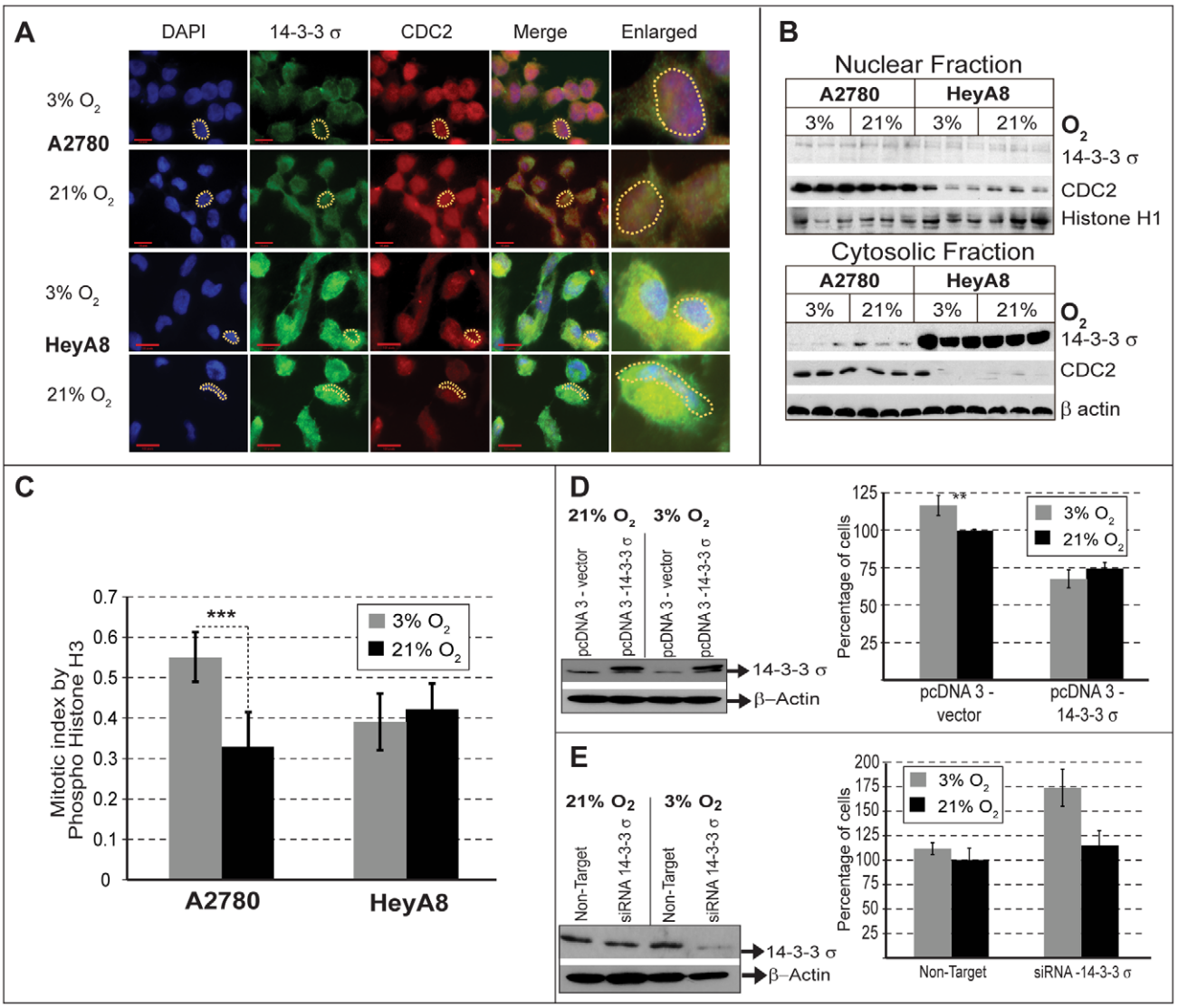

Figure 5. 14-3-3 σand O_2 sensitivity. (A) Cellular localization by immunofluoresence shows that 14-3-3 σ (Green) is located in the cytoplasm and CDC2 (Red) is present in the nucleus (Blue). Compared to O_2 sensitive A2780 cells, the level of 14-3-3 σ is higher and CDC2 is low in the O_2 insensitive HeyA8 cells. In the O_2 sensitive A2780, 14-3-3 σ is localized both in the nucleus and cytoplasm at 21% O_2. (A dotted yellow line, outlines a representative nuclei to indicate relative localization of 14-3-3 σ and CDC2 in these cells). (B) Western blot analysis of nuclear and cytoplasmic fractions show low levels of 14-3-3 σ in the nucleus compared to cytoplasm, with increased amounts of 14-3-3 σ being present in the cytoplasm of the O_2 insensitive HeyA8 cells. The level of CDC2 is higher both in the nucleus and cytoplasm of the O_2 sensitive A2780, but present in lower amount only in the nucleus of O_2 insensitive HeyA8 cells. Histone H1 and β−actin were used as loading controls for nuclear and cytoplasmic fractions, respectively. (C) Mitotic cells were determined by counting the cells that stained positively for a mitosis specific marker, Phospho-Histone H3 from the total cell population. Mitotic fractions present at 3% or 21% O_2 were counted in both A2780 and HeyA8 and represented as bar graph. A significant increase in mitotic index ($p>0.001$, indicated by asterisk) was observed in the O_2 sensitive A2780 at 3% O_2, but not in the O_2 insensitive HeyA8 cells. (D) Over-expression of 14-3-3 σ in the O_2 sensitive A2780 (Western Blot) results in loss of O_2 sensitivity (Bar graph). For the cells transfected with empty vector (mock transfection) or 14-3-3 σ over-expression construct, the percent of cell proliferation was compared with proliferation of mock transfected cells grown under standard tissue culture conditions consisting of 21% O_2 (ambient), and (E) in the converse experiment performed with O_2 insensitive HeyA8, reducing the levels of 14-3-3 σ by siRNA (Western blot) results in restoration of O_2 sensitivity (Bar graph). For the cells transfected with scrambled siRNA (mock transfection) or siRNA against 14-3-3 σ, the percent of cell proliferation was compared with proliferation of mock transfected cells grown under standard tissue culture conditions consisting of 21% O_2.
doi:10.1371/journal.pone.0015864.g005

thus far characterized have high 14-3-3 σ (Figure 5A) and low CDC2 protein levels. It is conceivable that the same phenotypic defect might result from cells with unchecked CDC2 activity, irrespective of 14-3-3 σ levels. To determine the frequency of commonly available cancer cell lines that have the hallmarks of O_2-insensitivity, we used a reverse phase protein array (RPPA) and screened 57 different ovarian cancer cell lines for the levels of 14-3-3 σ and CDC2, as well as phospho-RB as an indicator of CDC2 activity. Cell lines with the same name but from different labs or different passages were considered to be different. We therefore set the analysis criteria on the RPPA array to detect high phospho-RB (P-RB) and either high 14-3-3 σ or high CDC2. In the context of high levels of P-RB, this criteria should indicate that either 14-3-3 σis dysfunctional or that active CDC2 is uninhibited,

perhaps due to methylated 14-3-3 σ or inhibition of CDC2 degradation [42] We observed that of the 57 ovarian cancer cell lines represented in the RPPA, 28 cell lines (49%) showed high levels of 14-3-3 σ (Figure 6A) of which 16 cell lines (28%) also had increased P-RB, corresponding to the O_2 insensitivity pattern we have described. Amongst these 16 cell lines, 6 also have increased levels of CDC2 while the remainder had decreased levels of CDC2. This suggests that this protein profile is not exclusive to the cell lines we originally identified and might be representative of a relatively common phenomenon. We therefore determined whether this O_2-insensitive associated 14-3-3 σ/CDC2/P-RB protein profile is also observed in ovarian tumor samples. Using the same criteria as with the cell line RPPA, we examined 205 ovarian tumor specimens using RPPA. This analysis revealed that 27% of ovarian tumors (56) had elevated levels of both 14-3-3 σ and P-RB, and amongst these, 34 also had elevated levels of CDC2 expression (Figure 6B). These results are very comparable with the RPPA analysis of the ovarian cancer cell lines (Figure 6A).

Ovarian cancer has a poor survival rate and this is often associated with metastatic progression [43]. The O_2-insensitive associated 14-3-3 σ/CDC2/P-RB protein profile suggests an unrestricted G2/M control in response to changes in O_2 levels, such as a migrating or metastatic cancer would encounter. Therefore, it is possible that this protein profile is associated with poor prognosis. Using the O_2-insensitive associated protein profile (high P-RB with either high 14-3-3 σ or high CDC2) we identified 47 of 158 tumors with associated clinical data. A Kaplan-Meier survival estimate shows that patients with the O_2-insensitive associated protein profile have a poor survival outcome (less than 90 months compared to 200 months observed otherwise, $p = 0.016$, Figure 6C). Altogether it appears that the O_2-insensitive associated protein profile suggests that unrestricted G2/M accompanies a substantial proportion of ovarian cancer cells and primary tumor samples. Further, this O_2-insensitive profile is associated with poor prognosis for this disease.

Elevated 14-3-3 σ expression in metastatic ovarian tumors

Having observed that the O_2-insensitive associated protein profile (high P-RB with either high 14-3-3 σ or high CDC2) is both relatively common in ovarian cancer and associated with poor prognosis, we went on to determine directly whether metastatic ovarian tumors exhibit an overt 14-3-3 σ signature. Of note, the ovarian tumors represented in the ovarian tumor RPPA are from primary sites and thus do not necessarily provide an accurate representation of the protein profile in the metastatic cancer. We therefore expect that metastatic tumors or primary tumors that give rise to metastatic tumors will exhibit a more overt 14-3-3 σ signature than primary tumors. In fact, an increased expression of 14-3-3 σ has been previously reported with other tumors [44] and a functional involvement for 14-3-3 σ in metastatic disease is known [45,46]. We analyzed 14-3-3 σ expression using immunohistochemistry on paraffin embedded tissues obtained from 10 different metastatic ovarian tumors and their corresponding primary site tumors. We consistently observed intense immunostaining of 14-3-3 σ in 8/10 metastatic tumors and the corresponding primary tumors (Figure 7*j–l*). In contrast, the primary tumors without metastasis at diagnosis showed moderate immunostaining for 14-3-3 σ, and occasionally intense staining was also noted (Figure 7*i*). Borderline tumors showed a mild to moderate staining pattern for 14-3-3 σ, while in normal tissues, protein levels were absent or diffusely present (Figure 7 *a–c*). Increased expression of 14-3-3 σ in the metastatic primary tumors compared to normal tissue or malignant tumors without metastasis were observed to be statistically significant by the Fisher's exact test (Figure 7, Bar Graph). The high level of 14-3-3 σ expression offers the first indication of the manner in which regulation of G2/M may be dysfunctional in these tumors.

Over-expression of 14-3-3 σ in metastatic disease is not unexpected and has been previously noted [45,46,47]. However, we speculate the reason for this association is due to a loss of O_2-sensitivity and that this provides a selective advantage for metastatic progression. Our conclusion is that O_2-sensitive and insensitive patterns of 14-3-3 σ and CDC2 expression are readily detectable and common to cancer cells, regardless of whether they are grown *in vivo* or *in vitro*. Further, these expression patterns may have prognostic implications, but additional experiments will be required to confirm the mechanistic relevance of O_2-sensitivity in the clinical progression of cancer.

Discussion

There is an increasing interest to study cell biology under the context of physiological O_2 levels. Investigations with primary mouse embryonic fibroblasts comparing the effects of physiological (3%) and ambient (21%) oxygen, show that 21% O_2 causes increased oxidative stress and induces senescence [4]. Several studies conducted with embryonic stem (ES) cells reported that characteristic stem cell properties are preserved only when ES cells are maintained under physiological O_2- ES cells otherwise differentiate under ambient O_2 as reviewed in [2]. This prompted us to investigate the effects of physiological (3%) and ambient (21%) oxygen in the context of cancer. With A2780 ovarian cancer cells grown under 21% or 3% O_2, a 20% growth suppression was observed with 21% O_2 by three days (Figure 2) and although the proportional changes to cell cycle profile appear small, they were significant (Table 1). The accumulated effect of these differences in proliferation and cell cycle resulted in a 2.6 fold difference to the growth of the cancer cells by 12 days in the presence of different O_2 concentrations (Figure 1). This observation demonstrates that standard tissue culture conditions may adversely impact the *in vitro* proliferation of cancer, which is primarily a disease of proliferation. Previous studies compared the growth of primary mouse embryonic fibroblast cells [4], adult human fibroblasts [48] and human cancer cells [8] grown under physiological (3–5%) or ambient (21%) O_2 and observed increased cell proliferation under physiological O_2. In this study, we observed similar effects with ovarian cancer cells (A2780, OVCAR5, OVCAR8 and HOC8 - Figure 2), however other cells lines failed to respond to O_2 concentration (HeyA8 and SKOV3) (Figure 2). These proliferative responses to O_2 seem to affect all phases of the cell cycle, particularly the G1 and S phases of cell cycle, in all cell lines. However, only the G2 phase was affected in cell lines which displayed proliferative response to 3% O_2 (Table 1), suggesting the possibility that the G2 phase transition of the cell cycle is crucial for regulating proliferation in response to differences in 3% O_2 levels. A change in the G2 phase in response to O_2 levels was reported in only one other study performed with Fanconi anemia (FA) cell lines [49]. Analogous to our study, the experiments with FA cells demonstrated a characteristic G2 delay with standard tissue culture conditions (20% O_2), but a reduced proportion of cells in G2 and increased proliferation when cultured at 5% O_2 [49]. Furthermore, growth of different human fibroblast cells under physiological O_2 has also been observed to be accompanied by a reduction in the G2 cell population [27,48]. Overall, it appears that the G2 phase is the most O_2-sensitive phase of the cell cycle. Exploring the possible molecular mechanisms that render ovarian cancer cells either sensitive or insensitive to oxygen has

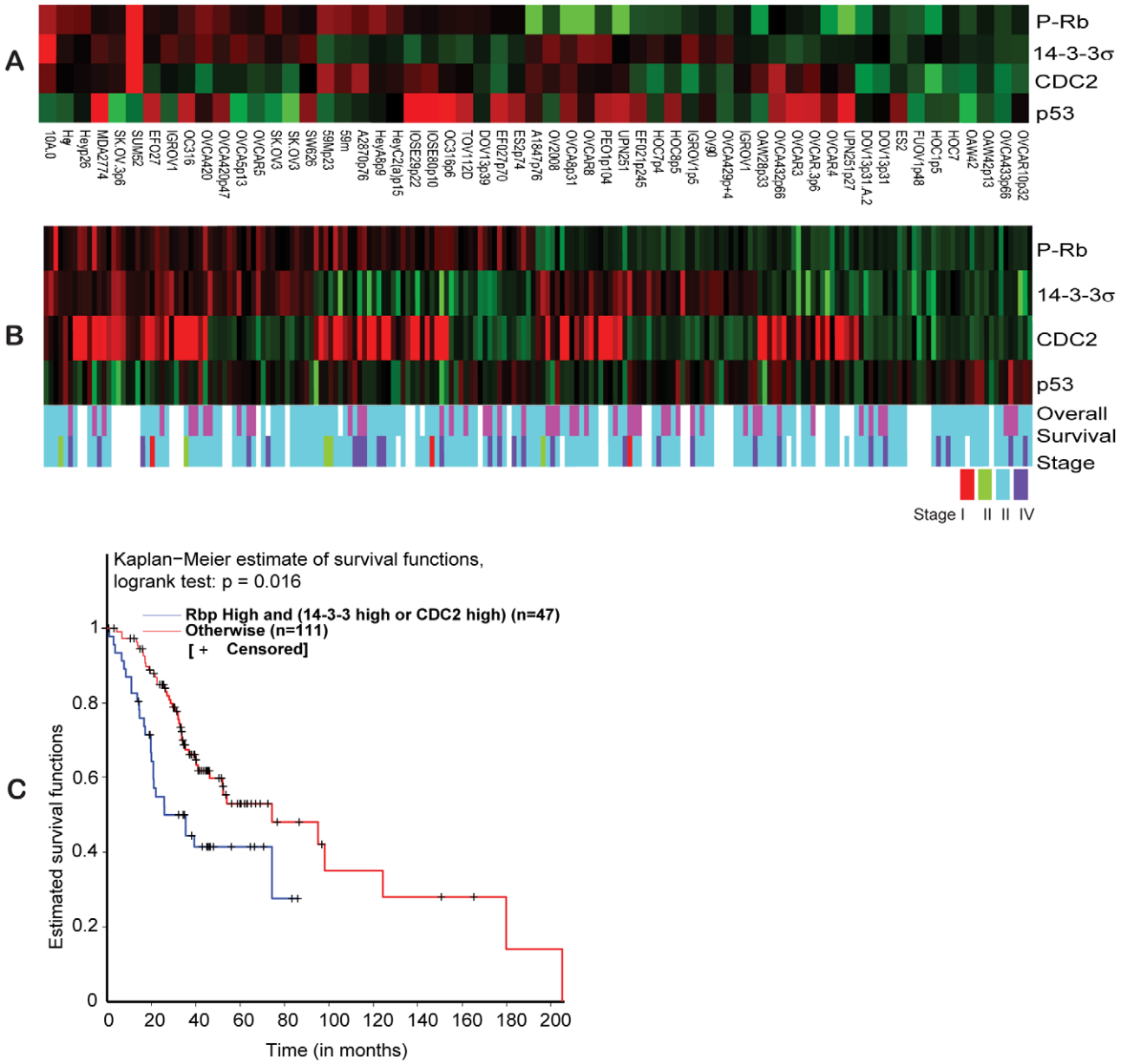

Figure 6. Reverse phase protein array data analysis. (A) Hierarchical clustering of normalized RPPA data over Phospho-RB (Ser 807/811), 14-3-3 σ, CDC2 and p53 across 57 ovarian cancer cell lines. (B) Hierarchical clustering of normalized RPPA data over Phospho-RB (Ser 807/811), 14-3-3 σ, CDC2 and p53 across 205 ovarian tumors. The color codes for overall survival represents overall survival >24 months (blue) and overall survival <24 months (pink). The color codes for tumor stage represent stage I (red), stage II (green), stage III (light-blue) and stage IV (dark-blue). (C). Kaplan-Meier survival curve for the RPPA results comparing the group of ovarian tumors with high Phospho-RB and high 14-3-3 σ or CDC2 (blue line) with other expression profiles (red line).
doi:10.1371/journal.pone.0015864.g006

clearly demonstrated that it is 14-3-3 σ and its inability to control CDC2 dependent G2/M transition in response to O_2 levels that results in oxygen-insensitive cell lines. Although expression of 14-3-3 σ is regulated by p53 [25], we observed no difference in the levels of p53 expression under different oxygen concentrations (Figure S1), suggesting that the involvement of 14-3-3 σ in O_2-sensitivity is independent of p53. If the decrease in 14-3-3 σ is associated with oxygen-sensitive increase in proliferation, then silencing the expression of 14-3-3 σ in oxygen-insensitive cell lines should restore proliferative sensitivity to oxygen. In fact, our experiments show that RNAi mediated silencing of 14-3-3 σ in HeyA8 cells restored oxygen sensitivity (Figure 5E) and in a converse experiment, over-expression of 14-3-3 σ abolished oxygen sensitivity in the A2780 cell line (Figure 5D). This suggests that high levels of 14-3-3 σ protein is sufficient to restrict the regulation of CDC2 mediated G2/M progression. The cytoplasmic restriction of overexpressed 14-3-3 σ in the O_2-insenstive HeyA8 cells provides the first indication for the possible mechanistic basis of this dysregulation (Figure 5A). Other reports also show preferential changes to cellular localization of 14-3-3 σ during different phases of the cell cycle [50], suggesting that cell cycle changes observed with oxygen could be relevant to the 14-3-3 σ localization and pattern in our experiments. Furthermore, 14-3-3 σ is actively exported out of nucleus by CRM1, [51], a nuclear

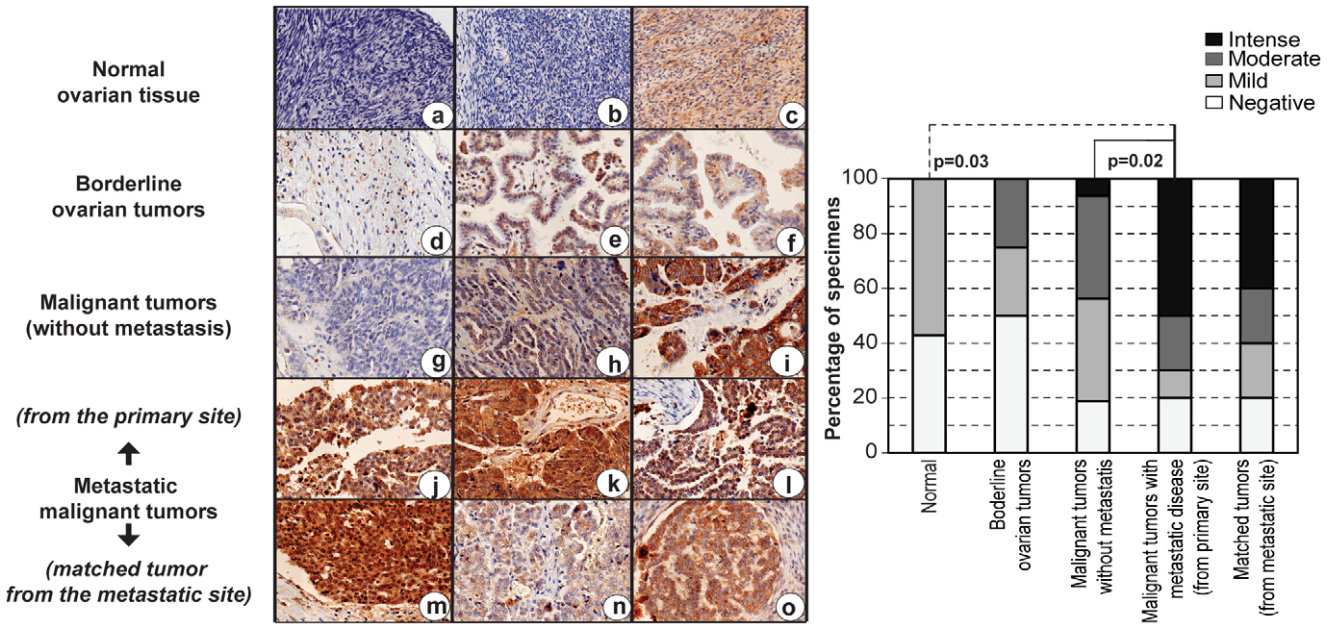

Figure 7. 14-3-3 σ expression and ovarian tumor metastasis. Immunohistochemical analysis of 14-3-3 σ in ovarian tissues show negative (hematoxylin stained blue nucleus) to diffuse staining pattern for 14-3-3 σ (brown) in normal ovarian tissues (a–c), and a moderate increase in the staining intensity localized to the cytoplasm is observed in the borderline ovarian tumors (d–f). In the malignant tumors without any metastatic disease at diagnosis, 14-3-3 σ expression was either absent (g), or stained at moderate to intense levels (h–i), with occasional nuclear staining (i). Intense nuclear and cytoplasmic staining for 14-3-3 σ was observed in ovarian tumors with metastatic disease, obtained from the primary site of the disease, and a moderate to intense staining for 14-3-3 σ in the cytoplasm or both nucleus and cytoplasm of the corresponding tumors obtained from the metastatic site was observed [site of metastasis - (m) appendix, (n) lymph node and (o) omentum]. The quantitative relationship between 14-3-3 σ expression and various stages of ovarian cancer progression is represented in the bar graph, and the statistical analysis for correlation of expression with pathological grades were determined by a Fisher's exact test.
doi:10.1371/journal.pone.0015864.g007

protein that is frequently over-expressed in ovarian cancer [52]. A host of other factors such as, BRCA1, p63 and estrogen induced zinc finger protein (EFP) are also known to regulate the levels of 14-3-3 σ [53]. Therefore, it is possible that 14-3-3 σ expression and its cellular distribution could be influenced by several factors, independent of p53 (as must be the situation in the O_2 insensitive p53 null cell line SKOV3).

The differences in O_2-sensitivity and, consequently, cell proliferation is most important when trying to recapitulate *in vivo* responses where physiological O_2 tensions vary from 2.7–5% in the interstitial space (where many cancer cells reside) to 14.7% in the arterial circulation and lung [18]. Thus, it is reasonable to predict that if O_2-sensitive cancer cells were to dislodge from a primary interstitial space and migrate to the lungs via blood circulation, the increased O_2 concentration would restrict proliferation. In contrast, we speculate that oxygen insensitive cancer cells would have a selective advantage compared to sensitive ones, being better able to thrive in the conditions of increased oxygen concentration. In fact, 14-3-3 σ is frequently over-expressed in many thyroid [54], colorectal [55] and prostate [56] tumors, and is also a potential target for therapeutic modulation [55,56]. Our results provide one rationale for selecting the cancers best suited for 14-3-3 σ targeted therapy. Oxygen insensitivity observed in HeyA8 or SKOV3 is less likely an adaptation to *in vitro* growth conditions because transient over-expression of 14-3-3 σ renders O_2-sensitive A2780 cell line insensitive to increased levels of O_2 (Figure 5D), and over-expression of 14-3-3 σ is observable in primary tumors with metastatic potential (Figure 7). Oxygen sensitivity could therefore be an important factor in the context of metastatic spread of cancer because over-expression of 14-3-3 σ is frequently observed in metastatic cancers, including this study (Figure 7) and others (gastric [57], endometrial [58] and pancreatic [59]). However, epigenetic inactivation of 14-3-3 σ by gene methylation has also been reported to correlate with decreased expression of 14-3-3 σ in cancer progression [60] and metastasis of certain types of tumors [61]. Further, a correlation with a functional role for 14-3-3 σ in promoting tumor invasion and metastasis has also been demonstrated [45,47,62]. Taken together, there is ample evidence to support that over-expression of 14-3-3 σ is relevant to tumor metastasis and therefore, it is likely that O_2 insensitivity associated with over-expression of 14-3-3 σ may have a pivotal role in metastatic dissemination of tumors. Further support to demonstrate the explicit role of 14-3-3 σ in *in vivo* O_2 sensitivity and its relevance to metastasis would require experiments with animal models.

In conclusion, there are many advantages to studying cancer biology under physiological O_2. In fact, compared to cell propagation under physiological O_2, ambient O_2 levels are expected to result in oxidative stress [4], mutation proneness and persistence of transformation [63]. In this context, we have demonstrated that growing cancer cells *in vitro* at low physiological O_2 (not hypoxia), compared with ambient (21%) O_2 is a prudent approach to identify and understand some of the behavioral diversity observed in cancer.

Materials and Methods

Cell culture and Transfection

Ovarian cancer cells were grown in RPMI 1640 (A2780, OVCAR5, OVCAR8, SKOV3) or DMEM (HeyA8 and HOC8)

supplemented with 10% heat inactivated Fetal Bovine Serum (Sigma Aldrich, St.Louis, MO, Cat# F6178) and 200 units of penicillin/streptomycin and 0.5 μg amphotericin-B. Transfection was performed using Amaxa Nucleofector technology (Lonza) as described previously [64]. Plasmid pcDNA 3.0 HA 14-3-3 σ was obtained from Addgene (plasmid 11946 [65]) and pcDNA 3.0 HA empty vector was a gift from Dr. Y. Shiio, UTHSCSA. 14-3-3 σ siRNA and non-targeting dsRNA were purchased from Dharmacon. For oxygen exposures we used Forma Series II 3110 water-jacketed multigas incubator (Thermo Fisher scientific, Waltham, MA) with built-in CO_2 and O_2 monitors and controllers. To maintain 3% O_2, the incubator received an additional supply of nitrogen gas.

Cell proliferation

Cell proliferation was determined using Celltitre-Glo (Promega, Madison, WI) per manufacturer instructions, as described previously [64]. Cells were seeded to a final density of 100, 200 or 400 cells per well in a 384 well plate containing 40 μl of growth medium consisting of 2%, 6% or 10% FBS and antibiotics. Plates were then placed in a humid chamber and returned to the incubators of appropriate oxygen pressure. After 3 days of incubation, the number of cells present per well was measured using Celltitre-Glo reagent, as described previously [64]. The number of cells per well was determined using a standard curve based on ATP concentration, as recommended by the manufacturer.

Mitotic Index

The number of mitotic cells were quantified based the method as described [66]. Briefly, 96 well collagen coated plates were used to seed cells at a final concentration of 1000 cells/well in their respective media. Cells were then incubated for three days at 37°C in 3% or 21% O_2. Finally, cells were washed, resuspended in phosphate buffered saline and stained with DAPI, as described [66]. Images of stained cells were acquired using a Zeiss Axiovert 200M inverted fluorescent microscope using 10X magnification and Openlab (PerkinElmer) image acquisition software. Using Image J, a set threshold for staining intensity was used to count the brightly stained nuclei, with obvious chromatin condensation and the mitotic index was determined based on the ratio of number of mitotic cells present in 1000 cells, as described [66].

Protein isolation and Western blot analysis

Protein lysates and western blot analysis were preformed as previously described [64]. The immunoblots were probed with the appropriate dilutions of primary antibody and visualized using either Lumiglo (Cell signaling technology) or the ECL plus system (GE Healthcare) with the appropriate horseradish peroxidase-conjugated secondary antibody. The primary antibodies used were Phospho - p53 (Ser 15), total p53, Phospho - CDC2 (Tyr 15) and Total CDC2, Phospho - Cyclin B1 (Ser 133), total Cyclin B1, Phospho - CDC25C (Thr 160), total CDC25C, Phsopho RB (Ser 807/811), total RB, Phospho - WEE1 (Ser 642) and total WEE1 (Cell signaling technology), p21, 14-3-3 σ (Millipore) and β-actin (Abcam). Primary antibody dilutions were used as per manufacturer instructions. RB and WEE1 immunoblots were performed using 4–15% gradient gel (Criterion precast gel, Biorad).

Flow Cytometry

Cells were trypsinized and seeded to a final density of 1×10^6 cells per well in a 10 cm dish containing growth medium, antibiotics and appropriate concentrations of FBS. Dishes were then returned to the incubators set for the different oxygen conditions. Following three days of incubation, cells were harvested and prepared for FACS analysis as described previously [67]. Experiments were performed in triplicate. Stained cells were analyzed using a FACS Canto I (BD Biosciences) flow cytometer using an argon laser at 488 nm wavelength. Cell cycle analysis was performed using Modfit LT (version 3.2) software (Verity Software House).

Quantification of M phase cells

The number of cells in M phase were quantified based on mitosis-specific histone H3 phosphorylation in the ovarian cancer cell lines using the Cellomics® Cell Cycle Kit I (Thermo Scientific) as per the manufacturer's recommended protocol. Briefly, 96 well collagen coated plates were used to seed cells at a final concentration of 1000 cells/well in their respective media. Cells were then incubated for three days at 37°C in 3% or 21% O_2. Control wells were treated with 1.5 μg/ml nocodazole (Sigma Aldrich) for 16 hours, fixed with 16% formaldehyde, permeabilized, blocked and stained with reagents consisting anti-phospho-histone H3 primary antibody, as per instructions provided in the kit. Stained cells were analyzed with a Zeiss Axiovert 200M inverted fluorescent microscope using 10X magnification and Openlab (PerkinElmer) image acquisition software. 100–250 cells per replicate were counted for phospho-histone H3 positive cells.

Immunolocalization of 14-3-3 σ and CDC2

A2780 cells transfected with a 14-3-3 σ cDNA expression construct or HeyA8 cells transfected with 14-3-3 σ siRNA were seeded at a final density of 10^5 cells per fibronectin (Sigma) coated 12.5 mm^2 glass coverslip mounted in each well of a 12-well plate. Cells were maintained in complete growth medium supplemented with 10% fetal bovine serum and allowed to grow for three days in the presence of 21% or 3% oxygen. For the detection of 14-3-3 σ or CDC2 by immunofluorescence, cells were processed as described previously [68]. The primary antibodies used were mouse monoclonal 14-3-3 σ at 1.0 μg/mL (Upstate) and rabbit polyclonal total CDC2 at 1:1000 (Cell Signaling). Following a PBS wash, the cells were incubated with secondary antibodies, goat anti-mouse AlexaFluor 488 and goat anti-rabbit AlexaFluor 568 (Invitrogen) at 1:1000 dilution in blocking buffer for 1 hour at room temperature. Cells were then counterstained with DAPI (1:3000 dilution in PBS) and mounted onto microscope slides using Fluoromount-G. Images were taken at 63X magnification using the Zeiss Axiovert 200M inverted fluorescent microscope and Openlab software (PerkinElmer).

Reverse Phase Protein Array

Protein lysates from 57 cancer cell lines or 205 primary ovarian cancer tumors were spotted in RPPA slides and processed for expression analysis, as described previously [69,70]. Data acquisition and processing were performed as described previously [69]. Ovarian cancer specimens were obtained from Gynecology Tumor Tissue Bank at MD Anderson Cancer Center, following approval from the Institutional Review Board (BT).

Normalization and Clustering

log-transformed RPPA data was first examined to remove non ovarian cancer cell lines. We then examined all replicated representations from the same source as annotated to reduce down to 57 ovarian cancer cell lines or 205 patient samples (from each source) by taking the median protein expression level of all replicates. An additional cell-line specific normalization step was performed in which median expression levels for each protein was

first determined and then subtracted from individual RPPA experiments. The anchored heatmap (termed after anchored over/under-expression orientation) was generated by requiring RB, 14-3-3 σ and CDC2 to be arranged from over-expressed to under-expressed recursively from the given cell-line order, but exact positions of each protein was determined by hierarchical clustering algorithm with Euclidean distance as similarity measure and average lineage from all cell-lines, as shown in Figure 6 A&B). Raw data obtained from RPPA for the expression of Phospho RB, 14-3-3 σ and CDC2 is provided in the supplementary tables (for ovarian cancer cell lines, see Table S2, and for ovarian cancer patient specimens, see Table S3)

Immunohistochemistry

Tissue arrays (OV951-1) consisting of normal and malignant tissues from primary or metastatic sites were purchased from US Biomax Inc. Slides were processed for immunohistochemistry and analyzed, as described previously [71]. 14-3-3 σ (Upstate) was used at 1:50 dilution for incubation with primary antibody and subsequent steps were performed using the Dako universal LSAB kit with DAB as described by the manufacturer.

Statistical Analyses

To determine significant differences to proliferation under 3% or 21% O_2, a Student *t-test* was performed, and *ANOVA* was performed to compare the different cell cycle profiles with the panel of ovarian cancer cell lines. Kaplan-Meier survival analysis with p-value determined with log-rank test was performed using MATLAB (Mathworks, Natick, MA) for RPPA data consisting patient specimens. For Kaplan-Meier survival analysis the data was censored based on patient's vital status. Statistical analysis for the correlation of 14-3-3 σ expression with the various pathological grades of ovarian tumors determined based on immunohistochemistry was analyzed by a Fisher's exact test using R.

Supporting Information

Figure S1 Western blot analysis of phospho and total p53, and p21, which are major upstream regulators of G2/M cell cycle progression and the relevance to 21% or 3% O_2 in ovarian cancer cells. O_2 insensitive cell lines are indicated by asterisk and italics.
(EPS)

Table S1 *In vitro* cell doubling time for the ovarian cancer cell lines.
(XLS)

Table S2 Raw data from cell line RPPA for Phospho-Rb, p53, CDC2 and 14-3-3 σ expression. The table contains following columns: 1) Unique ID, 2) Original cell-line or with treatment, 3) Cell-line's contributing Lab/source; 4) Cell type, 5) Cell-line name, 6–9) log2 transformed protein expression ratios (14-3-3 σ, CDC2, p-Rb, and p53) as the raw measurement provided by the MD Anders Cancer Center RPPA core facility.
(XLS)

Table S3 Raw data from OVSS2 RPPA for Phospho Rb, CDC2 and 14-3-3 σ expression. The table contains following columns: 1) Unique ID, 2) Tumor ID in various databases (DBs), 3) Tumor source institution; 4) patient age at diagnosis (in months), 5) tumor stage, 6) grade (HG: high grade, LG: low grade, empty: unknown), 7) Overall survival (in months), 8) Vital Status (0: alive, 1: dead), 9–12) log2 transformed protein expression ratios (14-3-3 σ, CDC2, p53 and p-Rb) as the raw measurement provided by the MD Anderson Cancer Center RPPA core facility.
(XLS)

Acknowledgments

We thank Ms. Jennifer Rebels at the Greehey Children's Cancer Research Institute core facility, UTHSCSA for FACS analysis. We thank Ms. Michelle M. Brady at the Greehey Children's Cancer Research Institute histology core facility for immunocytochemistry processing of tumor specimens and Ms. Uthra Suresh at the Greehey Children's Cancer Research Institute, UTHSCSA for the statistical analysis of the data. We thank Ms. Alison Claybon for grammar checks and making corrections to the manuscript. We thank Dr. Peter Hornsby, Department of Physiology, UTHSCSA for constructive criticism of the manuscript.

Author Contributions

Conceived and designed the experiments: DR AJRB. Performed the experiments: DR BK AB TTG. Analyzed the data: DR YC BK AB AJRB. Contributed reagents/materials/analysis tools: YC JL MSC BTH AJRB. Wrote the paper: DR YC BK AB AJRB.

References

1. Sullivan M, Galea P, Latif S (2006) What is the appropriate oxygen tension for in vitro culture? Mol Hum Reprod 12: 653.
2. Csete M (2005) Oxygen in the cultivation of stem cells. Ann N Y Acad Sci 1049: 1–8.
3. Hornsby PJ (2003) Mouse and human cells versus oxygen. Sci Aging Knowledge Environ 2003: PE21.
4. Parrinello S, Samper E, Krtolica A, Goldstein J, Melov S, et al. (2003) Oxygen sensitivity severely limits the replicative lifespan of murine fibroblasts. Nat Cell Biol 5: 741–747.
5. Shay JW, Wright WE (2007) Tissue culture as a hostile environment: identifying conditions for breast cancer progression studies. Cancer Cell 12: 100–101.
6. Ince TA, Richardson AL, Bell GW, Saitoh M, Godar S, et al. (2007) Transformation of different human breast epithelial cell types leads to distinct tumor phenotypes. Cancer Cell 12: 160–170.
7. Frieboes HB, Edgerton ME, Fruehauf JP, Rose FR, Worrall LK, et al. (2009) Prediction of drug response in breast cancer using integrative experimental/computational modeling. Cancer Res 69: 4484–4492.
8. Sridhar KS, Plasse TF, Holland JF, Shapiro M, Ohnuma T (1983) Effects of physiological oxygen concentration on human tumor colony growth in soft agar. Cancer Res 43: 4629–4631.
9. Gupta V, Krishan A (1982) Effect of oxygen concentration on the growth and drug sensitivity of human melanoma cells in soft-agar clonogenic assay. Cancer Res 42: 1005–1007.
10. Carrera S, de Verdier PJ, Khan Z, Zhao B, Mahale A, et al. (2010) Protection of cells in physiological oxygen tensions against DNA damage-induced apoptosis. J Biol Chem 285: 13658–13665.
11. Laser H (1937) Tissue metabolism under the influence of low oxygen tension. Biochem J 31: 1671–1676.
12. Green DR, Chipuk JE (2006) p53 and metabolism: Inside the TIGAR. Cell 126: 30–32.
13. Powers DE, Millman JR, Huang RB, Colton CK (2008) Effects of oxygen on mouse embryonic stem cell growth, phenotype retention, and cellular energetics. Biotechnol Bioeng 101: 241–254.
14. Pouyssegur J, Dayan F, Mazure NM (2006) Hypoxia signalling in cancer and approaches to enforce tumour regression. Nature 441: 437–443.
15. Magagnin MG, Koritzinsky M, Wouters BG (2006) Patterns of tumor oxygenation and their influence on the cellular hypoxic response and hypoxia-directed therapies. Drug Resist Updat 9: 185–197.
16. Brizel DM, Rosner GL, Prosnitz LR, Dewhirst MW (1995) Patterns and variability of tumor oxygenation in human soft tissue sarcomas, cervical carcinomas, and lymph node metastases. Int J Radiat Oncol Biol Phys 32: 1121–1125.
17. Brown JM, Giaccia AJ (1998) The unique physiology of solid tumors: opportunities (and problems) for cancer therapy. Cancer Res 58: 1408–1416.
18. Treacher DF, Leach RM (1998) Oxygen transport-1. Basic principles. Bmj 317: 1302–1306.

19. Pantel K, Brakenhoff RH (2004) Dissecting the metastatic cascade. Nat Rev Cancer 4: 448–456.
20. Sherr CJ (2004) Principles of tumor suppression. Cell 116: 235–246.
21. Payton M, Chung G, Yakowec P, Wong A, Powers D, et al. (2006) Discovery and evaluation of dual CDK1 and CDK2 inhibitors. Cancer Res 66: 4299–4308.
22. Taylor WR, Stark GR (2001) Regulation of the G2/M transition by p53. Oncogene 20: 1803–1815.
23. Graeber TG, Peterson JF, Tsai M, Monica K, Fornace AJ, Jr., et al. (1994) Hypoxia induces accumulation of p53 protein, but activation of a G1-phase checkpoint by low-oxygen conditions is independent of p53 status. Mol Cell Biol 14: 6264–6277.
24. Das KC, Dashnamoorthy R (2004) Hyperoxia activates the ATR-Chk1 pathway and phosphorylates p53 at multiple sites. Am J Physiol Lung Cell Mol Physiol 286: L87–97.
25. Hermeking H, Lengauer C, Polyak K, He TC, Zhang L, et al. (1997) 14-3-3 sigma is a p53-regulated inhibitor of G2/M progression. Mol Cell 1: 3–11.
26. Eguchi T, Takaki T, Itadani H, Kotani H (2007) RB silencing compromises the DNA damage-induced G2/M checkpoint and causes deregulated expression of the ECT2 oncogene. Oncogene 26: 509–520.
27. Balin AK, Goodman DB, Rasmussen H, Cristofalo VJ (1978) Oxygen-sensitive stages of the cell cycle of human diploid cells. J Cell Biol 78: 390–400.
28. Stark GR, Taylor WR (2006) Control of the G2/M transition. Mol Biotechnol 32: 227–248.
29. Kaldis P, Aleem E (2005) Cell cycle sibling rivalry: Cdc2 vs. Cdk2. Cell Cycle 4: 1491–1494.
30. Lindqvist A, Rodriguez-Bravo V, Medema RH (2009) The decision to enter mitosis: feedback and redundancy in the mitotic entry network. J Cell Biol 185: 193–202.
31. Kishimoto T (1994) Cell reproduction: induction of M-phase events by cyclin-dependent cdc2 kinase. Int J Dev Biol 38: 185–191.
32. Lees JA, Buchkovich KJ, Marshak DR, Anderson CW, Harlow E (1991) The retinoblastoma protein is phosphorylated on multiple sites by human cdc2. Embo J 10: 4279–4290.
33. Berry LD, Gould KL (1996) Regulation of Cdc2 activity by phosphorylation at T14/Y15. Prog Cell Cycle Res 2: 99–105.
34. Shibuya EK (2003) G2 cell cycle arrest—a direct link between PKA and Cdc25C. Cell Cycle 2: 39–41.
35. Roy S, Khanna S, Bickerstaff AA, Subramanian SV, Atalay M, et al. (2003) Oxygen sensing by primary cardiac fibroblasts: a key role of p21(Waf1/Cip1/Sdi1). Circ Res 92: 264–271.
36. Lees SJ, Childs TE, Booth FW (2008) p21(Cip1) expression is increased in ambient oxygen, compared to estimated physiological (5%) levels in rat muscle precursor cell culture. Cell Prolif 41: 193–207.
37. Kim SY, Ferrell JE, Jr. (2007) Substrate competition as a source of ultrasensitivity in the inactivation of Wee1. Cell 128: 1133–1145.
38. Dalton S (1992) Cell cycle regulation of the human cdc2 gene. Embo J 11: 1797–1804.
39. Smith EM, Proud CG (2008) cdc2-cyclin B regulates eEF2 kinase activity in a cell cycle- and amino acid-dependent manner. Embo J 27: 1005–1016.
40. Astanehe A, Arenillas D, Wasserman WW, Leung PC, Dunn SE, et al. (2008) Mechanisms underlying p53 regulation of PIK3CA transcription in ovarian surface epithelium and in ovarian cancer. J Cell Sci 121: 664–674.
41. Armaiz-Pena GN, Mangala LS, Spannuth WA, Lin YG, Jennings NB, et al. (2009) Estrous cycle modulates ovarian carcinoma growth. Clin Cancer Res 15: 2971–2978.
42. Urano T, Saito T, Tsukui T, Fujita M, Hosoi T, et al. (2002) Efp targets 14-3-3 sigma for proteolysis and promotes breast tumour growth. Nature 417: 871–875.
43. Ramirez PT, Landen CN, Jr., Coleman RL, Milam MR, Levenback C, et al. (2008) Phase I trial of the proteasome inhibitor bortezomib in combination with carboplatin in patients with platinum- and taxane-resistant ovarian cancer. Gynecol Oncol 108: 68–71.
44. Li Z, Liu JY, Zhang JT (2009) 14-3-3sigma, the double-edged sword of human cancers. Am J Transl Res 1: 326–340.
45. Ghahary A, Karimi-Busheri F, Marcoux Y, Li Y, Tredget EE, et al. (2004) Keratinocyte-releasable stratifin functions as a potent collagenase-stimulating factor in fibroblasts. J Invest Dermatol 122: 1188–1197.
46. Ghahary A, Marcoux Y, Karimi-Busheri F, Li Y, Tredget EE, et al. (2005) Differentiated keratinocyte-releasable stratifin (14-3-3 sigma) stimulates MMP-1 expression in dermal fibroblasts. J Invest Dermatol 124: 170–177.
47. Lam E, Kilani RT, Li Y, Tredget EE, Ghahary A (2005) Stratifin-induced matrix metalloproteinase-1 in fibroblast is mediated by c-fos and p38 mitogen-activated protein kinase activation. J Invest Dermatol 125: 230–238.
48. Poot M, Schindler D, Kubbies M, Hoehn H, Rabinovitch PS (1988) Bromodeoxyuridine amplifies the inhibitory effect of oxygen on cell proliferation. Cytometry 9: 332–338.
49. Poot M, Gross O, Epe B, Pflaum M, Hoehn H (1996) Cell cycle defect in connection with oxygen and iron sensitivity in Fanconi anemia lymphoblastoid cells. Exp Cell Res 222: 262–268.
50. Moreira JM, Shen T, Ohlsson G, Gromov P, Gromova I, et al. (2008) A combined proteome and ultrastructural localization analysis of 14-3-3 proteins in transformed human amnion (AMA) cells: definition of a framework to study isoform-specific differences. Mol Cell Proteomics 7: 1225–1240.
51. van Hemert MJ, Niemantsverdriet M, Schmidt T, Backendorf C, Spaink HP (2004) Isoform-specific differences in rapid nucleocytoplasmic shuttling cause distinct subcellular distributions of 14-3-3 sigma and 14-3-3 zeta. J Cell Sci 117: 1411–1420.
52. Noske A, Weichert W, Niesporek S, Roske A, Buckendahl AC, et al. (2008) Expression of the nuclear export protein chromosomal region maintenance/exportin 1/Xpo1 is a prognostic factor in human ovarian cancer. Cancer 112: 1733–1743.
53. Mhawech P (2005) 14-3-3 proteins—an update. Cell Res 15: 228–236.
54. Ito Y, Miyoshi E, Uda E, Yoshida H, Uruno T, et al. (2003) 14-3-3 sigma possibly plays a constitutive role in papillary carcinoma, but not in follicular tumor of the thyroid. Cancer Lett 200: 161–166.
55. Perathoner A, Pirkebner D, Brandacher G, Spizzo G, Stadlmann S, et al. (2005) 14-3-3sigma expression is an independent prognostic parameter for poor survival in colorectal carcinoma patients. Clin Cancer Res 11: 3274–3279.
56. Quayle SN, Sadar MD (2007) 14-3-3 sigma increases the transcriptional activity of the androgen receptor in the absence of androgens. Cancer Lett 254: 137–145.
57. Tanaka K, Hatada T, Kobayashi M, Mohri Y, Tonouchi H, et al. (2004) The clinical implication of 14-3-3 sigma expression in primary gastrointestinal malignancy. Int J Oncol 25: 1591–1597.
58. Nakayama H, Sano T, Motegi A, Oyama T, Nakajima T (2005) Increasing 14-3-3 sigma expression with declining estrogen receptor alpha and estrogen-responsive finger protein expression defines malignant progression of endometrial carcinoma. Pathol Int 55: 707–715.
59. Okada T, Masuda N, Fukai Y, Shimura T, Nishida Y, et al. (2006) Immunohistochemical expression of 14-3-3 sigma protein in intraductal papillary-mucinous tumor and invasive ductal carcinoma of the pancreas. Anticancer Res 26: 3105–3110.
60. Cheng L, Pan CX, Zhang JT, Zhang S, Kinch MS, et al. (2004) Loss of 14-3-3sigma in prostate cancer and its precursors. Clin Cancer Res 10: 3064–3068.
61. Yi B, Tan SX, Tang CE, Huang WG, Cheng AL, et al. (2009) Inactivation of 14-3-3 sigma by promoter methylation correlates with metastasis in nasopharyngeal carcinoma. J Cell Biochem 106: 858–866.
62. Chavez-Munoz C, Morse J, Kilani R, Ghahary A (2008) Primary human keratinocytes externalize stratifin protein via exosomes. J Cell Biochem 104: 2165–2173.
63. Busuttil RA, Rubio M, Dolle ME, Campisi J, Vijg J (2003) Oxygen accelerates the accumulation of mutations during the senescence and immortalization of murine cells in culture. Aging Cell 2: 287–294.
64. Ravi D, Wiles AM, Bhavani S, Ruan J, Leder P, et al. (2009) A network of conserved damage survival pathways revealed by a genomic RNAi screen. PLoS Genet 5: e1000527.
65. Wilker EW, Grant RA, Artim SC, Yaffe MB (2005) A structural basis for 14-3-3sigma functional specificity. J Biol Chem 280: 18891–18898.
66. Tarnowski BI, Sens DA, Nicholson JH, Hazen-Martin DJ, Garvin AJ, et al. (1993) Automatic quantitation of cell growth and determination of mitotic index using DAPI nuclear staining. Pediatr Pathol 13: 249–265.
67. Ravi D, Muniyappa H, Das KC (2005) Endogenous thioredoxin is required for redox cycling of anthracyclines and p53-dependent apoptosis in cancer cells. J Biol Chem 280: 40084–40096.
68. Ravi D, Das KC (2004) Redox-cycling of anthracyclines by thioredoxin system: increased superoxide generation and DNA damage. Cancer Chemother Pharmacol 54: 449–458.
69. Zhang L, Wei Q, Mao L, Liu W, Mills GB, et al. (2009) Serial dilution curve: a new method for analysis of reverse phase protein array data. Bioinformatics 25: 650–654.
70. Stemke-Hale K, Gonzalez-Angulo AM, Lluch A, Neve RM, Kuo WL, et al. (2008) An integrative genomic and proteomic analysis of PIK3CA, PTEN, and AKT mutations in breast cancer. Cancer Res 68: 6084–6091.
71. Ravi D, Ramadas K, Mathew BS, Nalinakumari KR, Nair MK, et al. (1999) De novo programmed cell death in oral cancer. Histopathology 34: 241–249.

7538–7545 Nucleic Acids Research, 2010, Vol. 38, No. 21 Published online 21 July 2010
doi:10.1093/nar/gkq624

PARP1 suppresses homologous recombination events in mice *in vivo*

Alison Claybon[1,2], Bijal Karia[1,2], Crystal Bruce[3] and Alexander J. R. Bishop[1,2,*]

[1]Greehey Children's Cancer Research Institute, [2]Department of Cellular and Structural Biology, The University of Texas Health Science Center at San Antonio, San Antonio, TX 78229 and [3]Department of Biochemistry and Molecular Biology, Oklahoma State University, Stillwater, OK 74078, USA

Received April 1, 2010; Revised June 27, 2010; Accepted June 28, 2010

ABSTRACT

Recent studies suggest that PARP1 inhibitors, several of which are currently in clinical trial, may selectively kill *BRCA1/2* mutant cancers cells. It is thought that the success of this therapy is based on immitigable lethal DNA damage in the cancer cells resultant from the concurrent loss or inhibition of two DNA damage repair pathways: single-strand break (SSB) repair and homologous recombination repair (HRR). Presumably, inhibition of PARP1 activity obstructs the repair of SSBs and during DNA replication, these lesions cause replication fork collapse and are transformed into substrates for HRR. In fact, several previous studies have indicated a hyper-recombinogenic phenotype in the absence of active PARP1 *in vitro* or in response to DNA damaging agents. In this study, we demonstrate an increased frequency of spontaneous HRR *in vivo* in the absence of PARP1 using the p^{un} assay. Furthermore, we found that the HRR events that occur in *Parp1* nullizygous mice are associated with a significant increase in large, clonal events, as opposed to the usually more frequent single cell events, suggesting an effect in replicating cells. In conclusion, our data demonstrates that PARP1 inhibits spontaneous HRR events, and supports the model of DNA replication transformation of SSBs into HRR substrates.

INTRODUCTION

Poly (ADP-ribosyl)ation is the posttranslational transfer of long chains of negatively charged ADP-ribose moieties to proteins. The resultant increase in negative charge causes the target protein to lose DNA-binding affinity (1). Poly (ADP-ribose) polymerases, or PARPs, comprise a large family of genes that have shared homology with the catalytic domain of the founding member, PARP1 (1). PARP1 has been widely implicated in a multitude of cellular processes including replication (2–4), transcription [reviewed in (5)], chromatin remodeling [reviewed in (5)], telomere maintenance (6) and perhaps most notably, the repair of DNA damage through the base excision repair (BER) pathway (7–9).

Current understanding is that the key BER proteins actually participate in several distinct pathways such as short-patch BER, long-patch BER, single strand break (SSB) repair and nucleotide incision repair (10). However, the common factor for all of these pathways is an SSB—be it the initiating lesion or an intermediate step in a repair process. PARP1 readily binds SSBs (11,12) and recruits the scaffolding protein XRCC1 (13). PARP1 poly (ADP-ribosyl)ates itself (13), reducing its DNA-binding affinity, thus allowing other repair factors to bind the lesion site (9,14).

A recent study demonstrated that chemical inhibition of PARP1 decreased the efficiency of SSB repair (15), conjecturing that chemically inhibited PARP1 remains bound to DNA and blocks other repair proteins from the SSB site. However, the same study revealed that despite PARP1 silencing via RNA interference, cells were able to repair SSBs (15), indicating that an alternative pathway, possibly homologous recombination repair (HRR), can compensate for this loss. Loss of *Parp1* by way of gene targeting in human cells does not hinder formation of nuclear RAD51 foci (an indicator of RAD51-dependent HRR) (16), nor does PARP1 inhibition appear to obstruct HRR *in vitro* (16,17). Waldman and Waldman (18) found a 4-fold increase in intrachromosomal homologous recombination in mouse fibroblasts grown in the poly(ADP-ribose) polymerase inhibitor, 3-methoxybenzamide, compared to controls. Furthermore, PARP1 does not co-localize to RAD51 foci following DNA damage (16) indicating that it is unlikely that PARP1 is directly involved in the HRR process. In addition, increased sister chromatid exchange has been observed with PARP1 inhibitors in Chinese

*To whom correspondence should be addressed. Tel: +1 210 562 9000; Fax: +1 210 562 9014; Email: bishopa@uthscsa.edu

hamster ovary cells (19) and in PARP1 null mice (20), whereas over-expression of *Parp1* decreases the incidence of sister chromatid exchange following DNA damage (21). Resolution of SSBs by way of HRR in the absence of PARP1 activity may be due either to stalled replication fork or DSBs resulting from replication fork collapse. The requirement of such activity is the postulated basis for synthetic lethality observed when treating breast and ovarian cancer cells deficient for either BRCA1 or BRCA2 with PARP1 inhibitors (4,22–24). This is because BRCA1 and BRCA2, amongst their various functions, are required for RAD51 dependent double-stranded DNA break induced HRR (25–27). Together, these *in vitro* observations indicate that loss or inhibition of PARP1 leads to a hyper-recombinogenic phenotype.

Here, we evaluate the spontaneous frequency of HRR *in vivo* using the well-established and highly sensitive p^{un} eye spot assay (28–30). The murine pink-eyed dilution gene, *p*, encodes a protein that functions in the pigmentation of the fur and the retinal pigment epithelium (RPE) of the mouse (31). Mice lacking a functional copy of this gene are hypopigmented, having a dilute (gray) coat and pink eyes (the cells of the RPE are rendered transparent) (31). One such mutant, the 'pink-eyed unstable' (p^{un}) allele contains a 70-kb duplication of exons 6–18 (32–34, Figure 1) and causes this autosomal recessive phenotype. However, the p^{un} allele is subject to a relatively high frequency of spontaneous, somatic reversion to wild-type (35). Reversion can only be attributed to HRR mediated deletion of the duplicated exons, which restores functionality of *p* (32,33) and consequently pigmentation to the fur and RPE. Equivalent assays in yeast have demonstrated that such intrachromosomal deletions between homologous tandem repeats may be mediated by either a RAD51-dependent pathway (canonical HRR pathway) or a RAD51-independent pathway [single strand annealing (SSA), an alternative HRR pathway)] (36). Therefore, the frequency of p^{un} reversion is indicative of the somatic occurrence of spontaneous HRR events (28,29,37). Here we use the p^{un} eye spot assay to demonstrate that the absence of PARP1 results in increased spontaneous somatic HRR events *in vivo*. The significant increase in rare multi-cell clones of eye spots in *Parp1* nullizygous mice suggests that the normal function of PARP1 is to remove DNA lesions prior to their becoming HRR substrates during DNA replication. Our observations substantiate current models of the relationship between PARP1 and HRR, providing formal *in vivo* evidence of a spontaneous, hyper-recombination phenotype.

MATERIALS AND METHODS

Generation of mice

Mice heterozygous for a targeted null allele of *Parp1*, 129S-*Parp1tm1Zqw* (38), were obtained from Jackson Laboratories (Bar Harbor, ME) and genotyped for *Parp1* as described (http://parplink.u-strasbg.fr/protocols/tools/parp1_typing.html) earlier. The $Parp1^{+/-}$ mice were made C57BL/6J congenic by five backcrosses followed by two crosses to C57BL/6J $p^{un/un}$ mice. Mice with homozygous $p^{un/un}$ genotype were selected by their phenotypic gray coat color. The resulting C57BL/6J N7 $Parp1^{+/-}$ $p^{un/un}$ mice (hereafter referred to as $Parp1^{+/-}$) were self-crossed to create the necessary experimental ($Parp1^{-/-}$) and control animals ($Parp1^{+/-}$ and $Parp1^{+/+}$).

P^{un} assay

The p^{un} frequency assay was performed as described earlier (29). Briefly, eyes were harvested, with the investigator blinded to the genotypes until after p^{un} eye spot data was collected. Three types of data were collected for each RPE: the total number of eye spots, the number of cells comprising each eye spot, and the position of each eye spot relative to the optic nerve. Following Bishop *et al.* (29), a p^{un} reversion event or eye spot was defined as 'a pigmented cell or a cluster of pigmented cells, separated by no more than one unpigmented cell'. Eyes were viewed at 15× using a Zeiss Axiovert microscope and methodically scanned for pigmented spots. A 5× mosaic photograph was taken of each RPE using a Zeiss Lumar V.12 stereomicroscope, Zeiss Axiovision MRm camera and Zeiss Axiovision 4.6 software (Thornwood, NY, USA). In cases where a suspected clone consisted of pigmented cells separated by clear cell(s), the Adobe Photoshop CS2 (San Jose, CA, USA) measure tool was used to assess if the unpigmented area between pigmented cells was consistent with the single cell diameter in that part of the RPE (Figure 1). The p^{un} positional assay was then performed as described earlier (28). Briefly, the position of each spot relative to the optic nerve was calculated using simple measurements. In Photoshop, the brush tool was used to mark the approximate center of the optic nerve and the measure tool was then used to obtain two distances for each eye spot: (i) from the center of the optic nerve to the proximal edge of the eye spot, and (ii) from the center of the optic nerve to the edge of the RPE. By dividing the former by the latter, the position of each eye spot relative to the optic nerve was determined.

Primary mouse embryonic fibroblasts and cell culture

Primary mouse embryonic fibroblasts (MEFs) were obtained by intercrossing *Parp1* heterozygous mice to obtain *Parp1* null embryos and littermate controls. Pregnancies were timed by the observation of a vaginal copulation plug and embryos were harvested on Day E14. Embryos were mechanically homogenized and allowed to incubate in 0.05% Trypsin–EDTA for 20 min. Cells were cultured in Dulbecco's modified Eagle's medium supplemented with 10 000 U/ml penicillin, 10 000 μg/ml streptomycin, 25 μg/ml Amphotericin B (Cellgro). The cells were grown at 37°C in the presence of 5% CO_2 in a humidified incubator.

RAD51 nuclear foci immunofluorescence

HRR frequency was determined by immunofluorescence using an antibody against RAD51 (RK-70-005, MBL) as described earlier (39). Cells were grown on acid-washed fibronectin coated cover slips at a density of 1×10^5 cells/cover slip. Cells were then fixed with 4% paraformaldehyde and permeabilized using Triton X-100

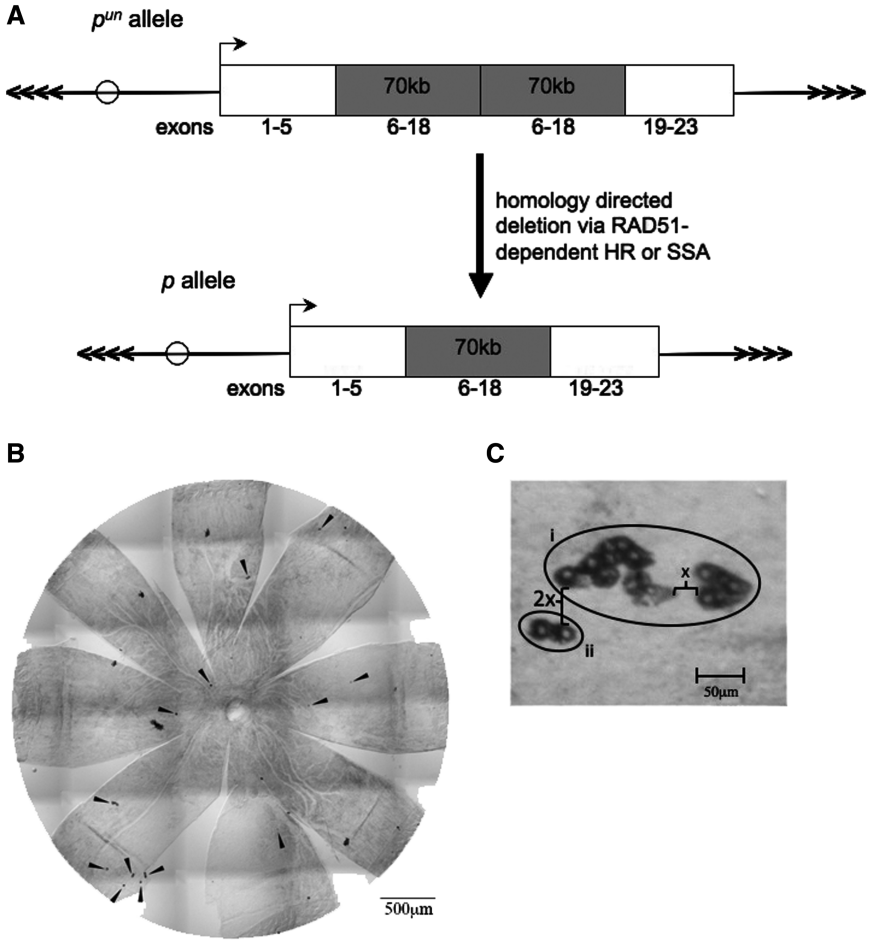

Figure 1. HR-mediated reversion of the p^{un} allele. (**A**) Schematic of the p^{un} mutation. HR events mediate the deletion of one copy of a tandem repeat (of Exons 6–18) rendering the *p* gene functional, thus causing pigmentation of RPE cells. Circles represent centromeres and arrows telomere DNA. (**B**) Mosaic image of a *Parp1*$^{-/-}$ RPE wholemount. The 13 p^{un} reversion spots are indicated with black arrowheads. (**C**) Example of two distinct p^{un} reversion events within a cluster of pigmented cells. *x* is the diameter of one cell in this region of the RPE and 2× is twice this diameter. For example, the two clusters of cells labeled *i*, are separated by a distance of *x* and are scored as one event. The cluster labeled ii is a distance of 2× from cluster *i*, and therefore represents a distinct event.

for 10 min at room temperature. Blocking was performed with 1% BSA–4% goat serum for 1 h followed by an overnight incubation with RAD51 antibody (1:2000) in a humidified chamber. Goat antichicken Alexa Fluor 488 (Invitrogen) diluted 1:1000 was applied to each cover slip for 1 h followed by DAPI staining and Fluoromount G slide mounting. A minimum of 100 nuclei were examined for each genotype, repeated with three technical replicates per genotype.

Statistics

Parametric analysis of variance was performed in Microsoft Excel 1994 for Mac (Redmond, Washington). The F_{max} test was done by hand per Hartley (40) and Rohlf and Sokal (41). Measurements of skew and kurtosis were obtained using descriptive statistics in Microsoft Excel 1994 for Mac (Redmond, Washington). Non-parametric Kruskal–Wallis test was performed using Stata (College Station, TX, USA). Dunn's test was done by hand per Siegel (42). Chi-squared contingency analysis was performed using the VasserStats online calculator (http://faculty.vasser.edu/lowry/VasserStats.html, accessed 11/2009). Fisher's Exact test (43) was used to compare RAD51 foci quantification using the sum of the technical replicates per genotype.

RESULTS

Loss of *Parp1* leads to a significant increase in HRR *in vivo*

PARP1, amongst its various activities, is involved in SSB repair (11,12). Inhibition of the PARP1 protein in BRCA1 and BRCA2 mutant cells leads to their selective cell death (23,44). This has led to the working model that the observed cell death is due to immitigable DNA damage caused by the loss of two key DNA repair pathways: (i) HRR, due to loss of *BRCA1/2*, and (ii) SSB repair due to inhibition of PARP1 (4,23,24). This model suggests that lack of PARP1 alone will cause an increase in HRR frequency in the absence of exogenous damage. To test this assumption, we determined the spontaneous frequency of

HRR in *Parp1*$^{-/-}$, $^{+/-}$ and $^{+/+}$ animals using the *in vivo* p^{un} assay.

The frequency of p^{un} reversion was determined in *Parp1*$^{-/-}$, $^{+/-}$ and $^{+/+}$ animals using p^{un} eye spot assay (Table 1 and Figure 2). There is a clear increase in the frequency of p^{un} reversion events observed in the absence of PARP1 compared to wild-type and heterozygous littermate controls. Considering that the data is non-parametric and not normal, we used the non-parametric Kruskal–Wallis test (followed by Dunn's test to determine which groups are different from one another). This analysis revealed that *Parp1*$^{-/-}$ animals had a highly statistically significant increase in p^{un} reversion, and thus increased HRR, compared to controls ($P = 0.0001$).

Parp1 null mice have an earlier incidence of p^{un} reversion than controls

The RPE develops radially outward from the optic nerve during development (45), therefore, much like the concentric annual rings of a tree, the positions of eye spots indicate the developmental time at which they occurred (28,29). p^{un} reversion events closer to the optic nerve occurred earlier in development and events further from the optic nerve occurred later in development (29). To investigate whether the increased number of events occurred at a particular time during development, we analyzed the relative positions of the p^{un} reversion events on the RPE of differing *Parp1* genotype (35 wild-type, 28 heterozygous and 24 *Parp1* null RPE). A Kruskal–Wallis test was used to compare the positional distribution of spots and indicated that there is a significant difference between genotypes ($P = 0.0043$, Figure 3). Subsequently, a Dunn's test indicated that the *Parp1* null group is different from the control groups.

To determine whether the difference in the positions of spots was due to early or late events, comparison was done between the numbers of events with proximal positions (earlier in development, 0–0.50) versus the numbers of events with distal positions (later in development, 0.51–1.0). A 2×3 contingency table analysis comparing wild-type, heterozygous and null revealed a highly statistically significant difference in the proportion of spots on the proximal half of the RPE ($\chi^2 = 32.09$, $P < 0.0001$). To verify that the difference was due to the null group, groups were analyzed pairwise. There was no significant difference between wild-type and heterozygous ($P = 0.865$), whereas the null group was significantly different from each of them ($P = 0.005$ and $P = 0.004$, respectively). Finally, 2×2 analysis was performed comparing the null group against the combined heterozygotes and wild-type, confirming a highly statistically significant difference ($\chi^2 = 17.86$, $P < 0.0001$), indicating that there is a shift of p^{un} reversion events to earlier in development. One interpretation of this result is that there is an increased rate of homologous recombination that occurs in the absence of PARP1.

Table 1. Summary of RPE examined and p^{un} reversion frequency by *Parp1* genotype

Genotype	No. of RPE	Total no. of spots	Average no. of spots/RPE	Average spot size (no. cells)
Parp1$^{+/+}$	42	287	6.8	3.5
Parp1$^{+/-}$	34	264	7.8	2
Parp1$^{-/-}$	28	545	19.5	6.2

Clonal expansion of p^{un} reversion events is associated with PARP1 absence

On initial analysis of the RPE, there appeared be a greater number of large (consisting of multiple cells) spots in the *Parp1*$^{-/-}$ RPE (Table 1). Previous studies have shown that spots with greater than 10 cells are very rare (28,30, Bishop, unpublished data). Therefore, a 2×3 contingency table analysis (Chi-square) was computed comparing the number of spots with 10 or fewer cells and the number of spots with 11 or more cells between genotypes ($\chi^2 = 32.65$, $P < 0.0001$, Figure 4). To determine if the null group is

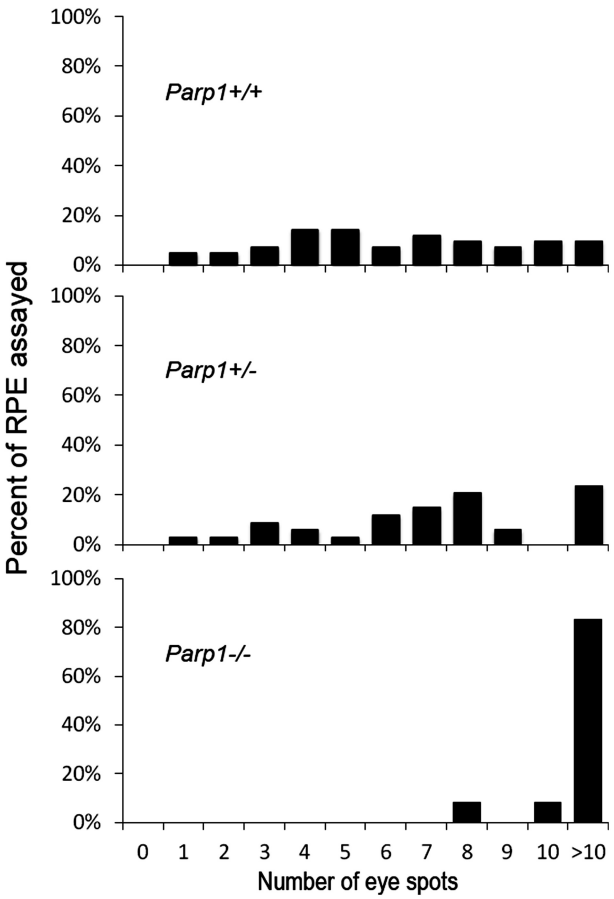

Figure 2. The frequency of p^{un} reversion events in the RPE (pigmented eye spots) in mice with differing *Parp1* genotypes. There is a highly statistically significant difference between the frequency of eye spots in *Parp1*$^{-/-}$ mice compared to wild-type and heterozygous controls ($P = 0.0001$ using the non-parametric Kruskal-Wallis test. A Dunn's test determined that the null group is different from the other two). The *x*-axis is expressed as whole number counts of eye spots, while the *y*-axis is expressed as percent of RPE assayed for that genotype. For example, over 80% of the *Parp1*$^{-/-}$ RPE had greater than 10 eye spots.

Figure 3. Positional distribution of spots in mice with differing *Parp1* genotypes. The position of an eyespot is a measurement relative to the optic nerve head. The position '0', which represents the optic nerve head, correlates to p^{un} reversion events that occurred relatively early in eye development. The position '1', which represents spots at the edge of the RPE, correlates to reversion events that occurred at a later time in eye development. Non-parametric analysis with a Kruskal–Wallis test ($P = 0.013$) followed by a Dunn's Test indicated that there is an increase in HRR more proximal to the optic nerve, and presumably earlier in eye development, in *Parp1* null mice compared to wild-type and heterozygous controls. Wild-type and heterozygous controls showed no difference, so data were combined in this graphical representation to compensate visually for disparity in sample sizes between the null group and either of the controls. The position (along the *x*-axis) and size (along the *y*-axis) of each individual eye spot is represented as a dot. The vertical marker delineates the position that is halfway between the optic nerve head and the edge of the RPE. The horizontal marker represents the divide between large and small eye spots and is therefore at the 11-cell size marker. Any dot on or above this line represents a 'large' eye spot.

the cause of statistical significance and because our frequency and positional analysis showed no difference between wild-type and heterozygous, the data for these two groups were combined and compared against the null group in a 2×2 contingency table analysis ($\chi^2 = 28.64$, $P < 0.0001$). These results indicate that there is a significant increase in the incidence of large spots in the *Parp1* null mice compared to controls, indicating an increase in HRR in proliferating cells.

To investigate whether a particular subset of spots (single cell or multi-cell) caused the observed shift in spots to an earlier time in development in *Parp1* null mice, a Kruskal–Wallis test was used to analyze the relative positions of these subsets of eye spots between genotypes. This test revealed that multi-cell eye spots are shifted toward the optic nerve in the null mice as compared to heterozygous and wild-type ($P = 0.0001$). Furthermore, analysis of the single-cell eye spots showed no difference between groups ($P = 0.5762$, Kruskal–Wallis test), indicating that the positional shift observed when analyzing all spots is in fact due to the multi-cell eye spots. Considering that the *Parp1* null mice display both an increase in the large eye spots and the position of these eye spots, we examined whether these large eye spots are significantly increased in the proximal half of the RPE in the absence of PARP1. A 2×2 contingency table analysis revealed that indeed there was a significant increase in large, multi-cell events ($\geq$11 cells) in the proximal half of the RPE in null mice compared to control RPE ($\chi^2 = 5.49$, $P = 0.019$, Figure 3). This suggests that many more highly replicative cells are prone to p^{un} reversion events during early RPE development in the absence of PARP1.

Loss of *Parp1* leads to an increase in RAD51 nuclear foci

It has been previously reported that human cells either deficient or inhibited for PARP1 have increased RAD51 nuclear foci, an indicator of increased HRR (16,17). To demonstrate that the same cellular phenomenon is observed here with the mouse *Parp1* knockout model, we examined spontaneous levels of RAD51 nuclear foci in MEFs isolated from these mice (Figure 5). As expected, the observed frequency of spontaneous RAD51 foci for wild-type MEFs displayed a very low background, mostly in the category of 0–5 RAD51 foci per cell. However, *Parp1* null MEFs showed a high number of cells with RAD51 foci with 68.3% having >6 foci per cell compared to wild-type MEFs (23.5%) ($P = 2.6e{-}29$). In addition, comparing 0 foci to either the 6–10 or >10 foci per cell groups demonstrates a significant increase in numbers of foci per cell in the *Parp1* null cells ($P = 3.3e{-}15$ and $P = 8.3e{-}25$, respectively). This data suggests a significantly higher frequency of HRR in

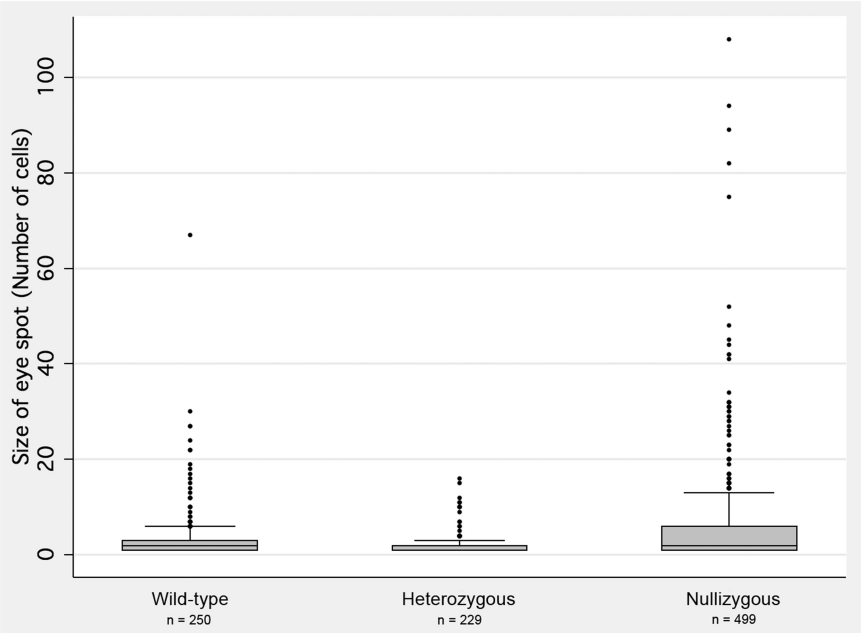

Figure 4. The size of eye spots in mice with differing *Parp1* genotypes**.** Eye spot size is expressed as the number of pigmented RPE cells comprising the eye spot (*y*-axis). A statistically significant increase in the number of large eye spots in *Parp1* null mice ($\chi^2 = 32.65$, $p < 0.0001$) compared to wild-type and heterozygous controls is shown by using a 2×3 contingency table. Comparison of null against combined wild-type and heterozygous data in a 2×2 contingency table also demonstrated a statistically significant difference in the null group ($\chi^2 = 28.64$, $p < 0.0001$).

Parp1 null MEFs compared to wild-type, correlating well with our *in vivo* p^{un} assay observations.

DISCUSSION

The inhibition of PARP1 activity is an exciting novel therapy used in the treatment of BRCA1 and BRCA2 hereditary breast and ovarian cancers (22). The mechanism by which this therapy is thought to work is by synthetic lethality resulting from an inability to repair SSBs by either PARP1-dependent SSB repair or BRCA1/2-dependent HRR (after replication fork stall/ collapse) (4,23,24). This model would suggest an increase in the spontaneous frequency of HRR in the absence of PARP1. *In vitro* evidence for a hyper-recombination phenotype has been presented in various tissue culture experiments (16,17,19–21). Here, we provide *in vivo* evidence that spontaneous HRR frequency is indeed increased in the absence of PARP1 protein by using an established mouse model for measuring HRR events. HRR dependent repair of SSBs has been proposed to be due to DNA replication fork collapse at the SSB that converts these lesions into HRR substrates. Our data supports this notion, with a significant increase in large clonal eye spots in the *Parp1* null background compared to controls. There is no selective advantage for p^{un} reversion, thus it is likely that similar somatic homologous recombination events are occurring in replicating cells throughout all tissues of the body and not just in the developing RPE and at the p^{un} locus.

The p^{un} HRR assay is based on the loss of one copy of a DNA duplication that encompasses exons 6–18 of the

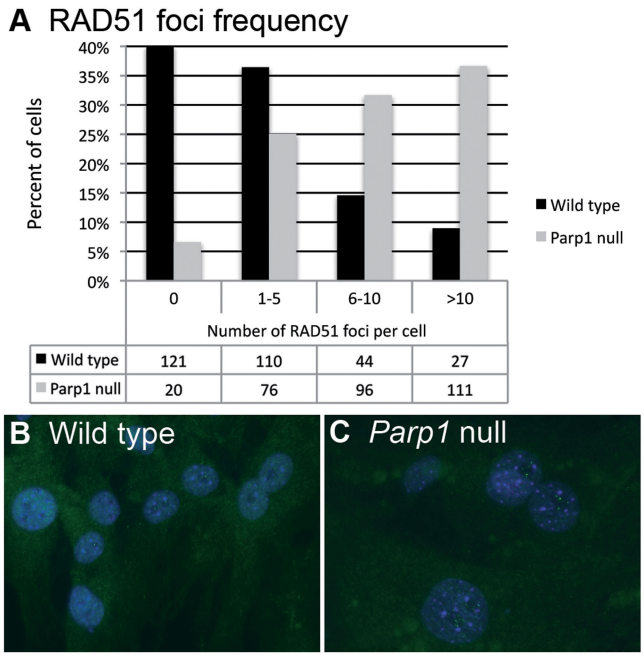

Figure 5. Spontaneous frequency of RAD51 nuclear foci in wild-type and *Parp1* null MEFs. (**A**) Frequency of RAD51 foci per cell by genotype categorized in 0, 1–5, 6–10 and >10 foci by *Parp1* genotype provided as a percentage of cells in the bar graph and actual numbers of cells in the table. There is a statistically significant increase in cells with RAD51 foci in *Parp1* null MEFs compared to wild-type MEFs (comparing 0–5 foci per cell to >6 foci, $P = 2.6e{-}29$). Furthermore, there are more RAD51 foci present per cell in the absence of PARP1. Representative field of cells with RAD51 foci positive cells are presented in (**B**) for wild-type and (**C**) for *Parp1* null MEFs. Blue is DAPI and green is RAD51, taken with a 40× objective.

p gene, restoring the function of this pigmentation gene. Theoretically the p^{un} reversion event, a homology directed deletion, may be mediated by either of two alternative mechanisms (36). First, there is the canonical, RAD51/BRCA1-dependent HRR pathway and is likely instigated by either a double-stranded DNA break or DNA replication fork collapse. The alternative homology-dependent repair pathway is SSA. SSA is a RAD51-independent pathway that can mediate intrachromosomal deletions between homologous DNA sequences, but is unlikely to be dependent upon the DNA replication process and is more likely to act in response to a double-stranded DNA break than an SSB-induced replication fork collapse (46,47). In contrast, RAD51-dependent HRR is considered a high fidelity DNA repair pathway and is likely a favored mechanism in replicating cells. Therefore, RAD51-dependent HRR provides the most obvious explanation for the observation that earlier p^{un} reversion events in proliferating cells will lead to larger eye spots.

Using the p^{un} assay, we previously reported that there is a significant increase in HRR in *Atm*, *p53* and *Gadd45a* null mice compared to controls (28). While these models showed differing shifts in the timing of events (position of eye spots) (28), the distribution of eye spot size was equivalent to wild-type (a majority of single cell eye spots, fewer two cell eye spots, and so forth, Bishop, unpublished data). In contrast, in the *Parp1* null mice we observed a significant increase in the number of multi-cell spots, particularly those greater than 10 cells (Figure 4). It is possible that different HRR pathways are at work in these different mutant mice, with a preference for replication-tied RAD51-dependent HRR events observed in PARP1 null mice.

It has already been postulated that the mechanism by which *Parp1* nullizygosity increases HRR is through replication fork collapse. Therefore, it is probable that it is the RAD51/BRCA1-dependent HRR pathway that results in the hyper-recombination phenotype we have observed in the *Parp1* null animals. In such a case, it would logically follow that more of the spots consist of a greater number of cells because the original cell in which the p^{un} reversion occurred was a proliferating cell; the daughter cells would have inherited the reverted *p* allele and thus will also be pigmented. However, in wild-type, as well as in *Atm*, *p53* and *Gadd45a* null mice, the majority of spots are single-cell events. These events follow the same general pattern of positions as larger spots, but with a phase shift toward the optic nerve. This relative distribution suggests that the single-cell events were likely to have occurred in cells that were in their terminal division at the rear of the proliferating region of the RPE (28). Therefore, it is possible that these single-cell events were not necessarily tied to active replication machinery, but rather could be due to SSA, in a DNA replication-independent manner. BRCA1-dependent HRR is thought necessarily to involve RAD51 (48) yet SSA is thought to be a RAD51-independent event (36). In support of this, we observe a significant increase in spontaneous nuclear RAD51 foci in the absence of PARP1. Though we cannot determine the proportion of p^{un} reversions that result from SSA events, it appears that the absence of PARP1 results in a clear increase in p^{un} reversion events that are tied to cellular proliferation and DNA replication. Overall, our observations provide formal evidence that the absence of PARP1 protein results in a spontaneous hyper-homologous recombination phenotype that supports the proposed mechanisms of PARP1 inhibition and BRCA1/2 null synthetic lethality.

ACKNOWLEDGEMENTS

The authors thank Ting Ting Gu for general technical support and Jo Ann Martinez for helping to establish the mouse lines. The authors also thank members of the Bishop lab for critical reading of the manuscript.

FUNDING

National Institutes of Health (K22ES012264 to A.J.R.B.); US Department of Defense Breast Cancer Research Program Predoctoral Traineeship Award (W81XWH-10-1-0026 to B.K.); Greehey Children's Cancer Research Institute's summer program (to C.B.). Funding for open access charge: Greehey Children's Cancer Research Institute.

Conflict of interest statement. None declared.

REFERENCES

1. Diefenbach,J. and Burkle,A. (2005) Introduction to poly(ADP-ribose) metabolism. *Cell. Mol. Life Sci.*, **62**, 721–730.
2. Simbulan-Rosenthal,C.M., Rosenthal,D.S., Boulares,A.H., Hickey,R.J., Malkas,L.H., Coll,J.M. and Smulson,M.E. (1998) Regulation of the expression or recruitment of components of the DNA synthesome by poly(ADP-ribose) polymerase. *Biochemistry*, **37**, 9363–9370.
3. Dantzer,F., Nasheuer,H.P., Vonesch,J.L., de Murcia,G. and Menissier-de Murcia,J. (1998) Functional association of poly(ADP-ribose) polymerase with DNA polymerase alpha-primase complex: a link between DNA strand break detection and DNA replication. *Nucleic Acids Res.*, **26**, 1891–1898.
4. Bryant,H.E., Petermann,E., Schultz,N., Jemth,A.S., Loseva,O., Issaeva,N., Johansson,F., Fernandez,S., McGlynn,P. and Helleday,T. (2009) PARP is activated at stalled forks to mediate Mre11-dependent replication restart and recombination. *EMBO J.*, **28**, 2601–2615.
5. Kim,M.Y., Zhang,T. and Kraus,W.L. (2005) Poly(ADP-ribosyl)ation by PARP-1: 'PAR-laying' NAD+ into a nuclear signal. *Genes Dev.*, **19**, 1951–1967.
6. d'Adda di Fagagna,F., Hande,M.P., Tong,W.M., Lansdorp,P.M., Wang,Z.Q. and Jackson,S.P. (1999) Functions of poly(ADP-ribose) polymerase in controlling telomere length and chromosomal stability. *Nat. Genet.*, **23**, 76–80.
7. Dantzer,F., Schreiber,V., Niedergang,C., Trucco,C., Flatter,E., De La Rubia,G., Oliver,J., Rolli,V., Menissier-de Murcia,J. and de Murcia,G. (1999) Involvement of poly(ADP-ribose) polymerase in base excision repair. *Biochimie*, **81**, 69–75.
8. Dantzer,F., de La Rubia,G., Menissier-De Murcia,J., Hostomsky,Z., de Murcia,G. and Schreiber,V. (2000) Base excision repair is impaired in mammalian cells lacking Poly(ADP-ribose) polymerase-1. *Biochemistry*, **39**, 7559–7569.
9. Herceg,Z. and Wang,Z.Q. (2001) Functions of poly(ADP-ribose) polymerase (PARP) in DNA repair, genomic integrity and cell death. *Mutat. Res.*, **477**, 97–110.

10. Almeida,K.H. and Sobol,R.W. (2007) A unified view of base excision repair: lesion-dependent protein complexes regulated by post-translational modification. *DNA Rep.*, **6**, 695–711.
11. de Murcia,G. and Menissier de Murcia,J. (1994) Poly(ADP-ribose) polymerase: a molecular nick-sensor. *Trends Biochem. Sci.*, **19**, 172–176.
12. Gradwohl,G., Menissier de Murcia,J.M., Molinete,M., Simonin,F., Koken,M., Hoeijmakers,J.H. and de Murcia,G. (1990) The second zinc-finger domain of poly(ADP-ribose) polymerase determines specificity for single-stranded breaks in DNA. *Proc. Natl Acad. Sci. USA*, **87**, 2990–2994.
13. Masson,M., Niedergang,C., Schreiber,V., Muller,S., Menissier-de Murcia,J. and de Murcia,G. (1998) XRCC1 is specifically associated with poly(ADP-ribose) polymerase and negatively regulates its activity following DNA damage. *Mol. Cell. Biol.*, **18**, 3563–3571.
14. Satoh,M.S. and Lindahl,T. (1992) Role of poly(ADP-ribose) formation in DNA repair. *Nature*, **356**, 356–358.
15. Godon,C., Cordelieres,F.P., Biard,D., Giocanti,N., Megnin-Chanet,F., Hall,J. and Favaudon,V. (2008) PARP inhibition versus PARP-1 silencing: different outcomes in terms of single-strand break repair and radiation susceptibility. *Nucleic Acids Res.*, **36**, 4454–4464.
16. Schultz,N., Lopez,E., Saleh-Gohari,N. and Helleday,T. (2003) Poly(ADP-ribose) polymerase (PARP-1) has a controlling role in homologous recombination. *Nucleic Acids Res.*, **31**, 4959–4964.
17. Yang,Y.G., Cortes,U., Patnaik,S., Jasin,M. and Wang,Z.Q. (2004) Ablation of PARP-1 does not interfere with the repair of DNA double-strand breaks, but compromises the reactivation of stalled replication forks. *Oncogene*, **23**, 3872–3882.
18. Waldman,A.S. and Waldman,B.C. (1991) Stimulation of intrachromosomal homologous recombination in mammalian cells by an inhibitor of poly(ADP-ribosylation). *Nucleic Acids Res.*, **19**, 5943–5947.
19. Oikawa,A., Tohda,H., Kanai,M., Miwa,M. and Sugimura,T. (1980) Inhibitors of poly(adenosine diphosphate ribose) polymerase induce sister chromatid exchanges. *Biochem. Biophys. Res. Commun.*, **97**, 1311–1316.
20. de Murcia,J.M., Niedergang,C., Trucco,C., Ricoul,M., Dutrillaux,B., Mark,M., Oliver,F.J., Masson,M., Dierich,A., LeMeur,M. *et al.* (1997) Requirement of poly(ADP-ribose) polymerase in recovery from DNA damage in mice and in cells. *Proc. Natl Acad. Sci. USA*, **94**, 7303–7307.
21. Meyer,R., Muller,M., Beneke,S., Kupper,J.H. and Burkle,A. (2000) Negative regulation of alkylation-induced sister-chromatid exchange by poly(ADP-ribose) polymerase-1 activity. *Int. J. Cancer*, **88**, 351–355.
22. Fong,P.C., Boss,D.S., Yap,T.A., Tutt,A., Wu,P., Mergui-Roelvink,M., Mortimer,P., Swaisland,H., Lau,A., O'Connor,M.J. *et al.* (2009) Inhibition of poly(ADP-ribose) polymerase in tumors from BRCA mutation carriers. *N Engl. J. Med.*, **361**, 123–134.
23. Farmer,H., McCabe,N., Lord,C.J., Tutt,A.N., Johnson,D.A., Richardson,T.B., Santarosa,M., Dillon,K.J., Hickson,I., Knights,C. *et al.* (2005) Targeting the DNA repair defect in BRCA mutant cells as a therapeutic strategy. *Nature*, **434**, 917–921.
24. Turner,N., Tutt,A. and Ashworth,A. (2005) Targeting the DNA repair defect of BRCA tumours. *Curr. Opin. Pharmacol.*, **5**, 388–393.
25. Bhattacharyya,A., Ear,U.S., Koller,B.H., Weichselbaum,R.R. and Bishop,D.K. (2000) The breast cancer susceptibility gene BRCA1 is required for subnuclear assembly of Rad51 and survival following treatment with the DNA cross-linking agent cisplatin. *J. Biol. Chem.*, **275**, 23899–23903.
26. Moynahan,M.E., Chiu,J.W., Koller,B.H. and Jasin,M. (1999) Brca1 controls homology-directed DNA repair. *Mol. Cell.*, **4**, 511–518.
27. Moynahan,M.E., Pierce,A.J. and Jasin,M. (2001) BRCA2 is required for homology-directed repair of chromosomal breaks. *Mol. Cell.*, **7**, 263–272.
28. Bishop,A.J., Hollander,M.C., Kosaras,B., Sidman,R.L., Fornace,A.J. Jr and Schiestl,R.H. (2003) Atm-, p53-, and Gadd45a-deficient mice show an increased frequency of homologous recombination at different stages during development. *Cancer Res.*, **63**, 5335–5343.
29. Bishop,A.J., Kosaras,B., Carls,N., Sidman,R.L. and Schiestl,R.H. (2001) Susceptibility of proliferating cells to benzo[a]pyrene-induced homologous recombination in mice. *Carcinogenesis*, **22**, 641–649.
30. Bishop,A.J., Kosaras,B., Sidman,R.L. and Schiestl,R.H. (2000) Benzo(a)pyrene and X-rays induce reversions of the pink-eyed unstable mutation in the retinal pigment epithelium of mice. *Mutat. Res.*, **457**, 31–40.
31. Brilliant,M.H. (2001) The mouse p (pink-eyed dilution) and human P genes, oculocutaneous albinism type 2 (OCA2), and melanosomal pH. *Pigment Cell Res.*, **14**, 86–93.
32. Brilliant,M.H., Gondo,Y. and Eicher,E.M. (1991) Direct molecular identification of the mouse pink-eyed unstable mutation by genome scanning. *Science*, **252**, 566–569.
33. Gondo,Y., Gardner,J.M., Nakatsu,Y., Durham-Pierre,D., Deveau,S.A., Kuper,C. and Brilliant,M.H. (1993) High-frequency genetic reversion mediated by a DNA duplication: the mouse pink-eyed unstable mutation. *Proc. Natl Acad. Sci. USA*, **90**, 297–301.
34. Oakey,R.J., Keiper,N.M., Ching,A.S. and Brilliant,M.H. (1996) Molecular analysis of the cDNAs encoded by the pun and pJ alleles of the pink-eyed dilution locus. *Mamm. Genome*, **7**, 315–316.
35. Melvold,R.W. (1971) Spontaneous somatic reversion in mice. Effects of parental genotype on stability at the p-locus. *Mutat. Res.*, **12**, 171–174.
36. Ira,G. and Haber,J.E. (2002) Characterization of RAD51-independent break-induced replication that acts preferentially with short homologous sequences. *Mol. Cell. Biol.*, **22**, 6384–6392.
37. Bodenstein,L. and Sidman,R.L. (1987) Growth and development of the mouse retinal pigment epithelium. II. Cell patterning in experimental chimaeras and mosaics. *Dev. Biol.*, **121**, 205–219.
38. Wang,Z.Q., Auer,B., Stingl,L., Berghammer,H., Haidacher,D., Schweiger,M. and Wagner,E.F. (1995) Mice lacking ADPRT and poly(ADP-ribosyl)ation develop normally but are susceptible to skin disease. *Genes Dev.*, **9**, 509–520.
39. Busuttil,R.A., Munoz,D.P., Garcia,A.M., Rodier,F., Kim,W.H., Suh,Y., Hasty,P., Campisi,J. and Vijg,J. (2008) Effect of Ku80 deficiency on mutation frequencies and spectra at a LacZ reporter locus in mouse tissues and cells. *PLoS ONE*, **3**, e3458.
40. Hartley,H.O. (1950) The use of range in analysis of variance. *Biometrika*, **37**, 271–280.
41. Rohlf,F.J. and Sokal,R.R. (1995) *Statistical Tables*, 3rd edn. Freeman and Company, New York.
42. Siegel,S. and Castellan,N.J. (1956) *Non-Parametric Statistics for Behavioral Sciences*. McGraw Hill, New York.
43. Fisher,R. (1922) On the interpretation of $\chi 2$ from contingency tables, and the calculation of P. *J. Roy. Statist. Soci.*, **85**, 87–94.
44. Bryant,H.E., Schultz,N., Thomas,H.D., Parker,K.M., Flower,D., Lopez,E., Kyle,S., Meuth,M., Curtin,N.J. and Helleday,T. (2005) Specific killing of BRCA2-deficient tumours with inhibitors of poly(ADP-ribose) polymerase. *Nature*, **434**, 913–917.
45. Bodenstein,L. and Sidman,R.L. (1987) Growth and development of the mouse retinal pigment epithelium. I. Cell and tissue morphometrics and topography of mitotic activity. *Dev. Biol.*, **121**, 192–204.
46. Galli,A. and Schiestl,R.H. (1998) Effect of Salmonella assay negative and positive carcinogens on intrachromosomal recombination in S-phase arrested yeast cells. *Mutat. Res.*, **419**, 53–68.
47. Galli,A. and Schiestl,R.H. (1998) Effects of DNA double-strand and single-strand breaks on intrachromosomal recombination events in cell-cycle-arrested yeast cells. *Genetics*, **149**, 1235–1250.
48. Cousineau,I., Abaji,C. and Belmaaza,A. (2005) BRCA1 regulates RAD51 function in response to DNA damage and suppresses spontaneous sister chromatid replication slippage: implications for sister chromatid cohesion, genome stability, and carcinogenesis. *Cancer Res.*, **65**, 11384–11391.

[CANCER RESEARCH 63, 5335–5343, September 1, 2003]

Atm-, p53-, and Gadd45a-Deficient Mice Show an Increased Frequency of Homologous Recombination at Different Stages during Development[1]

Alexander J. R. Bishop,[2] M. Christine Hollander, Bela Kosaras, Richard L. Sidman, Albert J. Fornace, Jr., and Robert H. Schiestl[3]

Department of Genetics and Howard Hughes Medical Institute, Harvard Medical School, Boston, Massachusetts 02115 [A. J. R. B.]; National Institutes of Health, National Cancer Institute, Bethesda, Maryland 20892 [M. C. H., A. F.]; Department of Neurology, Beth Israel Deaconess Medical Center, Harvard Institutes of Medicine, Boston, Massachusetts 02115 [B. K., R. L. S.]; and Department of Pathology, University of California at Los Angeles School of Medicine, Los Angeles, California 90095 [R. H. S.]

ABSTRACT

Atm, p53, and Gadd45a form part of a DNA-damage cellular response pathway; the absence of any one of these components results in increased genomic instability. We conducted an *in vivo* examination of the frequency of spontaneous homologous recombination in Atm-, p53-, or Gadd45a-deficient mice. In the absence of p53, we observed the greatest increase in events, a lesser increase in the absence of Atm, and only a modest increase in the absence of Gadd45a. The striking observation was the difference in the time at which the spontaneous events occurred in *atm* and *trp53* mutant mice. The frequency of homologous recombination in *atm* mutant mice was increased later during development. In contrast, p53 appears to have a role in suppressing homologous recombination early during development, when p53 is known to spontaneously promote p21 activity. The timing of the increased spontaneous recombination was similar in the Gadd45a- and p53-deficient mice. This temporal resolution suggests that Atm and p53 can act to maintain genomic integrity by different mechanisms in certain *in vivo* contexts.

INTRODUCTION

After cellular DNA damage, cells respond to and often repair the damage in an orchestrated manner. One signaling pathway that has been demonstrated to play a key role is the Trp53 (p53) damage response pathway (1–5). After the activation and stabilization of p53, p53 plays a central part in the type of responses that cells mount to a variety of damages. These responses include apoptosis, cell cycle arrest and DNA repair (reviewed in Ref. 6). It is now understood that p53 is normally maintained at a level within the cell that does not result in any significant transcriptional activation of its downstream effectors.

Atm is a protein kinase (7–9) that is activated in the cell after ionizing radiation exposure (10, 11). It is now clear that Atm has many targets (for a review see Ref. 12), among them is p53, which is effected both directly (2, 13–17) and indirectly (18–20). p53 can subsequently transcriptionally up-regulate effectors such as Cdkn1a (p21; see Ref. 21) and Gadd45a (2) to produce a coordinated cellular response. The up-regulation of p21 results in a cell cycle arrest at the G_1-S border (21–27), which is thought to allow time for repair reactions to be enacted. In what manner any repair reaction is controlled by p53 is not fully understood, although the absence of p53 or Gadd45a has been related to a decreased level of nucleotide excision repair (28). From the point of view of this report, it is interesting to note that the absence of the p53 damage response pathway components Atm (29–34), p53 (35, 36), or Gadd45a (37) has been observed to confer an increased level of genomic instability.

Our understanding of recombination is that there are a number of different types of recombination mechanisms, broadly divided into HR[4] and nonhomologous endjoining. HR is mediated by regions of homologous DNA and is the basis of the assay used in this study.

To determine the frequency of HR *in vivo*, we identified the number of cells or clones of cells that had deleted a 65-kb DNA duplication to a single copy (see Fig. 1). The duplication allele, called pink-eyed unstable (p^{un}; see Refs. 38, 39), interrupts the murine pigmentation gene, pink-eyed dilution (*p*). In the absence of a functional *p* gene, mice have pink eyes and a dilute coat color (40). Only a HR event will result in the correct reconstitution of the *p* gene and the phenotypic pigmentation that is assayed (38, 39). Molecular analysis has confirmed that these events are the result of p^{un} reversion (38, 39, 41). The *p* gene is normally transcribed in melanocytes and cells of the RPE, so that when a deletion/reversion event of p^{un} occurs somatically in a precursor of a melanocyte or RPE cell, this cell will proliferate and differentiate into a clone of pigmented cells. Such patches or spots have been observed in both the fur (38, 41) and eyes (42–44) of p^{un} mice. On the C57BL/6J inbred background, approximately 5–10% of p^{un} mice spontaneously display visible fur-spots (38, 41) and 4 to 5 eyes-pots are observed per RPE (44, 45).

Deletions reverting the p^{un} allele to p^{+} resulting in fur spots (fur-spot assay) are increased in frequency after exposure to different DNA-damaging agents (41, 46, 47), as well as in different cancer predisposing genetic backgrounds (34, 48). In those *in vivo* studies, *atm* mutant mice had an increased frequency of recombination (34), whereas the *trp53* mutant mice did not (49). This was surprising because a number of tissue culture studies with p53-deficient cells have demonstrated an increased frequency of recombination (50–54). To address this issue, we developed the p^{un} eye-spot assay. This assay has already proven to be more sensitive in detecting the frequency of recombination after exposure to DNA-damaging agents than the fur-spot assay (45). In addition, we demonstrated that because of the well-defined developmental pattern of the RPE (55), we were able to define the time at which a recombination event occurred by its position within the RPE (56). Here we use the p^{un} eye-spot assay to examine the frequency of spontaneous recombination in mice deficient for Atm, p53, or Gadd45a. The results demonstrated an increased frequency of HR in all three genetic backgrounds, but the timing of the instability was different between Atm-deficient and p53- or Gadd45a-deficient mice. This study confirms our earlier suggestion of an increased frequency of HR in *atm* mutant mice, while demonstrating that *trp53* and *gadd45a* mutant mice also display an increased frequency of HR early during development.

Received 12/18/02; revised 5/22/03; accepted 6/26/03.

The costs of publication of this article were defrayed in part by the payment of page charges. This article must therefore be hereby marked *advertisement* in accordance with 18 U.S.C. Section 1734 solely to indicate this fact.

[1] Supported by grants from the National Institute of Environmental Health Sciences, NIH, RO1 Grant ES09519 and KO2 Award ES00299 (to R. H. S.), NIH RCDA Award F32GM19147 (to A. J. R. B.), and an A-T Children's Fund award (to B. K. and R. L. S.).

[2] To whom requests for reprints should be addressed, at Department of Genetics, Harvard Medical School, 200 Longwood Avenue, Boston, MA 02115. Phone: (617) 432-7553; Fax: (617) 432-7663; E-mail: abishop@genetics.med.harvard.edu.

[3] To whom requests for reprints should be addressed, at Department of Pathology, UCLA School of Medicine, 650 Charles E. Young Drive South, Los Angeles, CA 90095. Phone: (310) 267-2087; Fax: (310) 267-2578; E-mail: rschiestl@mednet.ucla.edu.

[4] The abbreviations used are: HR, homologous recombination; RPE, retinal pigment epithelium; dpc, days post coitum.

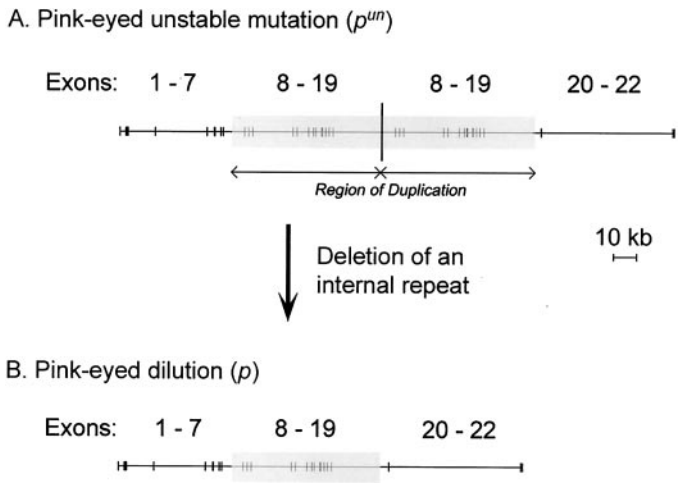

Fig. 1. A schematic representation of the pink-eyed unstable mutation (p^{un}; *A*) and the wild-type gene pink-eyed dilution (*p*; *B*). The publicly available murine sequences for the wild-type gene were obtained from the NIH (Internet address: www.ncbi.nlm.nih.gov/cgi-bin/Entrez/map_srchdb?chr = mouse_chr.inf). The duplication junction sequenced identified previously (39) were identified within the genomic region to generate the schematic. The duplication was found to include sequences from within intron 7 to within intron 19, spanning ~65 kb. The sequence representations are drawn to scale, a *10-kb scale bar* is given. The translation start is in exon 3 and, assuming correct splicing of all exons, the duplication will result in the insertion of a novel alanine created at the junction of exons 19 and 8, followed by 433 amino acids of the duplicated exons 8 to 19. After deletion of one of the internal repeats by HR, a functional protein can be produced and will result in pigmentation in either melanocytes or cells of the RPE.

MATERIALS AND METHODS

Mice. C57BL/6J- $p^{un/un}$ mice were obtained from the Jackson Laboratory (Bar Harbor, ME). C57BL/6J $p^{un/un}$ *Atm* $^{+/-}$ and C57BL/6J $p^{un/un}$ *Trp53*$^{+/-}$ have been described previously (34, 49). Mice heterozygous for *Atm* or *Trp53* and homozygous for p^{un} were bred to generate mice of all three *Atm* or *Trp53* genotypes. *Gadd45a* mutant mice (37) were bred into the C57BL/6J $p^{un/un}$ genetic background with three back-crosses to produce C57BL/6J-$p^{un/un}$ *Gadd45a*$^{-/-}$ mice that were maintained. In the generation of this colony, C57BL/6J-$p^{un/un}$ *Gadd45a*$^{+/+}$ mice were also produced and maintained as a control. All mice were bred in the institutional animal facility under standard conditions with a 12-h light/dark cycle and were fed standard diet and water *ad libitum*. The $p^{un/un}$ genotype was observed phenotypically in the progeny of the second back-cross as mice with a dilute (gray) coat color.

PCR Genotype. The *Atm*, *Trp53*, and *Gadd45* genotypes were determined by PCR amplification as described previously (34, 37, 49). DNA was prepared from tail biopsies by standard protocols.

Dissection of the RPE. Eyes from sacrificed 20-day-old mice were removed, fixed, and dissected to expose the RPE layer, as described previously (45, 55). The RPE adjacent to the neural retina was isolated for analysis by removing the eye from its orbit, immersing it in fixative [4% paraformaldehyde in 0.1 M phosphate buffer (pH 7.4)] for 1 h and then in PBS until dissection. An incision was made at the upper corneo-scleral border to allow removal of the cornea and lens. Six to eight incisions were made into the eyecup from the corneo-scleral margin toward the centrally positioned optic nerve. The dissected eyecup was placed on a glass slide with the retina facing up. The retina was then gently removed and the flattened eyecup, with RPE facing up, was mounted in 90% glycerol for analysis.

Scoring a Single-Reversion Event, Visualized As an Eye-Spot. We defined two or more adjacent pigmented cells, or pigmented cells separated from each other by no more than one unpigmented cell, as an eye-spot that resulted from one reversion event (55). The number of eye-spots in each RPE and the number of cells that comprised each eye-spot were counted. Positions of eye-spots were mapped.

Distance Analysis of Eye-Spots from the Optic Nerve. Spots were identified under the microscope and compared with their scanned digital images. Distances were measured with the Adobe PhotoShop 5.5 Measurement Tool. Distances were converted from pixels to millimeters by counting the number of pixels per millimeter on the image of a micron scale reticule scanned at the same optical settings as the RPE. Two distances were measured for each eye-spot: the "eye-spot distance," the distance from the center of the optic nerve head to the most proximal edge of the eye-spot; and the "RPE distance" of an eye-spot, the distance from the optic nerve through the eye-spot to the outer edge of the RPE. Dividing the eye-spot distance by the RPE distance gave the proportional distance of each eye-spot from the outer edge of the RPE, or its "position." The position of each eye-spot was determined in this manner to compensate for differences in the size of the eyes.

Microscope, Digital Camera, and Software. Whole-mount RPE were scanned by a DC120 digital camera (Eastman Kodak Company) mounted on a DMLB microscope (Leica Microsystems, Inc., Wetzlar, Germany) using a ×2.5 N-plan objective. Embryonic sections were scanned by a RT Slider Spot camera (Diagnostic Instruments, Inc., MI) mounted on a Axioskop microscope (Zeiss, Göttingen, Germany). The images were assembled and examined in Adobe PhotoShop 5.5 on a Macintosh Power Computer. All data were stored and processed with Microsoft Excel 2001.

Statistical Analysis. Comparison between numbers of events was performed by a standard *G* test (57). The *G* test is equivalent to a contingency χ^2 test, but allows for classes with zero events. Comparison of the population of events per RPE between genotypes was performed by Wilcoxon rank-sum analysis (58, 59).

RESULTS

Eye-Spot Frequency. An examination was conducted on the p^{un} reversion frequency in the RPE. The C57BL/6J- $p^{un/un}$ *Atm*$^{+/+}$, C57BL/6J- $p^{un/un}$ *Trp53*$^{+/+}$ and C57BL/6J- $p^{un/un}$ colonies described in previously reported concurrently performed studies (45, 56) were not maintained separately, and comparison of the wild-type retinal pigment epithelia revealed no significant difference in p^{un} reversion frequency or pattern (data not shown). The *Gadd45a* mouse colony was maintained separately; therefore, an extensive analysis was performed to compare the RPE of that colony with the rest of the wild-type controls. Of all of the analyses performed, a significant difference was only found by the relative positional distribution of events ($Z = 2.4$; $P_{(z)} \geq 0.015$). Taking this minor difference into account, we performed all further analyses for the *Gadd45a* colony separately from the other colonies and their wild-type controls.

The reversion frequency of the p^{un} locus was determined for 20 C57BL/6J- $p^{un/un}$ *Atm*$^{-/-}$, 16 C57BL/6J- $p^{un/un}$ *Trp53*$^{-/-}$, 40 C57BL/6J- $p^{un/un}$ combined wild-type control, 32 C57BL/6J- $p^{un/un}$ *Gadd45a*$^{-/-}$, and 26 C57BL/6J- $p^{un/un}$ *Gadd45a*$^{+/+}$ control RPE (see Table 1). One unexpected observation that came from this analysis was that 2 of the 16 RPE obtained from C57BL/6J- $p^{un/un}$ *Trp53*$^{-/-}$

Table 1 *Summary of eye-spot and pigmented cell frequency*

	Totals			Averages					
Genotype	RPE	Cells[a]	Spots	Cells[a] RPE	± SD	spots (*n*)	± SD	Spot Size[b]	± SD
Wildtype control	40	610	242	16.3	11.2	6.1	3.5	2.6	3.1
Gadd45a control	26	621	157	24.1	25.7	6.0	2.8	4.0	8.9
atm mutant	20	425	188	21.3	9.5	9.4	3.2	2.3	2.5
trp53 mutant	16	1265	255	79.1	145.4	15.9	17.4	5.0	7.0
gadd45a mutant	32	1260	283	39.4	150.6	8.8	13.8	4.5	7.8

[a] Pigmented cells.
[b] Spot size in number of pigmented cells.

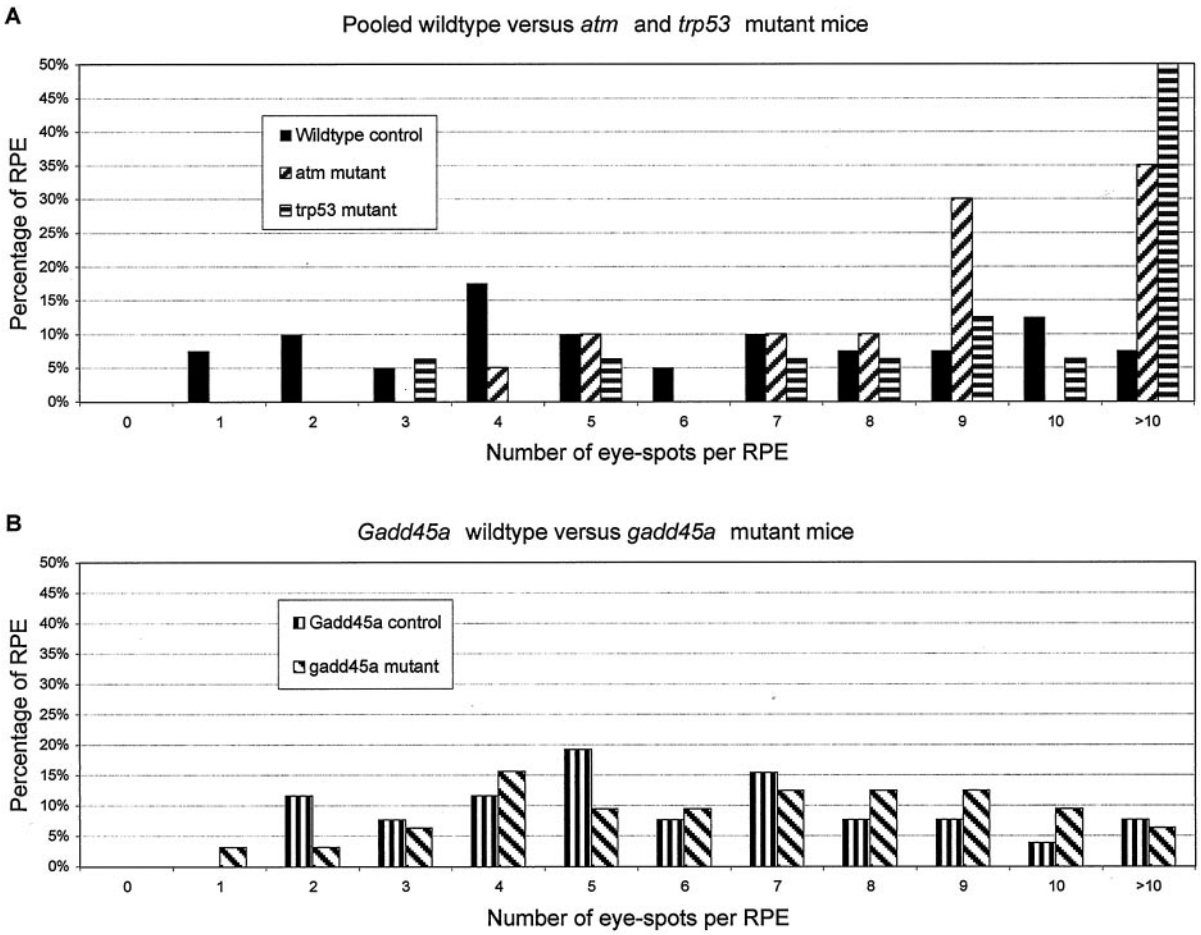

Fig. 2. Comparison of the number of eye-spots found per RPE in the each mutant genotype with their relevant control. *A*, a graphical representation of eye-spot frequency per RPE of *atm* and *trp53* mutant mice compared with the wild-type control. The majority of RPE obtained from the *atm* and *trp53* mutant mice have more than nine eye-spots, where the majority of wild-type control RPE have fewer than seven eye-spots. This difference is highly significant for both genotypes. *B*, a graphical representation of eye-spot frequency per RPE of *gadd45a* mutant mice compared with the *Gadd45a* control. There is no significant difference in the pattern of eye-spot frequency between these genotypes, although *Gadd45a* control RPE have six eye-spots on average whereas *gadd45a* mutant RPE have nine.

mice and 1 of 32 RPE obtained from C57BL/6J- $p^{un/un}$ *Gadd45a*$^{-/-}$ mice had what appeared to be a very early reversion events, possibly in progenitor RPE cells, resulting in many eye-spots. No such event has been observed in the 40 combined control RPE examined to date, nor the 26 C57BL/6J- $p^{un/un}$ *Gadd45a*$^{+/+}$, the additional 20 *Atm*$^{-/-}$ derived RPE reported here, or the 45 RPE obtained after either X-ray or benzo(*a*)pyrene exposure previously reported (45, 56). The frequency of such an early event in the *Trp53*$^{-/-}$ was significantly different from the combined control ($G = 5.199878$; $P_{(G)} \geq 0.023$), although the frequency observed for the *Gadd45a*$^{-/-}$ was not significantly different from the *Gadd45a* control ($G = 1.203654$; $P_{(G)} \geq 0.27$). The observation of these types of event is already indicative of an increased level of HR early in the development of the RPE in these genetic backgrounds.

The average number of reverted (pigmented) cells per RPE, eye-spots per RPE, and eye-spot size for all genotypes were determined (see Table 1). On average, all three mutant backgrounds had more reverted RPE cells and eye-spots compared with their controls, but only *trp53* and *gadd45a* mutant mice had an increased average eye-spot size. Because the SD in these analyses was similar to the average, a more correct method to examine the distribution of reversion frequency between the control and the mutant genotypes was to compare the distribution of RPE with a particular number of events, as shown graphically in Fig. 2. Performing a rank-sum analysis of these distributions demonstrated a significant difference between the pooled wild-type control and both *atm* and *trp53* mutant mice (see Fig. 2*A*; *atm* mutant mice: $Z = -3.2$; $P_{(Z)} \geq 0.0013$; *trp53* mutant mice: $Z = -3.6$; $P_{(Z)} \geq 0.0003$). The difference between *Gadd45a* wild-type and mutant mice was not significant (see Fig. 2*B*; *gadd45a* mutant mice: $Z = 0.9$; $P_{(Z)} \geq 0.37$). Therefore, after examining the overall frequency of spontaneous HR events, it was apparent that the *atm* and *trp53* mutant backgrounds displayed a greatly increased level of HR that was not observed in the *gadd45a* mutant background.

Examining the Frequency of Different Sized Eye-Spots. Eye-spots were categorized by size, that is, the number of reverted cells that constitute them. Previous reports have noted that the majority of eye-spots consisted of a single pigmented cell, with fewer two-cell eye-spots, even fewer three-cell eye-spots, and so on (44, 45, 56). We observed no difference in these ratios for either the *atm* mutant mice ($Z = 1.5$; $P_{(Z)} \geq 0.15$) or the *gadd45a* mutant mice ($Z = -0.2$; $P_{(Z)} \geq 0.85$) and their relevant controls (see Fig. 3, *B* and *D*, respectively). In contrast, *trp53* mutant mice had a significantly different eye-spot size distribution from both the pooled control ($Z = -4.1$; $P_{(Z)} \geq 4.2 \times 10^{-5}$) and even more so from the *atm* mutant mice ($Z = -5.1$; $P_{(Z)} \geq 3.3 \times 10^{-7}$). This size redistribution indicates that in the *trp53* mutant mice, more HR events occurred in cells that were likely to continue proliferating than was observed with either Atm-deficient or control mice. It is clear, however, that all three mutant backgrounds displayed an increased frequency of each sized eye-spot compared with their control (see Fig. 3, *A* and *C*).

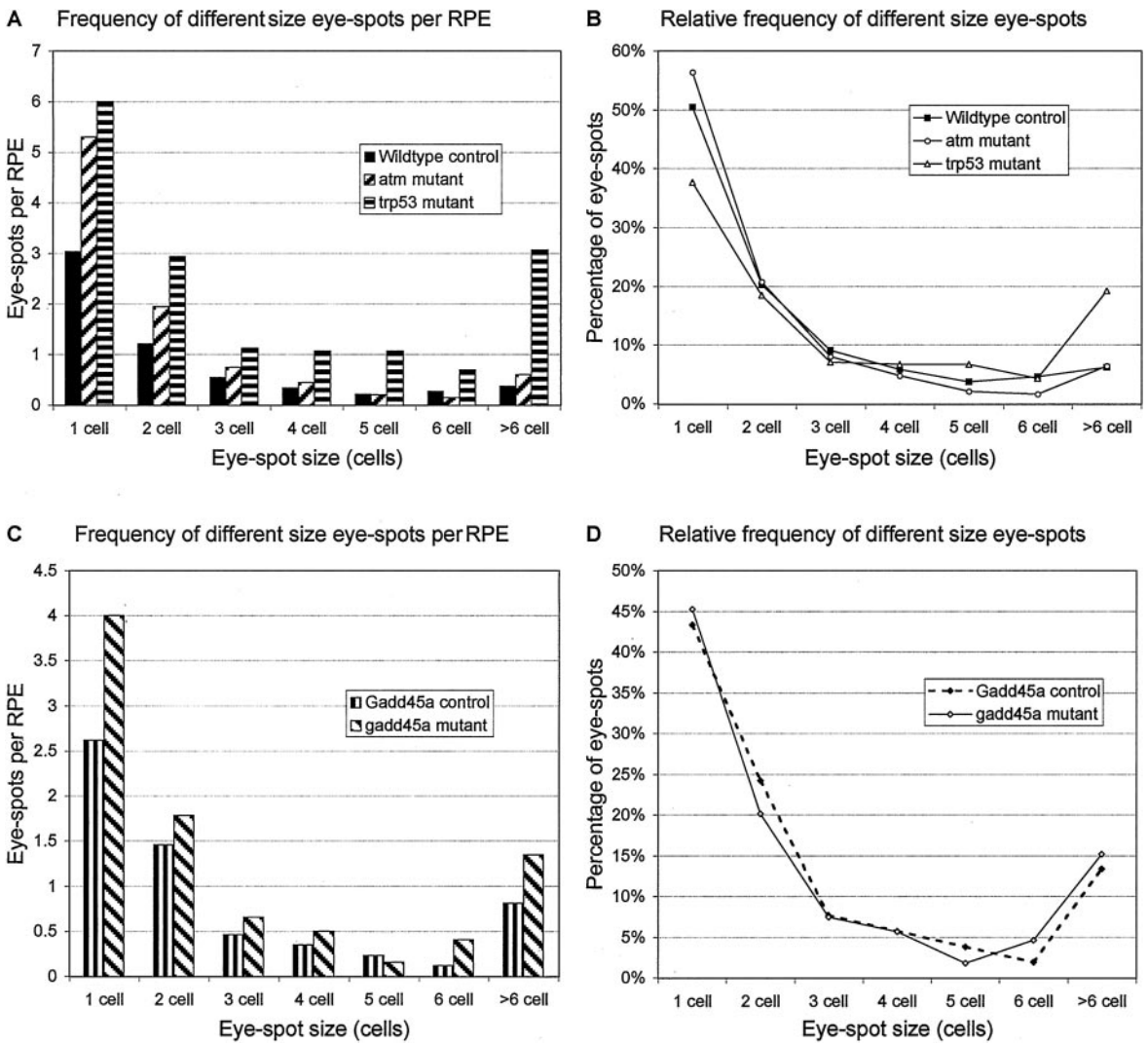

Fig. 3. Frequency and relative frequency of different size eye-spots in the RPE of the mutant mouse genotypes and their relevant controls. Eye-spot size is determined by the number of pigmented cells in the eye-spot. *A*, the frequency of different size eye-spots per RPE in *atm* and *trp53* mutant mice and the wild-type control. For all sizes of eye-spot, there is an increased frequency per RPE for both genotypes over the control. *B*, the relative frequency of each size eye-spot per RPE as a proportion of all of the other eye-spots found in *atm* and *trp53* mutant mice and the wild-type control. In both the control wild-type and *atm* mutant RPE >50% of the eye-spots consisted of only a single cell. Although *trp53* mutant RPE also displayed a majority of singlet eye-spots, there were proportionally more larger eye-spots. *C*, the frequency of different size eye-spots per RPE in *gadd45a* mutant mice and the *Gadd45a* control. The *gadd45a* mutant RPE had more of each size eye-spot per RPE than the control. *D*, the relative frequency of each size eye-spot per RPE as a proportion of all of the other eye-spots found in *gadd45a* mutant mice and the *Gadd45a* control. The distribution of the eye-spot sizes appear to be the same between this mutant genotype and its control.

Examining the Positional Distribution of Eye-Spots in the RPE. We examined the frequency of eye-spots located in different position intervals for the different mutant backgrounds and their relevant controls (see Figs. 4*A* and 5*A*). The data obtained are displayed either as a frequency per RPE over positional intervals or as a relative frequency distribution that more clearly illustrates the pattern of recombination frequency by position. To determine whether there was any significant difference between the positional distributions of these eye-spots in different genotypes, rank-sum analyses were performed. Because we determined previously that the pattern of eye-spots can be resolved into two populations, eye-spots consisting of a single pigmented cell (singlets) and larger eye-spots (56), with distinguishable distribution patterns, larger eye-spots generally lying more distal to the optic nerve head than the singlets (56), any positional analysis benefits from the individual consideration of each type of eye-spot population. The distributions of singlet (see Figs. 4*B* and 5B) and larger eye-spots (see Figs. 4*C* and 5*C*) are also given.

The *atm* mutant mice had an ~30% increase in the frequency of events compared with the wild-type control for each position examined (see Fig. 4*A*). The greatest increase in frequency of events was found in the singlet eye-spot class, as compared with the control (compare eye-spot frequency for *atm* mutant mice in Fig. 4, *C* and *E*). The most interesting aspect of these results, however, is that the overall distribution of these HR events was the same as the distribution found in the wild-type control (Fig. 4*B*; $Z = 0.4$; $P_{(Z)} \geq 0.66$). The same was found to be true with both the singlet (Fig. 4, *C* and *D*; $Z = -0.2$; $P_{(Z)} \geq 0.86$) and larger (Fig. 4, *E* and *F*; $Z = 0.7$; $P_{(Z)} \geq 0.48$) eye-spot populations. These results suggest that although there is an increased amount of HR in the *atm* mutant mouse, the timing and types of event is directly comparable with the pattern observed for wild-type mice.

The *trp53* mutant mice had an increased frequency of events at all positions compared with the wild-type control, irrespective of whether examining all eye-spots, the singlets or the larger eye-spots (see Fig. 4, *A*, *C*, and *E*, respectively). The largest increase in events was observed in the optical nerve head proximal region, leading to a significant redistribution in the relative positional pattern of HR events (all eye-spots, Fig. 4*B*: $Z = 6.0$, $P_{(Z)} \geq 2.4 \times 10^{-9}$; singlets,

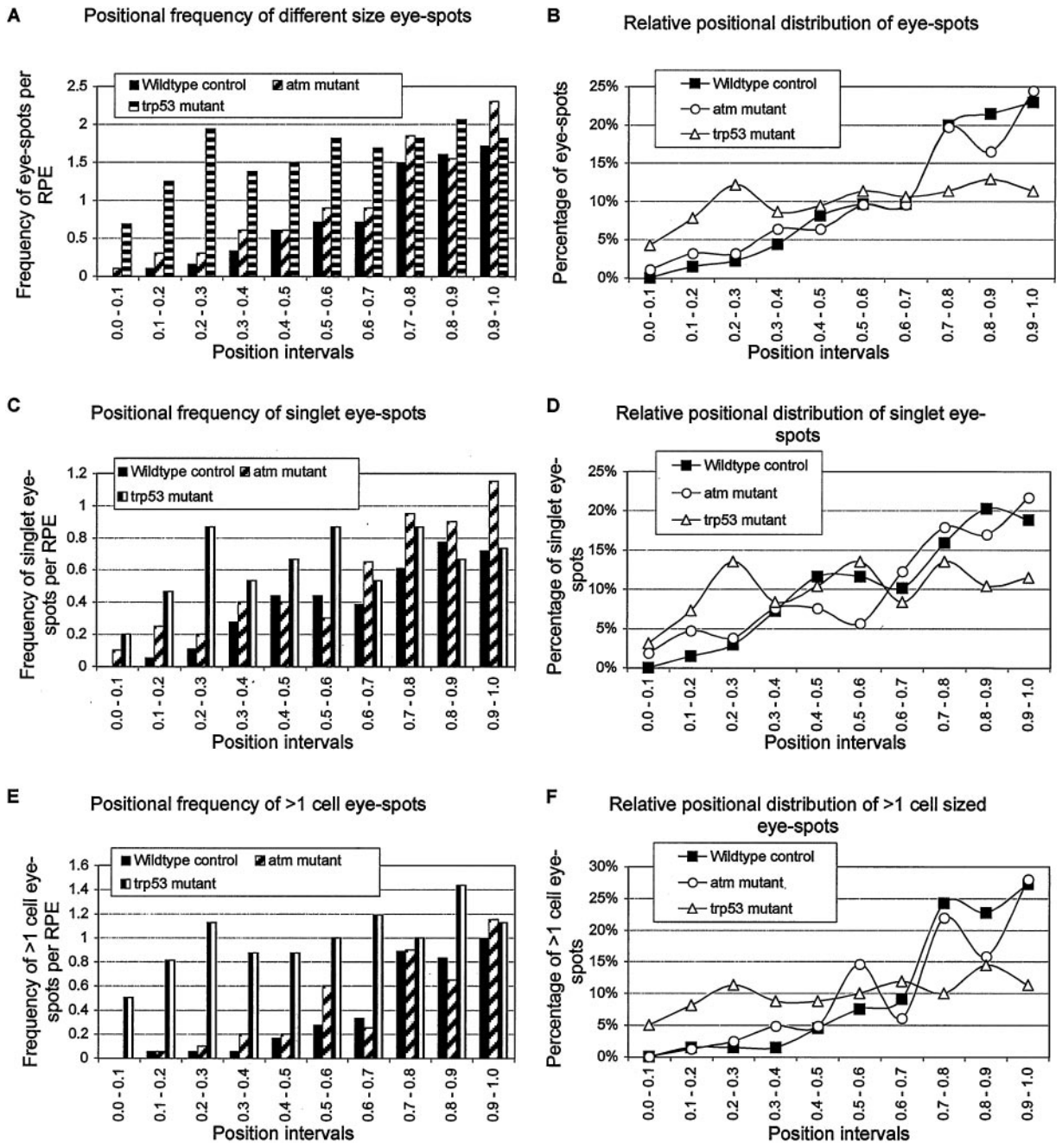

Fig. 4. An examination of the frequency of eye-spots in different regions of the RPE of *atm* and *trp53* mutant mice compared with the wild-type mice. Results are presented as either the absolute frequency per RPE (*A*, *C*, and *E*) or as a relative positional distribution (*B*, *D*, and *F*). A *position* of *0.0* is equivalent to the optic nerve head, whereas a *position* of *1.0* is at the edge of the RPE. Examination was conducted on all sized eye-spots combined (*A* and *B*), singlet eye-spots (*C* and *D*), or only the larger eye-spots (*E* and *F*). Examination of the absolute frequency of events for the 20 *atm* mutant and 18 of the wild-type RPE (*A*, *C*, and *E*) demonstrates that the frequency of eye-spots of all classes increase from the optic nerve to the periphery of the RPE. This is represented in the positional distributions (*B*, *D*, and *F*) by the increasing proportion of events from 0% at *positions 0.0–0.1* to 25% at *positions 0.9–1.0*, the edge of the RPE. The eye-spot distribution in the RPE derived from the 16 *trp53* mutant mice do not display this gradient effect, with the most obvious difference seen with the larger eye-spots (*E* and *F*).

Fig. 4*D*: $Z = 3.1$, $P_{(Z)} \geq 0.0017$; larger eye-spots, Fig. 4*F*: $Z = 5.4$, $P_{(Z)} \geq 7.6 \times 10^{-8}$), most dramatically in the larger eye-spot population. The distributions of eye-spots in the *atm* and *trp53* mutant mice were also compared and gave similar results, demonstrating a significant difference in the pattern of events for these two genotypes (all eye-spots, Fig. 4*B*: $Z = 5.9$, $P_{(Z)} \geq 4.8 \times 10^{-9}$; singlets, Fig. 4D: $Z = 3.5$, $P_{(Z)} \geq 0.00050$; larger eye-spots, Fig. 4*F*: $Z = 4.9$, $P_{(Z)} \geq 8.8 \times 10^{-7}$).

The positional distribution of events in the *gadd45a* mutant was compared with the *Gadd45a* control. An overall increased frequency of events was observed for most positions (Fig. 5*A*), although this increase seemed to be mostly attributable to the increase in larger eye-spots (compare Fig. 5, *C* and *E*). Similar to the results with the *trp53* mutant mice, the greatest increase in events were found proximal to the optic nerve head, although a significant difference was only found for the total events and more so for the larger eye-spots compared with the control distribution (all eye-spots, Fig. 5*B*: $Z = 2.8$, $P_{(Z)} \geq 0.0052$; singlets, Fig. 5*D*: $Z = 0.7$, $P_{(Z)} \geq 0.47$; larger eye-spots, Fig. 5*F*: $Z = 3.2$, $P_{(Z)} \geq 0.0016$).

An alternative method to examining the overall frequency dis-

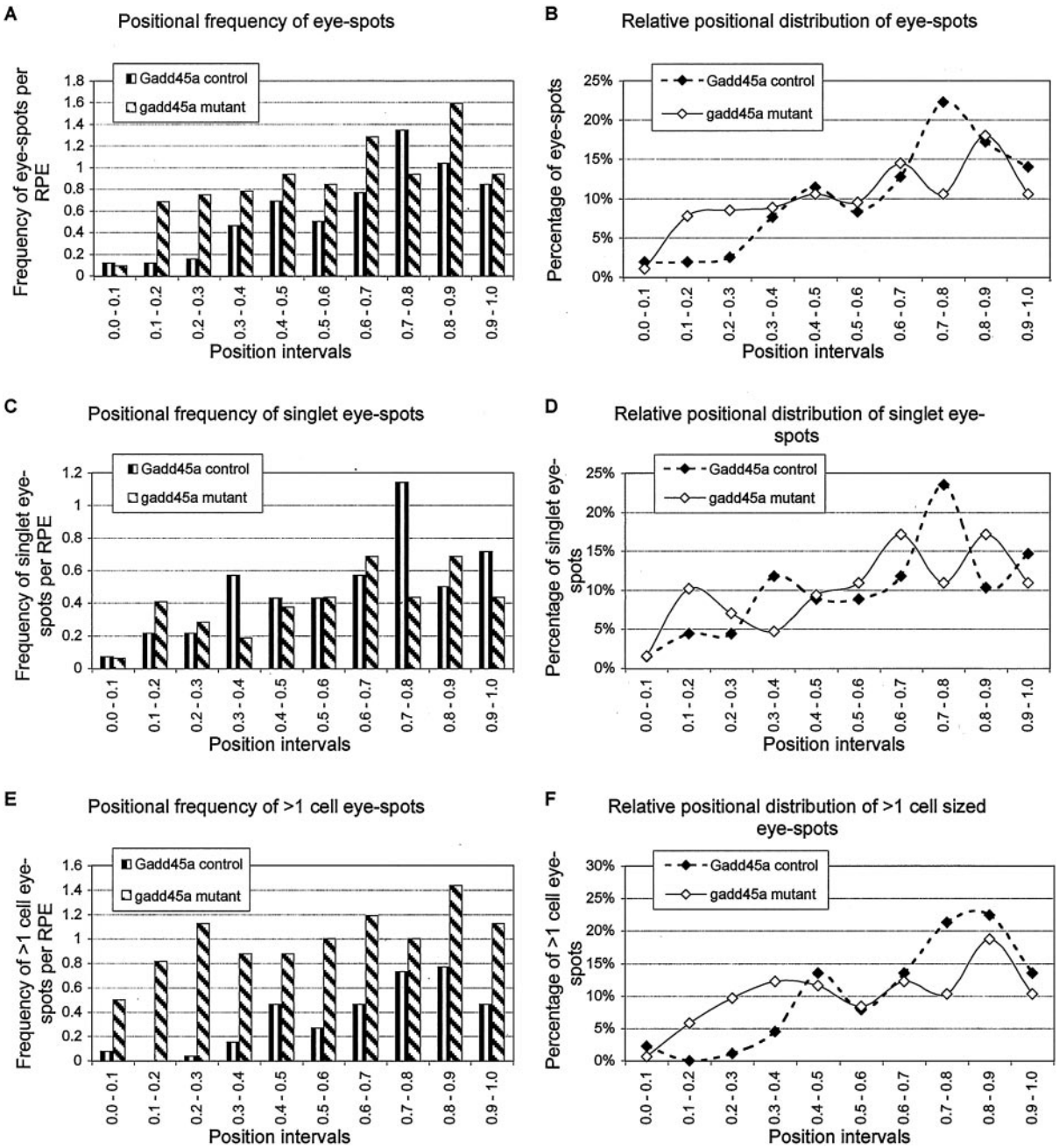

Fig. 5. An examination of the frequency of eye-spots in different regions of the RPE of *gadd45a* mutant mice compared with the *Gadd45a* control mice. Results are presented as either the absolute frequency per RPE (*A*, *C*, and *E*) or as a relative positional distribution (*B*, *D*, and *F*). A *position* of *0.0* is equivalent to the optic nerve head, whereas a *position* of *1.0* is at the edge of the RPE. Examination was conducted on all sized eye-spots combined (*A* and *B*), singlet eye-spots (*C* and *D*) or only the larger eye-spots (*E* and *F*). The distribution of eye-spots in the 32 *gadd45a* mutant RPE examined is significantly different from the eye-spot distribution of the 26 control RPE. The most significant difference between *gadd45a* mutant and the control eye-spot distribution can be observed for the larger eye-spots (*E* and *F*), with an increased proportion of eye-spots located proximal to the optic nerve in the mutant background.

tribution of eye-spots is to compare the frequency of events within a defined region *versus* the frequency of events outside of that region. Previously, we have used this method to identify specific regions into which there has been a redistribution of recombination events compared with control (56). The results of these analyses are given in Table 2 and correlate very well with the rank-sum analyses performed on the overall eye-spot distribution patterns (compare Table 2 regions with Fig. 4, *B*, *D*, and *F*, and Fig. 5, *B*, *D*, and *F*). Comparison between the *atm* mutant mice and the wild-type control revealed no region of significant difference and was, therefore, not included. *Trp53* mutant mice demonstrated regions of significant increase and a corresponding region of decrease, compared with the pooled wild-type control for every class of eye-spot. *Gadd45a* mutant mice demonstrated a very similar pattern to the *trp53* mutant mice with the exception that no region of significantly increased singlet eye-spots was identified, only a region of decrease distal to the optic nerve head. These results strongly suggest that the profile of events found in the *trp53* and *gadd45a* mutant backgrounds are very similar, and yet both are very different from the profiles observed for the *atm* mutant mice. In addition, examining either the total population distribution or limiting the analysis to specific regions demonstrates that the greatest effect of *trp53* and *gadd45a* mutations is an increased frequency of larger eye-spots. Region analysis locates these events

Table 2 *Comparing the frequencies of eye-spots of different classes in specific regions between mutant and control genotypes*

		Mutant frequency				Control frequency				Statistics	
Mutation	Region[a]	In[b]	Rest[c]	Total[d]	Percentage in[b]	In	Rest	Total	Percentage in	*G*	*P*
All eye-spots											
trp53 mutant	0.7–1.0	91	164	255	36%	87	48	135	64%	29.7	5.16×10^{-8}
trp53 mutant	0.0–0.4	84	171	255	33%	11	124	135	8%	33.6	6.83×10^{-9}
gadd45a mutant	0.7–0.8	30	253	283	11%	35	122	157	22%	10.5	1.17×10^{-3}
gadd45a mutant	0.0–0.3	46	237	283	16%	7	150	157	4%	15.2	9.49×10^{-5}
Singlet eye-spots											
trp53 mutant	0.7–1.0	34	62	96	35%	38	31	69	55%	6.3	1.20×10^{-2}
trp53 mutant	0.0–0.3	23	73	96	24%	3	66	69	4%	13.4	2.57×10^{-4}
gadd45a mutant	0.7–0.8	14	114	128	11%	16	52	68	24%	5.2	2.26×10^{-2}
>1-cell eye-spots											
trp53 mutant	0.7–1.0	57	102	159	36%	49	17	66	74%	28.3	1.01×10^{-7}
trp53 mutant	0.0–0.5	67	92	159	42%	6	60	66	9%	26.9	2.15×10^{-7}
gadd45a mutant	0.7–1.0	61	94	155	39%	51	38	89	57%	7.3	6.73×10^{-3}
gadd45a mutant	0.0–0.4	43	112	155	28%	5	84	89	6%	20.4	6.28×10^{-6}

[a] Region of RPE selected for comparison.
[b] Number of eye-spots in region selected.
[c] Number of eye-spots not in selected region.
[d] Total number of eye-spots.

proximal to the optic nerve head. Together, these observations suggest that there is an increased frequency of HR events initiated early during development in the *trp53* and *gadd45a* mutant mice, where the *atm* mutant mice have an increased frequency of events later in development in a pattern that recapitulates the pattern observed for wild-type mice.

DISCUSSION

The goal of this study was to examine the roles of Atm, p53, and Gadd45a in controlling the frequency of HR *in vivo*. Using a similar *in vivo* system (the p^{un} fur-spot assay), we previously reported that *atm* mutant mice have an increased frequency of HR and suggested that this increase came later during development (34). The increased level of recombination may not have been surprising, considering that cells from AT patients display a higher than normal frequency of genomic instability, but the timing aspect was unexpected. In addition, we also reported previously the spontaneous effect of *trp53* deficiency on the p^{un} fur-spot assay (49). In that study, we had the surprising finding that there was no observable increase in spontaneous HR frequency. Since that time, we developed and characterized the p^{un} eye-spot assay (45). With this assay, we defined a relationship between the regions in the adult mouse RPE where an increased level of HR occurred at the time of exposure to an HR-inducing agent during development and the region of proliferation of the RPE at that time of development (56). Thus, the p^{un} eye-spot assay provides both a more sensitive assay to determine the frequency of HR events *in vivo* and the ability to understand the timing of such events during development. With these tools, we have reexamined the roles of Atm and p53 in controlling the level of spontaneous HR during the development of the mouse embryo. In addition, we have included the *gadd45a* mutant mouse.

The study presented here clearly demonstrates that *atm* and *trp53* mutant mice have an increased frequency of spontaneous HR events compared with control mice. In addition, we have observed that the *gadd45a* mutant mice also have an increased frequency of HR, although only observable at a significant level by the positional distribution of events in the RPE. The striking result is that the profile of events in the *atm* mutant background is clearly different from the profile observed in the *trp53* and *gadd45a* mutant backgrounds, which are very similar to each other. In particular, the major spontaneous effect of the *trp53* and *gadd45* mutant backgrounds appears to be early in development, whereas the *atm* mutant background seems to affect spontaneous HR at later times of development, increasing at the same rate as wild-type spontaneous events.

The RPE of the mouse is a monolayer of pigmented cells derived from the neural epithelium. The development of this tissue in the mouse follows a well-defined pattern. RPE precursors enter the embryonic eyecup around the optic nerve head at about 8.5 dpc (60); the RPE then develops radially away from the optic nerve, with an outer edge-biased pattern of proliferation (55). In a previous study, we examined with the p^{un} eye-spot assay the effect of exposure to recombination-inducing agents at different times during development (56). We demonstrated that because of the well-defined developmental pattern of the RPE (55), we were able to define the time at which a recombination event occurred by its position within the RPE (56). The earliest exposure was at 8.5 dpc and resulted in a significant increase in events in almost the exact same position as observed here for the *trp53* and *gadd45a* mutant mice, if not slightly more distal from the optic nerve head. These results would suggest that the both *trp53* and *gadd45a* are playing a role in maintaining genomic stability early during development, before 8 dpc.

In our previous report on the effect of *trp53* on spontaneous HR frequency using the p^{un} fur-spot assay, we observed no difference in the frequency of events compared with wild-type control (49). In our efforts over the last decade to characterize the p^{un} fur-spot assay for the most responsive time during development to conduct an exposure to a DNA-damaging agent to demonstrate induction of HR, we found that exposure on 10.5 dpc had the best result. Exposure at 8.5 dpc resulted in little induction, presumably because of the low number of target melanoblasts, whereas exposure at 12.5 dpc resulted in fur-spots that were extremely difficult to detect, probably because of the number of cell divisions left was too limited to make an easily recognizable pigmented spot (data not shown). This would suggest that the p^{un} fur-spot assay would be insensitive to genomic instability at or before 8.5 dpc. Because we suggest that the time before 8 dpc is when an increased level of HR is seen in the *trp53* mutant mice, our previous study would have missed that effect.

There have been three reports in the literature on the spontaneous activity of p53 during mouse embryonic development (61–63), that is, the p53 dependent transcriptional activation of its downstream effector p21. All three studies reported that p53 is spontaneously active in the embryo up to approximately 8 dpc, when, depending on the tissue and level of differentiation, the spontaneous activity ceases. The lack of spontaneous activity later in development does not preclude the inducibility of p53 after exposure to DNA-damaging agents. These

reports have been substantiated by the early embryonic lethality of Mdm2-deficient mice and their rescue by a p53-null genetic background (64, 65), suggesting that p53 is highly active over this period and must be negatively regulated. In addition, the hypersensitivity of embryos to ionizing radiation over this same period (66, 67), before 8 dpc, also suggests an already potentiated damage response system that is easily triggered to promote an apoptotic response.

The timing of the increased HR frequency in the absence of p53 that we report here correlates surprisingly well with the spontaneous activity of p53 during embryonic development. The majority of events in the *trp53* and *gadd45a* mutant backgrounds appear to occur early, which, as a consequence, results in not only an increased number of events, but also an increase in larger eye-spots compared with singlets. These observations suggest a role for p53 and Gadd45a in maintaining genomic stability early in the developing embryo, similar to that seen in proliferating tissue culture studies (50–54). In addition, the results presented here strongly suggest that p53 and Gadd45a are acting in a similar fashion to control spontaneous HR, perhaps acting epistatically, as has already been established by the transcriptional regulation of Gadd45a by p53 in response to exogenous exposure to DNA-damaging agents (2). Considering that nucleotide excision repair is compromised in the p53 and Gadd45a-deficient backgrounds (28), it is possible that the HR machinery, in the absence of p53 or Gadd45a, has more opportunity to act on lesions that are normally repaired by nucleotide-excision repair. The result would be the observed increase in HR frequency in these mutant backgrounds. When p53 or Gadd45a are not spontaneously active, we would not expect to see a substantial increase in HR frequency above the background, correspondingly, the fold increase of HR over control is less later in development as determined by the eye-spot assay.

The results from the *atm* mutant mice directly correlates with our previous findings with the p^{un} fur-spot assay, an increased frequency of spontaneous recombination that increases more in later embryonic development. In addition, the majority of events, leading to greatest increase, were observed in the singlet eye-spots, unlike the observed profile of the *trp53* and *gadd45* mutant mice, where the greatest increase was in the frequency of larger eye-spots. This suggests that the role of Atm is very different from p53 in regulating spontaneous HR during development.

In the last few years, it has been demonstrated that Atm is involved in adult neurogenesis (68). To address the possibility that the observed HR patterning was attributable to a defect in RPE proliferation or development we examined the proliferation of RPE cells in 12.5 dpc embryos by BrdUrd incorporation (data not shown). Although markedly smaller and, in fact, 1-day developmentally delayed, determined by the lack of postmitotic ganglion cells, the RPE of *atm* mutant mice displayed no gross abnormality or any mispatterning of proliferation. We would, therefore, suggest that Atm does not have a tissue-specific role in RPE differentiation or development and is unlikely to be affecting the HR pattern in the RPE by perturbing its genesis.

In summary, we have demonstrated that p53 and Gadd45a play a role in suppressing HR during *in vivo* development similar to reports from tissue-culture studies. Unlike the tissue-culture studies, we have seen, both directly in this study and indirectly in our previous study (49), that this effect does not play a role later during the development of the embryo in either a neural epithelial or a neural crest derived tissue. This points to the necessity of relating tissue-culture studies on genomic stability with an *in vivo* model. In addition, this study also raises the question of the function of p53 and Gadd45a later in embryo development and how this function changes. Finally, we clearly demonstrate that Atm is functioning very differently from p53 and Gadd45a in suppressing HR, acting later in development. This synergy is supported by the increased prenatal death, severe runting, and increased rate of lymphoma reported in the generation of *atm trp53* double-mutant mice (69). Both Atm and p53 act as guardians for genomic stability, yet the differences in their time of action may offer some explanation as to the timing of carcinogenesis in these mouse models, with Atm-deficient mice suffering a more rapid rate of lymphoma onset (32, 33, 70) than p53-deficient mice (71, 72). If the level of HR stays abnormally high level in Atm-deficient mice, there is a great likelihood that HR events might directly cause oncogenic mutations or might more rapidly result in exposure of mutations in tumor suppressors. In p53-deficient mice, if the initial high burst of HR during development does not have a deleterious effect, the absence of p53 may have an effect later in the life when a cell is presented with a genomic insult and, in the absence of p53, will not be able to suppress an inappropriate HR event.

REFERENCES

1. Kastan, M. B., Onyekwere, O., Sidransky, D., Vogelstein, B., and Craig, R. W. Participation of p53 protein in the cellular response to DNA damage. Cancer Res., *51:* 6304–6311, 1991.
2. Kastan, M. B., Zhan, Q., el-Deiry, W. S., Carrier, F., Jacks, T., Walsh, W. V., Plunkett, B. S., Vogelstein, B., and Fornace, A. J., Jr. A mammalian cell cycle checkpoint pathway utilizing p53 and GADD45 is defective in ataxia-telangiectasia. Cell, *71:* 587–597, 1992.
3. Lu, X., and Lane, D. P. Differential induction of transcriptionally active p53 following UV or ionizing radiation: defects in chromosome instability syndromes? Cell, *75:* 765–778, 1993.
4. Zhan, Q., Carrier, F., and Fornace, A. J., Jr. Induction of cellular p53 activity by DNA-damaging agents and growth arrest (Published erratum in Mol. Cell. Biol. *13:* 5928, 1993). Mol. Cell. Biol., *13:* 4242–4250, 1993.
5. Hupp, T. R., Sparks, A., and Lane, D. P. Small peptides activate the latent sequence-specific DNA binding function of p53. Cell, *83:* 237–245, 1995.
6. Bargonetti, J., and Manfredi, J. J. Multiple roles of the tumor suppressor p53. Curr. Opin. Oncol., *14:* 86–91, 2002.
7. Keegan, K. S., Holtzman, D. A., Plug, A. W., Christenson, E. R., Brainerd, E. E., Flaggs, G., Bentley, N. J., Taylor, E. M., Meyn, M. S., Moss, S. B., Carr, A. M., Ashley, T., and Hoekstra, M. F. The Atr and Atm protein kinases associate with different sites along meiotically pairing chromosomes. Genes Dev., *10:* 2423–2437, 1996.
8. Chen, G., and Lee, E. The product of the *ATM* gene is a 370-kDa nuclear phosphoprotein. J. Biol. Chem., *271:* 33693–33697, 1996.
9. Jung, M., Kondratyev, A., Lee, S. A., Dimtchev, A., and Dritschilo, A. *ATM* gene product phosphorylates I κ B-α. Cancer Res., *57:* 24–27, 1997.
10. Shieh, S. Y., Ikeda, M., Taya, Y., and Prives, C. DNA damage-induced phosphorylation of p53 alleviates inhibition by MDM2. Cell, *91:* 325–334, 1997.
11. Siliciano, J. D., Canman, C. E., Taya, Y., Sakaguchi, K., Appella, E., and Kastan, M. B. DNA damage induces phosphorylation of the amino terminus of p53. Genes Dev., *11:* 3471–3481, 1997.
12. Shiloh, Y. ATM (ataxia telangiectasia mutated): expanding roles in the DNA damage response and cellular homeostasis. Biochem. Soc. Trans., *29:* 661–666, 2001.
13. Khanna, K. K., and Lavin, M. F. Ionizing radiation and UV induction of p53 protein by different pathways in ataxia-telangiectasia cells. Oncogene, *8:* 3307–3312, 1993.
14. Canman, C. E., Wolff, A. C., Chen, C. Y., Fornace, A. J., Jr., and Kastan, M. B. The p53-dependent G_1 cell cycle checkpoint pathway and ataxia- telangiectasia. Cancer Res., *54:* 5054–5058, 1994.
15. Savitsky, K., Bar-Shira, A., Gilad, S., Rotman, G., Ziv, Y., Vanagaite, L., Tagle, D. A., Smith, S., Uziel, T., Sfez, S., *et al*. A single ataxia telangiectasia gene with a product similar to PI-3 kinase. Science (Wash. DC), *268:* 1749–1753, 1995.
16. Barlow, C., Brown, K. D., Deng, C. X., Tagle, D. A., and Wynshaw-Boris, A. Atm selectively regulates distinct p53-dependent cell-cycle checkpoint and apoptotic pathways. Nat. Genet., *17:* 453–456, 1997.
17. Banin, S., Moyal, L., Shieh, S., Taya, Y., Anderson, C. W., Chessa, L., Smorodinsky, N. I., Prives, C., Reiss, Y., Shiloh, Y., and Ziv, Y. Enhanced phosphorylation of p53 by ATM in response to DNA damage. Science (Wash. DC), *281:* 1674–1677, 1998.
18. Khosravi, R., Maya, R., Gottlieb, T., Oren, M., Shiloh, Y., and Shkedy, D. Rapid ATM-dependent phosphorylation of MDM2 precedes p53 accumulation in response to DNA damage. Proc. Natl. Acad. Sci. USA, *96:* 14973–14977, 1999.
19. de Toledo, S. M., Azzam, E. I., Dahlberg, W. K., Gooding, T. B., and Little, J. B. ATM complexes with HDM2 and promotes its rapid phosphorylation in a p53-independent manner in normal and tumor human cells exposed to ionizing radiation. Oncogene, *19:* 6185–6193, 2000.
20. Maya, R., Balass, M., Kim, S. T., Shkedy, D., Leal, J. F., Shifman, O., Moas, M., Buschmann, T., Ronai, Z., Shiloh, Y., Kastan, M. B., Katzir, E., and Oren, M. ATM-dependent phosphorylation of Mdm2 on serine 395: role in p53 activation by DNA damage. Genes Dev., *15:* 1067–1077, 2001.
21. el-Deiry, W. S., Tokino, T., Velculescu, V. E., Levy, D. B., Parsons, R., Trent, J. M., Lin, D., Mercer, W. E., Kinzler, K. W., and Vogelstein, B. WAF1, a potential mediator of p53 tumor suppression. Cell, *75:* 817–825, 1993.
22. Xiong, Y., Hannon, G. J., Zhang, H., Casso, D., Kobayashi, R., and Beach, D. p21 is a universal inhibitor of cyclin kinases. Nature (Lond.), *366:* 701–704, 1993.

23. Harper, J. W., Adami, G. R., Wei, N., Keyomarsi, K., and Elledge, S. J. The p21 Cdk-interacting protein Cip1 is a potent inhibitor of G_1 cyclin- dependent kinases. Cell, *75:* 805–816, 1993.
24. Dulic, V., Kaufmann, W. K., Wilson, S. J., Tlsty, T. D., Lees, E., Harper, J. W., Elledge, S. J., and Reed, S. I. p53-dependent inhibition of cyclin-dependent kinase activities in human fibroblasts during radiation-induced G_1 arrest. Cell, *76:* 1013–1023, 1994.
25. Di Leonardo, A., Linke, S. P., Clarkin, K., and Wahl, G. M. DNA damage triggers a prolonged p53-dependent G_1 arrest and long-term induction of Cip1 in normal human fibroblasts. Genes Dev., *8:* 2540–2551, 1994.
26. Deng, C., Zhang, P., Harper, J. W., Elledge, S. J., and Leder, P. Mice lacking p21CIP1/WAF1 undergo normal development, but are defective in G_1 checkpoint control. Cell, *82:* 675–684, 1995.
27. Gu, W., and Roeder, R. G. Activation of p53 sequence-specific DNA binding by acetylation of the p53 C-terminal domain. Cell, *90:* 595–606, 1997.
28. Smith, M. L., Ford, J. M., Hollander, M. C., Bortnick, R. A., Amundson, S. A., Seo, Y. R., Deng, C. X., Hanawalt, P. C., and Fornace, A. J., Jr. p53-mediated DNA repair responses to UV radiation: studies of mouse cells lacking *p53*, *p21*, and/or *gadd45* genes. Mol. Cell. Biol., *20:* 3705–3714, 2000.
29. Bigbee, W. L., Langlois, R. G., Swift, M., and Jensen, R. H. Evidence for an elevated frequency of *in vivo* somatic cell mutations in ataxia telangiectasia. Am. J. Hum. Genet., *44:* 402–408, 1989.
30. Kojis, T. L., Gatti, R. A., and Sparkes, R. S. The cytogenetics of ataxia telangiectasia. Cancer Genet. Cytogenet., *56:* 143–156, 1991.
31. Meyn, M. S. High spontaneous intrachromosomal recombination rates in ataxia-telangiectasia. Science (Wash. DC), *260:* 1327–1330, 1993.
32. Barlow, C., Hirotsune, S., Paylor, R., Liyanage, M., Eckhaus, M., Collins, F., Shiloh, Y., Crawley, J. N., Ried, T., Tagle, D., and Wynshaw-Boris, A. Atm-deficient mice: a paradigm of ataxia telangiectasia. Cell, *86:* 159–171, 1996.
33. Elson, A., Wang, Y., Daugherty, C. J., Morton, C. C., Zhou, F., Campos-Torres, J., and Leder, P. Pleiotropic defects in ataxia-telangiectasia protein-deficient mice. Proc. Natl. Acad. Sci. USA, *93:* 13084–13089, 1996.
34. Bishop, A. J., Barlow, C., Wynshaw-Boris, A. J., and Schiestl, R. H. Atm deficiency causes an increased frequency of intrachromosomal homologous recombination in mice. Cancer Res., *60:* 395–399, 2000.
35. Purdie, C. A., Harrison, D. J., Peter, A., Dobbie, L., White, S., Howie, S. E., Salter, D. M., Bird, C. C., Wyllie, A. H., Hooper, M. L., *et al*. Tumour incidence, spectrum and ploidy in mice with a large deletion in the *p53* gene. Oncogene, *9:* 603–609, 1994.
36. Donehower, L. A., Godley, L. A., Aldaz, C. M., Pyle, R., Shi, Y. P., Pinkel, D., Gray, J., Bradley, A., Medina, D., and Varmus, H. E. Deficiency of p53 accelerates mammary tumorigenesis in Wnt-1 transgenic mice and promotes chromosomal instability. Genes Dev., *9:* 882–895, 1995.
37. Hollander, M. C., Sheikh, M. S., Bulavin, D. V., Lundgren, K., Augeri-Henmueller, L., Shehee, R., Molinaro, T. A., Kim, K. E., Tolosa, E., Ashwell, J. D., Rosenberg, M. P., Zhan, Q., Fernandez-Salguero, P. M., Morgan, W. F., Deng, C. X., and Fornace, A. J., Jr. Genomic instability in Gadd45a-deficient mice. Nat. Genet., *23:* 176–184, 1999.
38. Brilliant, M. H., Gondo, Y., and Eicher, E. M. Direct molecular identification of the mouse pink-eyed unstable mutation by genome scanning. Science (Wash. DC), *252:* 566–569, 1991.
39. Gondo, Y., Gardner, J. M., Nakatsu, Y., Durham-Pierre, D., Deveau, S. A., Kuper, C., and Brilliant, M. H. High-frequency genetic reversion mediated by a DNA duplication: the mouse pink-eyed unstable mutation. Proc. Natl. Acad. Sci. USA, *90:* 297–301, 1993.
40. Lyon, M. F., King, T. R., Gondo, Y., Gardner, J. M., Nakatsu, Y., Eicher, E. M., and Brilliant, M. H. Genetic and molecular analysis of recessive alleles at the pink-eyed dilution (*p*) locus of the mouse. Proc. Natl. Acad. Sci. USA, *89:* 6968–6972, 1992.
41. Schiestl, R. H., Aubrecht, J., Khogali, F., and Carls, N. Carcinogens induce reversion of the mouse pink-eyed unstable mutation. Proc. Natl. Acad. Sci. USA, *94:* 4576–4581, 1997.
42. Searle, A. G. The use of pigment loci for detecting reverse mutations in somatic cells of mice. Arch. Toxicol., *38:* 105–108, 1977.
43. Deol, M. S., and Truslove, G. M. The effects of the pink-eyed unstable gene on the retinal pigment epithelium of the mouse. J. Embryol. Exp. Morphol., *78:* 291–298, 1983.
44. Bodenstein, L., and Sidman, R. L. Growth and development of the mouse retinal pigment epithelium. II. Cell patterning in experimental chimaeras and mosaics. Dev. Biol., *121:* 205–219, 1987.
45. Bishop, A. J. R., Kosaras, B., Sidman, R. L., and Schiestl, R. H. Benzo(a)pyrene and X-rays induce reversions of the pink-eyed unstable mutation in the retinal pigment epithelium of mice. Mutat. Res, *457:* 31–40, 2000.
46. Schiestl, R. H., Khogali, F., and Carls, N. Reversion of the mouse pink-eyed unstable mutation induced by low doses of x-rays. Science (Wash. DC), *266:* 1573–1576, 1994.
47. Jalili, T., Murthy, G. G., and Schiestl, R. H. Cigarette smoke induces DNA deletions in the mouse embryo. Cancer Res., *58:* 2633–2638, 1998.
48. Lebel, M. Increased frequency of DNA deletions in pink-eyed unstable mice carrying a mutation in the Werner syndrome gene homologue. Carcinogenesis (Lond.), *23:* 213–216, 2002.
49. Aubrecht, J., Secretan, M. B., Bishop, A. J., and Schiestl, R. H. Involvement of p53 in X-ray induced intrachromosomal recombination in mice. Carcinogenesis (Lond.), *20:* 2229–2236, 1999.
50. Bertrand, P., Rouillard, D., Boulet, A., Levalois, C., Soussi, T., and Lopez, B. S. Increase of spontaneous intrachromosomal homologous recombination in mammalian cells expressing a mutant p53 protein. Oncogene, *14:* 1117–1122, 1997.
51. Mekeel, K. L., Tang, W., Kachnic, L. A., Luo, C. M., DeFrank, J. S., and Powell, S. N. Inactivation of p53 results in high rates of homologous recombination. Oncogene, *14:* 1847–1857, 1997.
52. Sturzbecher, H. W., Donzelmann, B., Henning, W., Knippschild, U., and Buchhop, S. p53 is linked directly to homologous recombination processes via RAD51/RecA protein interaction. EMBO J., *15:* 1992–2002, 1996.
53. Gebow, D., Miselis, N., and Liber, H. L. Homologous and nonhomologous recombination resulting in deletion: effects of p53 status, microhomology, and repetitive DNA length and orientation. Mol. Cell. Biol., *20:* 4028–4035, 2000.
54. Willers, H., McCarthy, E. E., Wu, B., Wunsch, H., Tang, W., Taghian, D. G., Xia, F., and Powell, S. N. Dissociation of p53-mediated suppression of homologous recombination from G_1/S cell cycle checkpoint control. Oncogene, *19:* 632–639, 2000.
55. Bodenstein, L., and Sidman, R. L. Growth and development of the mouse retinal pigment epithelium. I. Cell and tissue morphometrics and topography of mitotic activity. Dev. Biol., *121:* 192–204, 1987.
56. Bishop, A. J., Kosaras, B., Carls, N., Sidman, R. L., and Schiestl, R. H. Susceptibility of proliferating cells to benzo[a]pyrene-induced homologous recombination in mice. Carcinogenesis (Lond.), *22:* 641–649, 2001.
57. Sokal, R. R., and Rohlf, F. J. Biometrics, pp. 575–585. San Francisco: W. H. Freeman, 1969.
58. Wilcoxon, F. Individual comparisons by ranking methods. Biometrics, *1:* 80–83, 1945.
59. Mann, H. B., and Whitney, D. R. On a test of whether one of two random variables is stochastically larger than the other. Ann. Math. Stat., *18:* 50–60, 1947.
60. Nakayama, A., Nguyen, M. T., Chen, C. C., Opdecamp, K., Hodgkinson, C. A., and Arnheiter, H. Mutations in microphthalmia, the mouse homolog of the human deafness gene *MITF*, affect neuroepithelial and neural crest-derived melanocytes differently. Mech. Dev., *70:* 155–166, 1998.
61. MacCallum, D. E., Hupp, T. R., Midgley, C. A., Stuart, D., Campbell, S. J., Harper, A., Walsh, F. S., Wright, E. G., Balmain, A., Lane, D. P., and Hall, P. A. The p53 response to ionising radiation in adult and developing murine tissues. Oncogene, *13:* 2575–2587, 1996.
62. Gottlieb, E., Haffner, R., King, A., Asher, G., Gruss, P., Lonai, P., and Oren, M. Transgenic mouse model for studying the transcriptional activity of the p53 protein: age- and tissue-dependent changes in radiation-induced activation during embryogenesis. EMBO J., *16:* 1381–1390, 1997.
63. Komarova, E. A., Chernov, M. V., Franks, R., Wang, K., Armin, G., Zelnick, C. R., Chin, D. M., Bacus, S. S., Stark, G. R., and Gudkov, A. V. Transgenic mice with p53-responsive lacZ: p53 activity varies dramatically during normal development and determines radiation and drug sensitivity in vivo. EMBO J., *16:* 1391–1400, 1997.
64. Jones, S. N., Roe, A. E., Donehower, L. A., and Bradley, A. Rescue of embryonic lethality in Mdm2-deficient mice by absence of p53. Nature (Lond.), *378:* 206–208, 1995.
65. Montes de Oca Luna, R., Wagner, D. S., and Lozano, G. Rescue of early embryonic lethality in mdm2-deficient mice by deletion of p53. Nature (Lond.), *378:* 203–206, 1995.
66. Russell, L. B., and Russell, W. L. An analysis of the changing radiation response of the developing mouse embryo. J. Cell. Comp. Physiol., *43:* A103–A149, 1954.
67. Russell, L. B. Effects of low doses of x-rays on embryonic development in the mouse. Proc. Soc. Exp. Biol. Med., *95:* 174–178, 1957.
68. Allen, D. M., van Praag, H., Ray, J., Weaver, Z., Winrow, C. J., Carter, T. A., Braquet, R., Harrington, E., Ried, T., Brown, K. D., Gage, F. H., and Barlow, C. Ataxia telangiectasia mutated is essential during adult neurogenesis. Genes Dev., *15:* 554–566, 2001.
69. Xu, Y., Yang, E. M., Brugarolas, J., Jacks, T., and Baltimore, D. Involvement of p53 and p21 in cellular defects and tumorigenesis in Atm−/− mice. Mol. Cell. Biol., *18:* 4385–4390, 1998.
70. Xu, Y., Ashley, T., Brainerd, E. E., Bronson, R. T., Meyn, M. S., and Baltimore, D. Targeted disruption of ATM leads to growth retardation, chromosomal fragmentation during meiosis, immune defects, and thymic lymphoma. Genes Dev., *10:* 2411–2422, 1996.
71. Donehower, L. A., Harvey, M., Slagle, B. L., McArthur, M. J., Montgomery, C. A., Jr., Butel, J. S., and Bradley, A. Mice deficient for p53 are developmentally normal but susceptible to spontaneous tumours. Nature (Lond.), *356:* 215–221, 1992.
72. Jacks, T., Remington, L., Williams, B. O., Schmitt, E. M., Halachmi, S., Bronson, R. T., and Weinberg, R. A. Tumor spectrum analysis in p53-mutant mice. Curr. Biol., *4:* 1–7, 1994.